EEG SIGNAL PROCESSING AND MACHINE LEARNING FOR ANALYSIS OF THE RESPONSES TO DEEP BRAIN STIMULATION IN EPILEPSY

SEPEHR SHIRANI

A thesis submitted to Nottingham Trent University in candidature of the Degree of Doctor of Philosophy

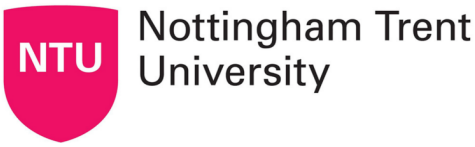

School of Science and Technology
Department of Computer Science
Nottingham Trent University

August 2024

Sepehr Shirani: *EEG SIGNAL PROCESSING AND MACHINE LEARNING FOR ANALYSIS OF THE RESPONSES TO DEEP BRAIN STIMULATION IN EPILEPSY* , A thesis submitted to Nottingham Trent University in candidature of the Degree of Doctor of Philosophy, © August 2024

SUPERVISORS:
Dr Jordan Bird
Dr Antonio Valentin
Dr Mufti Mahmud
Professor Saeid Sanei

DECLARATION

I hereby declare that the this thesis is my original work and it has been written by me in its entirety. I have duly acknowledged all the sources of information which have been used in the thesis. This thesis has also not been submitted for any degree in any university previously.

Nottingham, UK, August 2024

Sepehr Shirani

ACKNOWLEDGEMENTS

I would like to extend my heartfelt gratitude to my exceptional supervisors and mentors. Special thanks to Professor Saeid Sanei for his unwavering supervision and assistance, particularly in the theoretical and engineering aspects, throughout my PhD research period. I would also like to thank my second supervisor, Dr Antonio Valentin from King's College London, for providing the unique dataset used in this project and offering exceptional support from the clinical perspective. Additionally, I sincerely appreciate Dr Jordan Bird, my supervisor and director of studies, for his invaluable support during the final stages of my PhD journey. I would also like to thank Dr Mufti Mahmud for supporting the project. My deep gratitude goes to my dear friend and colleague, Dr Bahman Abdi-Sargezeh, for his continuous support.

To my friends and family, your unconditional love and support have been a constant source of strength.

Most importantly, to my father, my best friend, and my hero, Akbar: Daddy, you have given me everything, and the only reason I am where I am today is because of your sacrifices. Thank you. I will continue to work hard to make you proud. This one is for you. Love you now and always.

ABSTRACT

Single Pulse Electrical Stimulation (SPES) has emerged as a promising technique for the assessment of drug-resistant epilepsy (DRE). SPES offers a controlled method to probe the excitability and connectivity of neural circuits to identify regions associated with epileptic seizures. Current limited methods employed in practice for processing and diagnosing epilepsy using SPES sometimes fall short of explaining the underlying neurophysiological mechanisms and identifying the regions associated with seizure and seizure onset zone (SOZ). The unique nature of the data recorded during SPES sessions, such as the morphology and inconsistent behaviour of responses even for an individual case in a fixed setup, presents significant challenges for conventional processing algorithms. Such methods may lead to misleading results, underscoring the need for innovative approaches in SPES data analysis.

This PhD thesis focuses on increasing the efficacy of SPES used for the treatment of DRE cases by developing signal processing and machine learning pipelines to investigate the responses to SPES. We aim to answer the critical questions regarding the excitation and inhibition imbalance in regions associated with seizure, the relation between the source of responses to SPES and that of interictal epileptiform discharges (IEDs) as important biomarkers for epilepsy, and also provide accurate and robust tools for identifying the regions responsible for seizure generation focusing on array processing using beamforming.

By leveraging advanced techniques like adaptive and nonlinear signal processing, subspace analysis, single-channel source separation, regularised beamforming, and the related optimisations, this work is committed to improving the accuracy of the diagnosis stage, leading to more effective and individualised treatment strategies for DRE cases.

The excitatory and inhibitory components of brain responses to SPES are separated to study their imbalance associated with seizures. Moreover, more accurate and robust source localisation pipelines, including a distributed beamforming algorithm, are suggested and implemented to identify the regions responsible for generating abnormal responses to SPES. The source of these responses is compared with the origin of other epileptiform activities, such as IEDs and SOZ. The methods developed in this work not only offer a better insight into epilepsy and abnormal activity present in the intracranial electroencephalogram data recorded from DRE cases but also provide more reliable tools for their clinical diagnosis in the future, leading to more efficient and cost-effective DRE treatment techniques.

PUBLICATIONS RELATED TO PHD RESEARCH

Journals:

Shirani, S., Valentin, A., Alarcon, G., Kazi, F. & Sanei, S. (2023). "Separating inhibitory and excitatory responses of epileptic brain to single-pulse electrical stimulation." *International Journal of Neural Systems*, 33(02), 2350008.

Shirani, S., Valentin, A., Alarcon, G., Kazi, F. & Sanei, S. (2023). "Response to the Discussion on S. Shirani, A. Valentin, G. Alarcon, F. Kazi and S. Sanei, Separating Inhibitory and Excitatory Responses of Epileptic Brain to Single-Pulse Electrical Stimulation, International Journal of Neural Systems, Vol. 33, No. 2 (2023) 2350008." *International Journal of Neural Systems*, 33(9), 2375002.

Shirani, S., Valentin, A., Abdi-Sargezeh, B., Alarcon, G., & Sanei, S. (2023). "Localisation of Epileptic Brain Responses to Single-Pulse Electrical Stimulation by Developing an Adaptive Iterative Linearly Constrained Minimum Variance Beamformer." *International Journal of Neural Systems*, 2350050-2350050. **Received the 2024 International Journal of Neural Systems Award for Outstanding Contributions in Neural Systems.**

Shirani, S., Abdi-Sargezeh, B. Valentin, A., Alarcon, G., Bird, J. J., & Sanei, S. (2024). "Do Interictal Epileptiform Discharges and Brain Responses to Electrical Stimulation Come from the Same Location? An Advanced Source Localisation Solution." *IEEE Transactions on Biomedical Engineering*. **Selected by the Editorial Board as a Featured Article, in the TBME September Issue, 2024.**

Conferences:

S. Shirani, Abdi-Sargezeh, B., Valentin, A., Alarcon, G., D. Jarchi, J. Bird & Sanei, S. (2024) "Distributed Beamforming for Localisation of Brain Seizure Sources from Intracranial EEG Array." *European Conference on Signal Processing (EUSIPCO)*. **Selected to Compete for the "Student Best Paper" Award**

OTHER RESEARCH CONTRIBUTIONS DURING PHD STUDY

Journals:

Shirani, S., & Mohebbi, M. (2022). "Brain functional connectivity analysis in patients with relapsing-remitting multiple sclerosis: A graph theory approach of EEG resting state." *Frontiers in Neuroscience*, 16, 801774.

Abdi-Sargezeh, B., **Shirani, S.**, Sanei, S., Took, C. C., Geman, O., Alarcon, G., & Valentin, A. (2023). "A review of signal processing and machine learning techniques for interictal epileptiform discharge detection." *Computers in Biology and Medicine*, 107782.

Falcon-Caro, A. **Shirani, S.**, Ferreira, J. F., Bird, J. J., & Sanei, S. (2024). "Formulation of Common Spatial Patterns for Multi-task Hyperscanning BCI" *IEEE Transactions on Biomedical Engineering*.

Abdi-Sargezeh, B., **Shirani, S.**, Valentin, A. Alarcon, G., & Sanei, S. (2024). "EEG-to-EEG: Scalp-to-Intracranial EEG Translation using a Combination of Variational Autoencoder and Generative Adversarial Networks." *Submitted to International Journal of Neural Eengineering*, 107782.

Abdi-Sargezeh, B., **Shirani, S.**, Sharma, A., Green, A., Akram, H., Zrinzo, L., ... & Oswal, A. (2024). " Prediction of pathological subthalamic nucleus beta burst occurrence in Parkinson's disease." *Submitted to Brain*.

Sanei, S., Took, C. C., Tanaka, T., Abdi-Sargezeh, B., **Shirani, S.**, Valentin, A., & Alarcon, G. (2024). "Identification of Interictal Eplieptiform Discharges and Brain Responses to Electrical Stimulation." *Submitted to IEEE signal Processing Magazine*.

Conferences:

Yousefipour, B. **Shirani, S**, Mohebbi, M. & Abharian, P. H. (2022). "Evaluation of Brain Cortical Connectivity in Drug Abusers Using EEG Data." *29th National and 7th International Iranian Conference on Biomedical Engineering (ICBME)*, pp. 161-166.

CONTENTS

LIST OF FIGURES

LIST OF TABLES

LIST OF ABBREVIATIONS

ABMC	Adaptive Baysian with Multiple Constraints
ACPC	Anterior Commissure - Posterior Commissure
AI-LCMV	Adaptive Iterative LCMV
ASCI	Adaptive Signed Correlation Index
CCEP	Cortico-Cortical Evoked Potentials
CF-LCMV	Closed Form of LCMV
CG	Conjugate Gradient
CPD	Canonical Polyadic Decomposition
CT	Computed Tomography
DBS	Deep Brain Stimulation
DOA	Direction of Arrival
DR	Delayed Response
DRE	Drug Resistant Epilepsy
E	Excitation
ECDs	Equivalent Current Dipoles
ECG	Electrocardiogram
ECoG	Electrocorticography
EEG	Electroencephalography
EMD	Empirical Mode Decomposition
EOS	Engel Outcome Score
ER	Early Responses
ERP	Event Related Potentials
ESPRIT	Estimation of Signal Parameters via Rotational Invariance Techniques
EVD	Eigenvalue Decomposition

fMRI	Functional MRI
FR	Fast Ripple
HFO	High Frequency Oscillation
I	Inhibition
ICA	Independent Component Analysis
IED	Interictal Epileptiform Discharges
iEEG	Intracranial EEG
IMF	Intrinsic Mode Functions
LCMV	Linearly Constraint Minimum Variance
LCMV-RLS	LCMV with Recursive Least Squares
LCMV-SC	LCMV with Stochastic Gradient
LORETA	Low-Resolution Electromagnetic Tomography
MEG	Magnetoencephalography
MNE	Minimum Norm Estimation
MRI	Magnetic Resonance Imaging
MUSIC	Multiple Signal Classification
MVDR	Minimum Variance Distortionless Response
NES	Non-Epileptic Seizures
NTF	Non-negative Tensor Factorisation
PNES	Psychogenic NES
PSD	Power Spectrum Density
RAIS-LCMV	Robust Adaptive Iterative Suboptimal Solution for LCMV
RAP MUSIC	Recursively Applied and Projected MUSIC
RMS	Root Mean Square
ROI	Region of Interest
SBL	Sparse Bayesian Learning

sEEG	Stereo EEG
scEEG	Scalp EEG
SE	Status Epilepticus
SNR	Signal to Noise Ratio
SOZ	Seizure Onset Zone
SPES	Single Pulse Electrical Stimulation
SSA	Singular Spectrum Analysis
STFT	Short-Time Fourier Transform
UCA	Uniform Circular Arrays
ULA	Uniform Linear Arrays
URA	Uniform Rectangular Arrays
WHO	World Health Organization
WT	Wavelet Transform

1 INTRODUCTION

The brain is undeniably the most complex organ in the human body. It comprises a vast number of neurons that are anatomically or functionally connected. Researchers have been diligently investigating neuronal communication within the brain for many years. This extensive research has significantly enhanced our understanding of brain functionality and has led to improved methods for diagnosing and treating various neurological diseases and conditions, including autism, epilepsy, dementia, Parkinson's disease, and Alzheimer's disease [1].

To explore brain functionality, researchers employ various neuroimaging modalities. Among them, the electroencephalography (EEG) [2] and functional magnetic resonance imaging (fMRI) [3] are particularly prominent. fMRI is based on the brain's hemodynamic response, measuring the changes in blood flow to track alteration in neural activity. However, one of the limitations of fMRI is its low temporal resolution due to its nature, meaning it cannot capture and track the rapid changes in brain activity. Conversely, EEG records the brain's electrical activity directly, which provides a high temporal resolution and is invaluable for investigating the brain activities and overall functionality as a dynamic system.

EEG can be recorded either non-invasively from the scalp using wet or dry electrodes, known as scalp EEG (scEEG), or invasively by recording the electrical activity directly from the cerebral cortex or deeper brain areas called intracranial EEG (iEEG) [4]. Although scEEG is an easily available low-cost method for recording brain activity, it lacks sufficient precision in pinpointing their exact sources due to its limited spatial resolution. The volume conduction effect, a phenomenon where EEG signals generated by neuronal activity are spread and diffused through the various tissues of the head, causing a smearing effect on EEG [5], is worse for scEEG compared to iEEG as the signals propagate through extra layers of tissue (skull and scalp). In contrast, iEEG offers high spatial resolution, making it a powerful tool for detailed investigation of brain activity. This high spatial resolution is particularly crucial for patients with neurological conditions such as epilepsy, where precise localisation and characterisation of the brain activity are essential for effective diagnosis and treatment.

1.1 EPILEPSY AND EPILEPTIC SEIZURES

Epilepsy, a chronic brain disease, is characterised by epileptic seizures caused by an expected imbalance between excitatory and inhibitory activity in regions associated

with the epileptic seizure, known as epileptogenic regions [6]. Based on reports from the World Health Organization (WHO), epilepsy is the most prevalent neurological disease, affecting more than fifthy million people globally [7].

Epileptic seizures are characterised by sudden, uncontrolled electrical disruptions in the brain, which can lead to various symptoms, including loss of consciousness, and changed sensory perceptions [8]. The condition of epilepsy is diagnosed when a case experiences two or more unprovoked seizures, which are seizures not caused by identifiable factors such as head injury, stress, trauma, hypertensions, or fever. These rates can be influenced by demographic and regional factors, such as ageing populations and improvements in medical care and diagnosis, which may lead to variations over time [9].

The prognosis for individuals experiencing their first unprovoked seizure can vary significantly. Research indicates that approximately 27% of individuals experience a second seizure within six months of their first, and this risk increases to 43% within two years. This data is crucial for clinicians in counseling patients about the likelihood of recurrence and making informed treatment and management decisions [8, 10].

Approximately 30% of individuals with epilepsy do not respond positively to medication and show no improvement in their symptoms during or after the treatment, classifying them as drug-resistant epileptic (DRE) patients [11]. For these patients, alternative treatments such as resection surgery [12], where the regions responsible for seizures, if possible, are surgically removed, can be an option. Given the considerable global population afflicted by epilepsy and the complexities doctors and clinicians encounter in managing this condition, there has been a significant emphasis in research on enhancing the understanding of epilepsy and refining treatment approaches for the affected individuals.

Seizures are periods of unusual electrical activity in the brain that can manifest in various forms. They are generally grouped into epileptic and non-epileptic seizures, each with distinct etiologies, manifestations, and treatment approaches. Understanding these differences is necessary for accurate diagnosis and management [13].

Epileptic seizures stem from abnormal electrical discharges in the brain. These discharges disrupt normal brain function, leading to various symptoms such as convulsions, loss of consciousness, and sensory disturbances [14, 15]. The causes of epileptic seizures can be diverse, including genetic factors, brain injuries, strokes, brain tumors, and other neurological disorders [15].

Epileptic seizures are categorised into generalised and partial (focal) seizures. Generalised seizures affect the entire brain and are often associated with genetic factors. In contrast, partial seizures originate in a specific area in the brain and can be caused by localised brain damage or lesions [15]. Diagnosis typically involves EEG monitoring to detect abnormal electrical activity [16].

Non-epileptic seizures (NES) resemble epileptic seizures in appearance but are not due to changed brain electrical activity. Instead, they may result from psychological factors, such as stress or trauma, or physical conditions like metabolic imbalances or cardiovascular issues [14, 16]. NES can be further divided into functional (psychogenic) seizures and those with an organic cause [14, 16]. Functional seizures, also named psychogenic non-epileptic seizures (PNES), are physical manifestations of psychological distress. They occur unconsciously and are not under the individual's control [14, 17]. Diagnosis often involves ruling out epilepsy through EEG monitoring and assessing psychological factors [16, 17]. Organic NES has a physical cause, such as fainting or metabolic disturbances like hypoglycemia. These seizures are generally easier to diagnose and treat due to their identifiable physical causes [14, 16].

One important challenge in distinguishing between epileptic and non-epileptic seizures is their similar presentation. Both can involve convulsions, altered consciousness, and other seizure-like symptoms [16]. Hence, EEG monitoring is crucial for differentiation [17]. The paper "Differentiating between nonepileptic and epileptic seizures" addresses the complexities in distinguishing psychogenic nonepileptic seizures (PNES) from epileptic ones [13]. Wrong diagnosis can happen, which leads to inadequate treatment and prolonged patient distress. While clinical features such as seizure duration, motor activity, and responsiveness can offer the indications, none is definitive in isolation. Therefore, a comprehensive approach is required. The gold standard for diagnosis is video-electroencephalography (video-EEG), which can capture the brain's electrical activity during a seizure, helping distinguish between epileptic and nonepileptic events [13]. However, video-EEG alone may not be sufficient in all cases, and the paper advocates for integrating thorough neurological and psychiatric examinations to improve diagnostic accuracy [13].

Epileptic seizures are primarily managed with antiepileptic drugs and, in some cases, resection surgery to remove epileptogenic regions [18]. In contrast, treatment NES involves addressing the underlying psychological or physical causes. For PNES, cognitive behavioural therapy and psychiatric interventions are commonly used [17].

The iEEG recordings from ictal (during seizure) and interictal (between seizures) periods play a critical role in identifying the epileptogenic areas responsible for generating seizures during the clinical assessment stage, especially for DRE cases, prospected for resection surgery. Although monitoring the ictal recordings can be helpful during the treatment period, seizures are not always frequent and might not happen during the limited clinical assessment time in the clinical environment. The same applies to interictal epileptiform discharges (IEDs) observed during interictal periods [19]. Considering the sparsity of ictal periods and IEDs during interictal periods for a large number of DRE patients and the limited time they spend after electrode implantation at the telemetry unit, deep brain stimulation (DBS), mainly single pulse electrical stimulation (SPES) [20], is a method developed to investigate the brain responses to electrical stimulation

and identify the epileptogenic regions responsible for seizure generation. SPES results can help reduce the duration of chronic recordings, consequently lowering costs and the risk of infection during the assessment period. Additionally, various SPES modalities could be particularly relevant for patients who do not experience seizures during the intracranial recording periods [21]. Furthermore, exploring the relationship between SPES responses and IEDs can enhance the efficiency of pre-surgical assessments for patients undergoing evaluation for resection surgery [22].

Epilepsy research is continuously advancing, aiming to provide better diagnostic tools and treatment options for those affected by this neurological disorder. The integration of iEEG recordings and innovative techniques like SPES in clinical practice holds promise for improving the management and outcomes of epilepsy, particularly for those who are resistant to conventional treatments. These advanced methods allow for more precise localisation of seizure sources and mapping of the epileptogenic network in the brain, enabling tailored surgical interventions and possibly reducing the invasive procedures [23, 24]. Furthermore, recent studies have explored the use of machine learning algorithms to analyse iEEG data, enhancing the accuracy of seizure prediction and detection [25]. The combination of these cutting-edge approaches with traditional diagnostic methods, such as neuroimaging and standard EEG, paves the way for more personalised and effective epilepsy assessment and care, ultimately aiming to improve the quality of life for individuals living with this challenging condition [23, 26].

1.2 DBS AND SINGLE PULSE ELECTRICAL STIMULATION

The surgical procedure for DBS involves implanting electrodes where each electrode can be supplied by a pulse generator in targeted brain regions. This setup allows for the modulation of brain activity through electrical stimulation [27, 28]. DBS is mainly used for Parkinson's disease and epilepsy, but the mechanisms, targets, and outcomes differ between these conditions. DBS delivers electrical impulses to targeted brain areas, disrupting abnormal neural circuits. In both Parkinson's disease and epilepsy, DBS aims to modulate dysfunctional brain activity to alleviate symptoms. The procedure is reversible and adjustable, offering advantages over lesioning techniques [29, 30]. In addition to treatment, DBS has been used as a diagnostic tool for DRE cases [20].

The most common targets for DBS in Parkinson's are the subthalamic nucleus and the globus pallidus interna [31]. These areas are involved in motor control, and their stimulation helps alleviate symptoms like tremor, rigidity, and bradykinesia [27, 30].

The anterior nucleus of the thalamus is a common target for epilepsy. This area is involved in seizure propagation, and its stimulation can reduce seizure frequency in patients with refractory epilepsy [28]. In addition, DBS has been applied to various

regions in the brain to identify the epileptogenic regions responsible for seizure generation using the responses to electrical stimulation [20, 22].

The stimulation parameters, like frequency and intensity, can differ significantly between Parkinson's and epilepsy. Parkinson's DBS typically uses continuous high-frequency stimulation. At the same time, epilepsy may benefit from both open-loop and closed-loop systems, with the latter providing responsive stimulation based on detected seizure activity [22, 28, 29].

In Parkinson's disease, the DBS significantly improves motor symptoms and can reduce medication requirements. However, it does not halt disease progression and may not address non-motor symptoms like cognitive decline [27]. In epilepsy, the DBS can reduce seizure frequency and severity, particularly in patients with DRE. However, the efficacy can vary, and some patients may not achieve complete seizure control [28, 29]. The adverse effects of DBS can vary between the two conditions. In Parkinson's, cognitive and mood changes can occur, especially with subthalamic nucleus stimulation. In epilepsy, the side effects may include sleep disturbance and mood change, but these are often related to the specific brain target and the stimulation parameters [27, 30]. DBS may be used to treat refractory status epilepticus (SE). SE is a medical emergency where a seizure lasts for an unusually long time or when a person has repeated seizures without regaining full consciousness between the events. It is a condition that can occur in people with or without a history of epilepsy. DBS can be considered a salvage therapy for these conditions, which have high mortality rates. In some cases, DBS has resulted in a significant reduction or complete elimination of seizures in SE subjects [32].

In previous studies, the researchers have increasingly emphasised the synchronisation of brain cortical signals as a crucial predictor of impending epileptic events [33]. The balance between excitatory and inhibitory neural activities is fundamental for directing optimal information transmission within the brain necessary for normal brain functioning. Any deviation from this balance can disrupt normal brain function, impeding effective information processing [34–36].

Extensive research efforts have delved into elucidating the role of excitatory and inhibitory mechanisms in the transition from normal brain function to epileptic seizures. Traditional theories, such as the excitation (E)-inhibition (I) imbalance hypothesis, have posited that aberrant ion channel function and synaptic activity contribute to heightened seizure susceptibility [37]. However, recent advancements in understanding encompassing genetic mutations, neurotransmitter dynamics, medication mechanisms, and metabolic influences, necessitate a nuanced re-evaluation and expansion of this hypothesis [38].

In the context of epilepsy, where an imbalance between excitatory and inhibitory activities is anticipated within regions implicated in seizure initiation, the responses to electrical stimulation hold promise for assessing the E-I imbalance [22]. As a result of SPES the delicate interplay between E and I can be investigated. This technique records

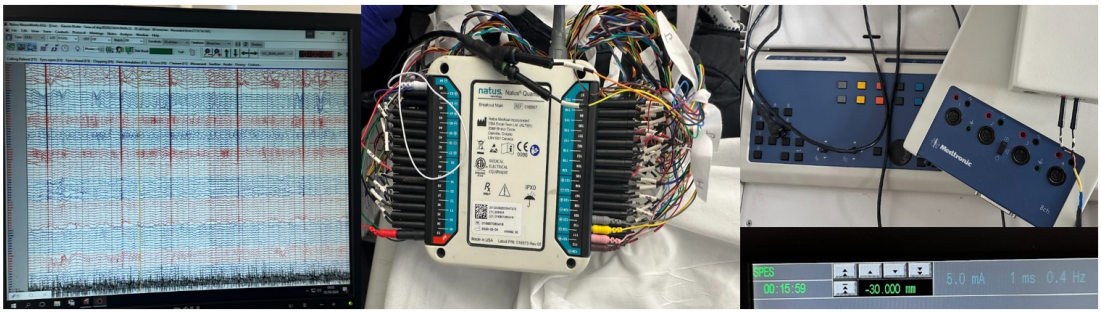

Figure 1.1: SPES setup and telemetry at King's College London Hospital.

the responses induced by applying the single electrical pulses to different cortical regions. Therefore, it is also known and referred to as cortico-cortical evoked potentials (CCEPs) [39]. By selectively activating localised populations of neurons, SPES generally elicits two distinct responses: early responses (ERs) and delayed responses (DRs) [20, 40].

The recorded responses in various brain regions typically exhibit a characteristic pattern, beginning with a negative spike or sharp wave, which frequently blends with the stimulation artefact. This initial phase is followed by a slow wave lasting for several hundred milliseconds. Termed ERs (or CCEPs) commence immediately following the stimulus (typically observed within 100ms post electrical stimulation) and are believed to reflect the brain's normal response to a stimulation. The detection of ERs at a specific site suggests the presence of functional connections with the stimulated region. Consequently, these responses serve as valuable indicators for mapping and quantifying brain functional connectivity [20, 39, 41].

Moreover, epileptogenic sites commonly demonstrate ERs followed by sharp waves or pronounced epileptiform discharges occurring between 100ms to 1s post-stimulation, known as DRs [20]. The presence of DRs typically signifies increased excitability, indicating a hyperexcitable region with potential epileptogenicity, often localised at the ictal onset zone. DRs play a crucial role in prognosticating seizure control, identifying epileptogenic areas, and pinpointing epileptogenic zones within the cortex [22].

Many researchers utilise single pulses for SPES characterised by a constant current intensity ranging from 2 to 6 mA [20, 39, 41]. These pulses typically display a biphasic waveform with a phase duration of 0.15 ms and an overall pulse span of 1 ms. They are administered at frequencies ranging from 0.2 Hz to 1 Hz. Apart from intensity, the number of pulses per second is another important parameter. Considering the presence of DRs serves as a helpful marker for identifying the seizure onset zone (SOZ), ensuring that the interval between pulses must be sufficiently long to capture these responses. As DRs may persist for as long as one second, employing a frequency of 1 Hz has the risk of misinterpreting DRs as seizures or inadvertently inducing real seizures. To balance test duration and the accurate interpretation of DRs, a frequency of 0.5 Hz could

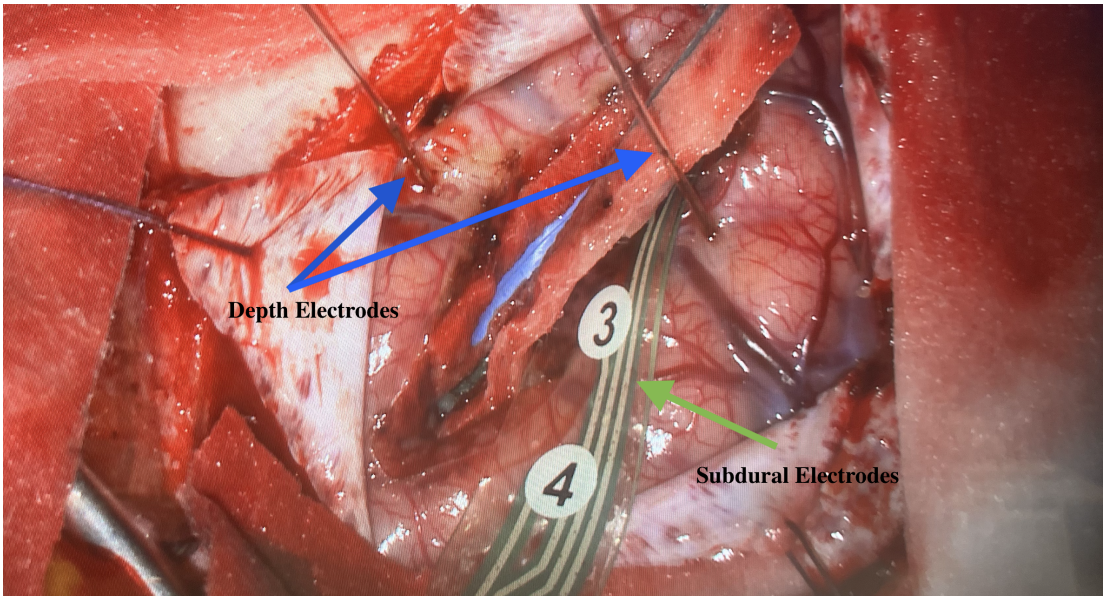

Figure 1.2: Implanting the iEEG electrodes for a DRE case at King's College London Hospital.

serve as a viable compromise [22]. Figure 1.1 shows the iEEG recordings alongside the SPES properties and equipment used for the assessment sessions at King's College London Hospital. The iEEG recordings can be obtained using two types of electrodes: subdural and depth electrodes. These two types differ significantly in their placement, structure, and the type of neural information they provide. Subdural electrodes are placed directly on the brain's surface (cortex), beneath the dura mater. These electrodes are typically arranged in grids or strips and provide extensive coverage over the cortical surface [42–44]. Depth electrodes are inserted into the brain tissue, targeting deeper brain structures. These electrodes are typically cylindrical and can monitor superficial and deep brain regions [42, 43]. Figure 1.2 shows the intracranial electrodes (depth and subdural) implantation for a DRE case.

1.3 SPES EARLY RESPONSES

Previous research has delved into the neuronal mechanisms underlying SPES responses [45]. The results suggest that SPES does not appear to alter the firing rate of approximately half of the neurons proximal to the stimulus. Among the remaining neurons, roughly 25% exhibit a brief burst of action potentials (indicative of E, typically lasting less than 100 ms), while 14% demonstrate a prolonged period of firing suppression (representing I, often lasting up to 800 ms). Additionally, 12% of neurons display a brief burst of action potentials followed by an extended period of suppression. The temporal dynamics of these action potential bursts and suppressions suggest that the initial N1 component of the ERs corresponds to E, whereas the subsequent slow wave reflects I [45].

To enhance the effectiveness of SPES for localising the SOZ, Hays et al. [46] undertook a study on the characteristics of ERs in patients undergoing intracranial recordings. Their investigation involved comparing ER characteristics across various stimulated regions and found that the first negative peak amplitude of responses was significantly higher within the SOZ compared to non-SOZ regions, regardless of whether the stimulation occurred within or outside the SOZ. This finding provided evidence of increased excitability at the SOZ. Additionally, by using progressive increments of current intensity, it was demonstrated that this approach could better estimate the SOZ than a fixed maximal stimulation intensity [46].

Furthermore, SPES and the corresponding ERs have been employed to explore brain functional connectivity in patients with epilepsy or brain tumors. The outcome of recent research has led to a paradigm shift in understanding brain function. While previous understanding considered highly localised hierarchical structures as the intermediate steps between the environmental stimuli and the responses, the current view asserts that brain functions are primarily intrinsic and involve the acquisition and integration of external stimuli to respond to environmental demands. ER analysis has proven instrumental in investigating the dynamic functional connections crucial to brain function as a dynamic system [47].

Studies focused on ERs to explore brain functionality have provided new insights into the limbic and, in general, language systems functionality [48]. Moreover, a sequential series of studies have been focused on using ERs to investigate the cortical motor network in and across hemispheres [49, 50]. ER studies face some limitations. First, as the data is recorded from epileptic brains or subjects with brain tumors, the reported ER cannot be assumed to correspond to a completely healthy brain and normal functional network. Also, the outcome of these studies are subject to the intracranial electrode implantation setup and their location. Therefore, these studies lack the information outside the coverage area. Finally, knowing that cognitive conditions can affect ER responses, it is essential to consider the influence of anesthetic agents, particularly during intraoperative ER monitoring [47].

1.4 SPES DELAYED RESPONSES

As mentioned earlier, studies focused on SPES for epileptic patients reveals two types of brain responses to electrical stimulation. Apart from ERs, DRs are also observed generally 100 ms to 1.5 seconds post-stimulation in regions believed to be epileptogenic and possibly responsible for seizure generation in the brain [20, 22]. A later study focuses on the outcome of resection surgery and investigate the relative location of the observed DRs and the resected sections in adults, emphasising the relation between the DRs and epileptogenic regions in the brain and their capability to identify these

regions, particularly when a frontal or temporal focus is suspected [40]. A sequential study targeting children shows similar results regarding the capability of DRs in SPES for identifying the epileptogenic cortex in children, demonstrating that in cases where these responses are present, the removal of the area responsible for generating them leads to improved conditions for these children after resection surgery [51].

Another study investigates the role of SPES in guiding electrode implantation under general anesthesia in the pre-surgical assessment of epileptic patients [52]. The findings of this study demonstrate that, when utilising general anesthesia, DRs can be consistently replicated without eliciting false positive epileptiform responses to SPES. However, it is noted that the sensitivity of the method is significantly diminished by the presence of spontaneous discharges [52]. These results advocate for using SPES as a supplementary technique, particularly beneficial for enhancing electrode placement accuracy during epilepsy surgery in cases where substantial interictal activity is absent.

1.5 CURRENT CHALLENGES IN SPES

Several challenges arise when applying SPES to pinpoint epileptogenic regions in the brain in its current form. Firstly, there is still ambiguity surrounding the nature of brain responses to SPES, including the underlying excitatory and inhibitory neural activities [53]. While an imbalance between E and I is expected, delving into alterations in E and I and the ratio between them can aid in pinpointing the SOZ.

Secondly, the weak and spike-like nature of brain responses to electrical stimulation (especially DRs) [20, 40] presents obstacles for conventional methods in the analysis of these waveforms. They also vary in morphology, and latency after stimulation, posing difficulties for conventional signal processing techniques to identify and analyse them effectively.

The third challenge arises from the current procedure of implanting intracranial electrodes based on presumed SOZ. Despite the higher spatial resolution of iEEG compared to scEEG, it's crucial to acknowledge that seizure-related stimulation responses can only be observed (visible in iEEG data) if the electrodes are planted close to the epileptogenic regions. Consequently, there's no assurance of precise electrode placement, potentially leading to a loss of necessary information in the recorded iEEG signals. Clinical reports from King's College London Hospital suggest instances where DRE cases underwent resection surgery multiple times (in some cases up to three times). This is due to ineffective surgery and no sign of improvement in the severity of the symptoms, highlighting the suboptimal nature of this approach in a considerable number of patients.

Finally, a noteworthy limitation of SPES sessions lies in the unique setup mandated for each patient. Ths is often tailored to their medical history and condition, while fol-

lowing the standardised clinical assessment approach for DRE cases eligible for surgery. This variability in SPES setups complicates comparison of the results across different subjects. Demonstrating the efficacy of advanced signal processing and machine learning techniques in analysing SPES responses and identifying epileptogenic regions helps developing the SPES processing pipelines. This which can lead to an improved clinical assessment and treatment plannig for the DRE patients.

1.6 AIMS AND OBJECTIVES

With the critical need to address the limitations in understanding abnormal epileptic activities in the brain, uncertainties surrounding seizure generators, and the existing challenges in SPES, this research is a timely and crucial endeavor. It aims to develop advanced signal processing and machine learning techniques that can significantly enhance the efficacy of DBS, notably SPES sessions.

Firstly, this thesis seeks a more profound insight into the nature and underlying brain responses to SPES by examining E-I imbalance from ERs and DRs in epileptogenic regions. The question that needs to be answered is: What is the alteration in the ratio of I to E during these responses? To answer this question, this thesis employs subspace analysis to extract and investigate the excitatory and inhibitory parts of SPES ERs and DRs. By means of an adaptive single-channel source separation algorithm suitable for non-stationary EEG signals, the E-I components are extracted, and the alterations in the I-to-E ratio are investigated. The adaptive source separation algorithm used in this thesis performs the E-I separation in the temporal domain without any prior assumptions about their spectral or spatial properties. Furthermore, this work aims to devise more effective methodologies for investigating these activities, enabling the identification of seizure sources with greater accuracy using recorded signals. The critical question that needs addressing is how to improve the performance of current conventional approaches. Having a more reliable method helps investigate better the source of abnormal epileptiform activities associated with seizures. This thesis introduces the concept of spatial filtering and beamforming as a well-known tool for source localisation. This thesis aims to use the concept of adaptive beamforming to improve the issues the conventional methods face when applied to identification of the source of SPES responses and other abnormal epileptic activities like IEDs. It aims to develop adaptive (regularised) beamforming algorithms tailored for identifying the source of these activities. In summary, the objectives of this thesis are to:

1. Review the state of the art research in SPES for epilepsy.
2. Develop and apply an adaptive single channel source separation to extract the excitatory and inhibitory components of the responses (ERs and DRs) to SPES.

3. Develop and apply a suitable source localisation approach to boost the performance of conventional methods in identifying the source of responses to the SPES and potentially SOZ.

4. Improve the overall adaptability and robustness of the source localisation pipeline by considering possible temporal delay mismatch and the effect of correlated sources.

5. Introduce a temporally distributed beamformer to increase the accuracy and consistency of source localisation

6. Incorporate tensor decomposition and temporal distributed approach in a hybrid localisation system to increase the consistency of results for each case.

1.7 ORGANISATION OF THE THESIS

Chapter 1 introduces the SPES method as a necessary tool for the assessment of epilepsy, especially for DRE cases, and outlines the necessity of advanced signal processing pipelines in analysing SPES results and iEEG data recorded during these sessions, considering challenges associated with SPES, leading to a delineation of aims and objectives.

Chapter 2 undertakes a comprehensive review of relevant publications on SPES that use pertinent methods for the investigation of brain functional connectivity and epileptogenicity. In this chapter, areas that can potentially be improved are pinpointed.

In Chapter 3, the concept of singular spectrum analysis (SSA) as a subspace analysis tool is introduced, followed by the development of an adaptive SSA pipeline for single channel iEEG to separate the excitatory and inhibitory components of SPES responses [54]. The chapter further explores the I-E ratio for the recorded responses to SPES in epileptogenic regions.

Chapter 4 introduces spatial filtering and the concept of beamforming, including the linearly constrained minimum variance beamformer (LCMV), as a prominent source localisation tool in various research fields, including EEG-related studies. Subsequently, a novel method, named "adaptive iterative LCMV (AI-LCMV)," [55] is introduced for localising DR sources, leveraging the morphology of DRs as an added constraint. The iterative algorithm that utilises iEEG data recorded via intracranial electrodes over the cortex is employed to optimise the beamformer weights.

The resemblance between IEDs and DRs [56] prompts inquiry into their shared brain origins in Chapter 5. An improved source localisation method, named "adaptive Bayesian beamformer with multiple constraints (ABMC)," [57] is proposed to determine sources of IEDs from interictal periods and SPES DRs associated with epileptogenic regions.

Chapter 6 aims to enhance the input SNR and exploit temporal variabilities through tensor factorisation and cooperative array processing in a temporally distributed beamformer. This endeavour seeks to strengthen source localisation pipelines by further adapting to the low-power and dynamic nature of DRs and IEDs.

Finally, in Chapter 7, the work presented in the thesis is summarised and concluded. The clinical impact of the overall work is highlighted, and possible areas for improvement in future works are mentioned.

2

LITERATURE REVIEW

The primary objective of this project is to uncover the data contained in the responses to SPES in order to pinpoint epileptogenic areas within the brain effectively. SPES stands out as a tool in epilepsy studies as it provides valuable glimpses into brain activity and possible treatment options. Through the employment of signal processing and machine learning techniques for SPES data analysis scientists can delve into neural reactions and derive vital insights, for comprehending epileptogenesis and creating specific remedies. This chapter discusses the current state of the art research on SPES data analysis, focusing on the signal processing and machine learning techniques. The aim here is to identify research gaps and areas needing improvement in this field.

2.1 BRAIN STIMULATION AND EVENT-RELATED RESPONSES

Most studies regarding brain stimulation are related to event-related potentials (ERPs) extracted from EEG signals, which are the brain responses evolving after visual, audio, or haptic stimulation and are cognitive or motor events [30]. However, here, events refer to electrical stimulations directly applied to brain tissue. In the context of SPES, ERPs can be used to study the brain's response to electrical stimulation to investigate E-I imbalance. Most SPES studies refer to the ERPs as early responses (ERs) or CCEPs and delayed responses (DRs) [20, 40]. The use of ERs and DRs allows researchers to investigate the dynamics of processing in the brain through the sequence of ER-DR components, making this technique valuable for testing theories of perception, attention, and cognition [58, 59]. The high temporal resolution of these responses makes them particularly useful for examining the precise timing of neural responses to electrical stimulation [58–60].

Common ERP analysis techniques include averaging and peak detection. Averaging multiple trials of SPES-evoked responses has been shown to significantly enhance the signal-to-noise ratio (SNR), offering a clearer insight into the underlying responses to SPES [58, 60].

One significant issue is the averaging procedure employed for ER analysis (considering that ERs are more consistent in appearance). Although averaging over several segments of data can lead to increased SNR, which is helpful for time-frequency analysis, it causes a loss of information related to the variability in time. Moreover, they need a timing cue to keep tracking the stimulation instants. Therefore, research has been diverted to tracking and monitoring the ERPs over single EEG trials [4]. Previously, a

large number of studies have used methods like particle filtering and Kalman filtering for single-trial EEG signal processing for ERP detection [61–63].

Particle filtering, a nonlinear and non-Gaussian filtering method, has been very useful for single-trial EEG signal processing. It is notably useful when dealing with complex, nonlinear models, as often encountered in EEG applications. One of its key applications is tracking the time-varying states of neural activity, a task that is inherently nonlinear and can benefit from the flexibility of particle filtering [61]. Another important application is decoding brain states from EEG signals, where the non-Gaussian nature of the brain dynamics can be effectively handled by this method [61, 63]. Particle filtering works by representing the posterior distribution of the state variables using a set of weighted particles, which are then propagated over time to model the system dynamics. This approach allows for the estimation of nonlinear and non-Gaussian processes that are common in EEG data, making it a powerful tool for tasks like real-time neural state estimation, and detecting transient events in EEG signals [61, 63].

Kalman filtering is another useful method previously used for EEG signal processing. Kalman filtering is a recursive linear filtering technique that estimates the state of a dynamic system from noisy observations, making it suitable for EEG signal processing where real-time tracking of brain activity is required [64]. It assumes that both the system and observation models are linear and that the estimated state and output noises are Guassian. Kalman filtering is widely used in EEG applications for smoothing and noise reduction, artefact removal, and real-time tracking of brain states [64, 65]. The filter works by predicting the next state of the system based on the previous state and updating this prediction using the new observations, leading to an optimal estimate of the current state. This method is computationally efficient and can be implemented in real-time systems, making it ideal for applications such as online ERP tracking.

A recent study introduced a novel method to investigate brain P300 (spike in EEG activity approximately 300ms following target stimulus presentation) variability across different trials. The method utilises spatial correlation between EEG channels through a nonlinear coupled particle filtering approach, which tracks these subcomponents in the temporal domain [63]. The algorithm incorporates physiological constraints and inter-channel information sharing to enhance accuracy and robustness, outperforming non-cooperative methods in single-trial estimation of P300 components.

While particle and Kalman filtering generally estimate dynamic systems' states from noisy data, they each bring unique features to the table. Kalman filtering offers computational efficiency, making it a preferred choice for real-time EEG applications. In contrast, particle filtering's ability to handle nonlinear, non-Gaussian models makes it useful for complex EEG signal processing tasks. These tasks usually involve highly nonlinear brain functions, where the rigid assumptions of Kalman filtering are not correct [66]. For example, in a previous study, a method based on WT and particle filtering was employed to estimate single-trial ERPs. Simulation results and results from real data

indicated the better performance of particle filtering over Kalman filtering for EEG signals [61].

The studies related to SPES show that the majority of them primarily focus on the ERs or CCEPs, as DRs lack consistency when using the same SPES setup and are not present across all regions. The averaging enables an overall comparison of SPES response characteristics across different brain regions, shedding light on disparities between normal and epileptogenic areas. However, as stated above the averaging process is not without its flaws.

2.2 SPES RESPONSE ANALYSIS

In the context of epilepsy research, ERs and DRs can provide insights into the functional connectivity of the brain and help identify abnormal neural activity associated with epileptogenic zones [60]. Brain functional connectivity refers to the temporal relation between spatially remote brain regions that share functional properties [67]. It is a measure of how different areas of the brain communicate or coordinate with each other during specific tasks or at rest [67, 68]. The temporal relationship is crucial because it helps reveal how different parts of the brain communicate and coordinate to perform cognitive functions, process sensory information, or maintain baseline activity. Functional connectivity is typically assessed using neuroimaging techniques together with estimation of casuality between the activities in different brain regions. These methods help identify networks of brain regions that work together to support cognitive functions, behaviour, and sensory processing [69]. In neuroimaging studies, the temporal dynamics of functional connectivity are often analysed using techniques like cross-correlation or coherence analysis to estimate the casuality. These methods assess how consistent the activity patterns are between regions over time. For example, if one brain region's activity consistently precedes or follows another area, this might indicate a directional or causal connection, leading to further investigation into the underlying neural mechanisms [70].

Wavelet transform-based time-frequency analysis is a technique used to examine how the frequency content of a signal evolves over time [71]. The key advantage of wavelet analysis is its ability to present the signals in the time-frequency domain in various scales. At lower frequencies, wavelets use wider time windows to capture slow oscillations accurately. For higher frequencies, narrower windows pinpoint rapid signal changes [71]. This adaptive approach enables wavelets to achieve an optimal balance between time and frequency resolution across different scales. In practice, the continuous wavelet transform (CWT) is commonly used for time-frequency analysis of non-stationary signals [72]. The CWT convolves the signal with wavelet functions at various scales and positions. This process generates a time-frequency representation

called a scalogram, which displays how the signal power is distributed across both time and frequency [72]. Unlike traditional Fourier analysis, which provides frequency information but does not capture temporal variations well, wavelet transform-based analysis allows for both time and frequency localisation [73].

Applying wavelet transform (WT)-based time-frequency analysis to SPES data elucidate evoked responses spanning the spectrum of spikes, ripples, and fast ripples (FRs). This investigation underscores the utility of time-frequency analysis in delineating the epileptogenic cortex, with particular emphasis on time-frequency single pulse-evoked fast ripples as a potential biomarker for epilepsy. The results of these studies provide valuable insights into the use of time-frequency analysis in epilepsy research and clinical practice. In a study by Van't Klooster et al. [74], ECoG data are gathered at a sampling rate of 2048 Hz from 13 patients. The experimental protocol involves SPES, consisting of 10 stimuli administered at one millisecond duration and 8 mA intensity, with a frequency of 0.2 Hz. Using pairs of adjacent electrodes the brain is stimulated. Morlet wavelet is used for transformation which is conducted within a time window of -1 second to 1 second around the stimulus instant, spanning a frequency range of 10–520 Hz. Morlet wavelets are complex wavelets that oscillate at a specific frequency and are localised in time. They are well-suited for capturing both low and high-frequency signal components of signals. Significant changes in power spectra, determined at a significance level of P = 0.05, were computed based on the averaging of 10 epochs, yielding event-related spectral perturbation images. These images facilitate the examination of single pulse-evoked responses across different frequency bands, specifically targeting spikes (10–80 Hz), ripples (80–250 Hz), and FRs (250–520 Hz). The sensitivity, specificity, and predictive value of time-frequency single pulse-evoked responses within these frequency ranges were compared against the SOZ and post-surgical outcomes, revealing intriguing patterns. For all patients, the evoked responses consistently include spikes, ripples, and FRs. Notably, within the SOZ, the median sensitivity of time-frequency single pulse-evoked responses decreased from 100% for spikes to 67% for FRs, while median specificity increases from 17% for spikes to 79% for FRs. The median positive predictive value for evoked responses within the SOZ is 17% for spikes, 26% for ripples, and 37% for FRs, suggesting potential implications for the assessment and treatment of epilepsy considering the significant alteration obsereved in SOZ.

A later study by Mouthaan et al. [75] investigates SPES as a tool to explore the epileptogenic cortex in iEEG recordings. It distinguishes pathological DRs linked to the SOZ and physiological ERs, reflecting cortical connectivity. Data from twelve refractory epilepsy patients were analysed, revealing that ERs, particularly those with frequencies higher than 80 Hz, are more prevalent in SOZ and seizure propagation areas. This association suggests that ER analysis can offer insights into epileptogenic pathology, as ERs are strongly linked to SOZ and coincide with areas of seizure propagation.

Power spectrum analysis of post-stimulation segments has shown alterations in higher frequency bands. As a result, high-frequency oscillations (HFOs) have become another widely used keyword in SPES and CCEP-related research for epileptic patients. SPES has been found to induce HFOs, including namely ripples and FRs. In a study by Van 't Klooster et al. [76], for ten patients with focal epilepsy, SPES was administered during ECoG at a sampling rate of 2048 Hz. Both evoked and spontaneous HFOs were visually analysed using time-frequency plots, comparing the occurrence of HFOs in electrodes located in the SOZ and outside the SOZ. The results illustrated that SPES successfully evoked HFOs, including ripples (80-250 Hz) and fast ripples (250-500 Hz). In comparison with spontaneous HFOs, two patients without spontaneous FRs exhibited evoked FRs in the SOZ. The percentages of electrodes with evoked and spontaneous HFOs in the SOZ were similar (ripples: 32% vs. 33%, FRs: 43% vs. 48%). Evoked HFOs demonstrate lower specificity but higher sensitivity for identifying the SOZ than spontaneous HFOs. Additionally, more electrodes with evoked ripples are found in areas outside the SOZ than spontaneous ripples. In [76], the multitaper method is used for spectral estimation. This method [77] is commonly employed in signal processing and data analysis where precise frequency information is required. The multitaper method improves spectral estimation by using multiple orthogonal tapers or windows instead of only one. Traditional spectral estimation techniques like the Fourier transform [78] apply a single window function to the entire signal. This can lead to spectral leakage, where the energy from one frequency leaks into the neighbouring frequency bands, causing a reduction in frequency resolution. In the multitaper method, multiple orthogonal window functions are employed instead of applying a single window function. These tapers are designed to be uncorrelated, which helps reduce the spectral estimate's variance. The signal is multiplied by each taper, and the Fourier transform is computed for each tapered signal segment. This results in multiple spectral estimates. The spectral estimates obtained from each taper are combined using appropriate weighting schemes. The weights are typically chosen to minimise bias or variance, depending on the specific requirements of the analysis.

One area worth focusing on is the application of single channel source separation or decomposition methods to investigate the SPES ERs and DRs, considering their unique nature and the expected imbalance between E and I as an underlying mechanism for epilepsy. Previously, various signal processing methods like SSA, Independent Component Analysis (ICA), Empirical Mode Decomposition (EMD), and Wavelet Transform (WT) [4, 79–81].

As an example, in a study by Corsini et al., [82] a new technique to quantify the dynamic changes of the brain using the scalp EEG was developed in which the scalp EEG is preprocessed using an effective block-based blind source separation technique to separate the underlying sources within the brain. The algorithm significantly excludes the effect of eye-blink artefacts.

2.3 SPES AND BRAIN CONNECTIVITY

Looking at the previously published research papers related to the SPES sessions and ERs or CCEPs, it is clear that the majority focus on using the brain responses to electrical stimulation to investigate the brain's functional and effective connectivity. In recent years, independent groups at the Cleveland Clinic [39, 83], University of Iowa [84], and King's College London [20] developed their methodologies using SPES to investigate functional connectivity and cortical excitability. Since then, SPES has been utilised in epilepsy surgery to examine the functional and seizure networks as well as the epileptogenicity. Since ERs to SPES show the brain's normal reaction to the stimulation, they can be used to study the functional relation between various brain regions in the epileptic brain. Although there might be differences in non-epileptic regions of the epileptic brain compared to a completely normal brain for these patients, the iEEG recordings from SPES sessions create an opportunity to study brain connectivity and investigate the differences in epileptogenic regions. Here, we summarise the overall research related to SPES for brain connectivity while focusing on the engineering side of this concept.

The earliest efforts to investigate connections using SPES in the human brain can be traced back to the early 1990s. Goldring et al. applied SPES to the sensorimotor cortices to record direct cortical responses nearby initially explored in animals [85, 86]. These preliminary attempts to map cortical responses aim to delineate the wave morphology of the N1 counterpart of CCEP specific to the primary motor, primary sensory, or premotor cortex. Wilson et al. pioneered SPES to examine adjacent and remote cortical responses [87, 88]. They utilised depth electrodes to apply SPES to mesial temporal structures and recorded cortical evoked responses in the ipsilateral and contralateral mesial temporal areas.

Functional connectivity refers to the statistical or temporal relations between the activities of different brain regions [89, 90]. In ER (CCEP) related studies, the functional connectivity is inferred from evoked potentials between cortical areas, indicating that they are functionally connected [90]. One the other hand, effective connectivity refers to the causal influence that one neural system exerts over another [89–91]. SPES and ER mapping can probe effective connectivity by directly perturbing a cortical region with electrical stimulation and measuring the evoked responses in other areas [90, 91]. The amplitude, latency, and propagation patterns of the ERs provide information about the direction and strength of functional connections between various regions, which might also help investigate seizure networks [90, 92].

Early studies investigate the functional connectivity between the stimulated regions using SPES to other regions of interest (ROI) simply by checking if any of the responses is visible in ROI [39, 41]. In addition, later studies have tried to examine the effective connectivity between various regions in the brain using the responses to SPES as it can

help better identify the directionality and nature of these connections. As an example, in the work performed by Krieg et al., [93] the effective connectivity based on the electrophysiological feature (for example, amplitude) of ERs is evaluated and subjected to node strength and betweenness centrality as graph metrics. These metrics are directly linked to how one node (small active region) influences the functionality of the overall network. This influence on the information transfer may depend on factors such as the strength of connections or the extent to which a node enhances the overall accessibility of other nodes within the network. The total of its weights determines node strength. Additionally, betweenness centrality refers to the proportion of all the shortest paths in the network that traverse a specific node. The shortest path between two nodes is the series of edges with the lowest sum of weights between the nodes. Nodes that bridge disconnected network segments tend to have higher betweenness centrality, which shows how important a node is to the flow of information through a network [94].

In another work by Prime, et al. [95], synthetic cortical responses are superimposed onto stereo EEG (sEEG) data to evaluate various metrics' ability to detect the simulated patterns. This study aims to compare the efficacy of different measures in analysing effective connectivity using SPES.

The assessment metrics include root mean square (RMS), which calculates the square root of the average of the squares of the values, providing a measure of the magnitude of the signals [96]. Standard deviation, a statistical measure, quantifies the variation or dispersion of a set of values, indicating how spread out the values are from the mean. Dynamic time warping is an algorithm for measuring similarity between two temporal sequences that may vary in speed, aligning the sequences in a way that minimises the distance between them [97]. Edit distance with real penalty determines the dissimilarity between two sequences by counting the minimum number of operations required to change one sequence into another, with penalties for real-valued differences.

Time warped edit distance is a variation of the edit distance that incorporates time elasticity, allowing for the comparison of time series data by considering both temporal and value differences [98]. Minimum jump cost measures the similarity between sequences by accounting for the minimal cost required to match segments of the sequences, considering both temporal shifts and amplitude changes [95]. The autoregressive model represents a time series using its previous values, providing a way to describe and predict temporal dependencies in the data [99]. Finally, Fourier coefficients are derived from the Fourier transform, which decomposes a signal into its constituent frequencies, offering a way to analyse the frequency components of the time series data [100]. These measures are compared to determine their capability for effective connectivity analysis using sEEG data and SPES. The results show different benefits and disadvantages for each measure to some degree. Before this work, only a few measures were applied to evaluate CCEP responses using sEEG. The most common approach

involves employing RMS or quadratic mean, which primarily addresses low-frequency trends [101].

Despite the valuable insights provided by SPES and ERs in studying the functional and effective connectivity of ROI in the brain, there are still areas that require refinement. For instance, a more detailed analysis of the connectivity of each ROI could provide a better understanding, accommodating the variability in structural epileptogenicity among patients, the variances in physiological connectivity, and the asymmetry of bidirectional effective connections. However, this level of detail would necessitate a more comprehensive sampling of each structure. Notably, while capable of investigating the relationship between different regions, the current measures are insufficient to account for spurious connections. This underscores the need for more advanced connectivity measures, especially for effective connectivity. Investigating brain effective connectivity using ERs can also help to provide valuable insights into the optimal placement of responsive neurostimulation electrodes for treating drug-resistant focal epilepsy. As an example, a recent study has shown that the functional connectivity investigated by the correlation between ERs offers valuable information for guiding the placement of responsive neurostimulation electrodes, potentially improving treatment efficacy [102].

2.4 SPES FOR SOZ LOCALISATION

Another area of focus for studies related to SPES and brain responses to stimulation is the SOZ localisation to aid surgical planning for DRE cases. Considering that ictal periods are not always present for a large number of DRE cases, localising the SOZ can be time-consuming and tedious, involving visual inspection of iEEG recordings captured during passive patient monitoring by trained clinical staff. One particular approach used to check if the responses to SPES can help identify the SOZ in recent studies is transfer function models. A recent study by Kamali et al. [103] involves constructing patient-specific transfer function models from SPES-evoked responses and iEEG recordings of 22 epilepsy patients. The authors analyse the system's frequency and connectivity-dependent peak gain using systems theory metrics. The results revealed that in cases where clinicians confidently localised the SOZ, the highest peak gains occurred when stimulating the clinically annotated SOZ and close regions.

Transfer function models are mathematical representations used to explain the relation between input and output signals in a system [104]. In the context of SPES, transfer function models are constructed to capture the relationship between the electrical stimulation and the resulting neural responses recorded through iEEG monitoring. These models quantify how the brain responds to SPES across different frequencies and connectivity patterns. By analysing the transfer function models, researchers can gain in-

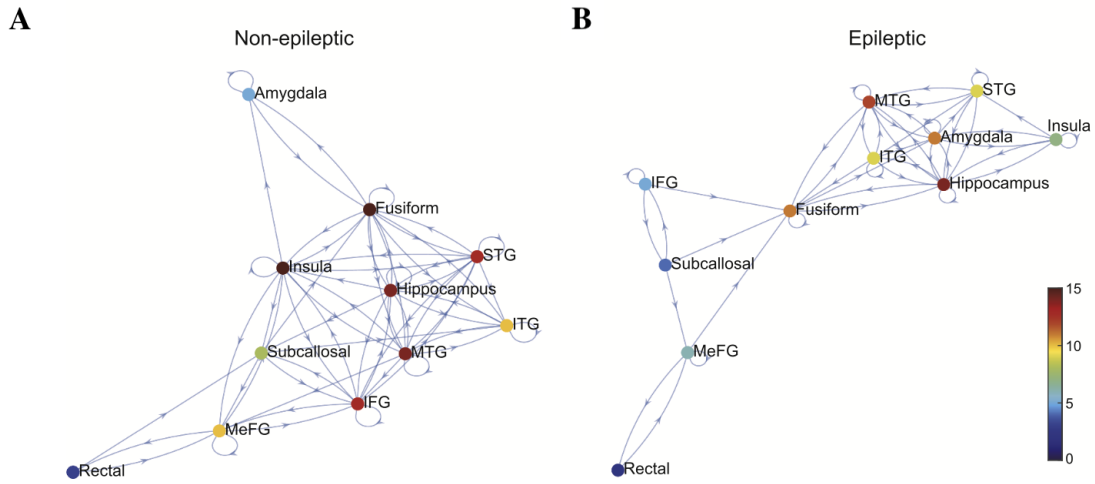

Figure 2.1: Epileptic and non-epileptic brain network analysis results from [106]. (A, B) Graph representation using degree measurements of the non-epileptic (A) and epileptic networks (B) in the temporal epilepsy patient group. SFG: superior frontal gyrus; MiFG: middle frontal gyrus; IFG: inferior frontal gyrus; MeFG: medial frontal gyrus; Rectal: Gyrus rectus; SPL: superior parietal lobe; IPL: inferior parietal lobe; STG: superior temporal gyrus; MTG: middle temporal gyrus; ITG: inferior temporal gyrus; TTG: temporal pole; SOG: superior occipital gyrus; MOG: middle occipital gyrus; ACC: anterior cingulate cortex; MCC: middle cingulate cortex; PCC: posterior cingulate cortex [106].

sights into the brain's response to electrical stimulation dynamics. In a previous study, parameters such as peak gain and floor gain were examined to understand how the brain's response varies depending on the location and complexity of the SOZ. The transfer function models provide a mathematical framework for understanding and predicting the behaviour of complex systems [105] like the brain in response to external stimuli, which can be valuable for various applications, including medical diagnosis and treatment planning.

Apart from transfer function models, other machine learning methods have recently been used to identify the SOZ. A study by Dou et al. aimed to enhance the localisation of epileptic brain zones employing iEEG data, mainly focusing on ERs alongside traditional oscillatory patterns and functional connectivity analysis [106]. The method involves developing a two-stream model utilising unsupervised learning and graph convolutional networks tailored for analysis of SPES datasets. A comparison with clinically marked electrode sites exhibited promising classification capabilities. Additionally, group-level analysis in this study revealed distinct epileptic and non-epileptic brain networks across different types of focal epilepsy. Figure 2.1 shows the results of epileptic and non-epileptic brain networks analysis presented in [106].

Another recent study aimed to develop a novel method for identifying the SOZ using ERs and compare the connectivity patterns from the patients with different clinical phenotypes [107]. Patients were analysed using logistic regression with six metrics as features. Results showed high accuracy in localising the SOZ. Additionally, differences

in ER metrics between clinical phenotypes were observed, with higher N1 RMS values in the hippocampus sclerosis group compared to the focal cortical dysplasia group. The sensitivity of localisation varied between seizure-free and non-seizure-free groups. The study suggests the potential of this machine learning approach for predicting SOZ localisation across different focal epilepsy phenotypes and highlights the impact of clinical phenotypes on epileptogenic network anomalies.

Deep learning methods have received substantial attention in various fields due to their capability to extract highly complex patterns and robust classification performance. Deep learning refers to a subgroup of machine learning methods that involves training artificial neural networks with multiple layers to automatically discover patterns and representations from large quantities of data [108, 109]. Unlike conventional machine learning, which often mandates manual feature extraction, deep learning models can discover complex patterns directly from raw input, which makes them extremely effective for pattern recognition tasks [108, 109].

Recent advancements in deep learning have also been applied to SPES responses to identify the SOZ for DRE cases. In a study by Johnson et al. [110], researchers explored machine learning methods to aid in localizing the SOZ. To identify SOZ, they train a multichannel convolutional neural network using CCEPs recorded via sEEG. The study involves SPES conducted on ten patients, utilising 500,000 unique post-stimulation sEEG segments to train the model to detect whether a SOZ is stimulated. Using a leave-one-patient-out testing approach, the model achieved a mean sensitivity of 78.1% and a specificity of 74.6%, with the best classification accuracy occurring within a 0 to 350-millisecond post-stimulation window. Further analysis indicated the model's capability to accurately differentiate between distinct SOZs, marking the first successful application of a deep learning framework to classify SOZs using SPES responses. The findings suggest that precise SOZ classification hinges on the complex temporal dynamics of evoked responses within the initial 350 milliseconds after stimulation.

In another research the authors try to address the problem of having an accurate SOZ localisation method. The researchers applied an existing deep learning model to compare two SPES analysis paradigms: divergent, which assesses outward effective connections, and convergent, which evaluates inward effective connections. In this study, the models' generalisability to the new patients and varying electrode placements using held-out test sets have been tested [111]. The results show considerable improvement when switching from the divergent to convergent approach. This research highlights the effectiveness of convolutional transformers with cross-channel attention in managing heterogeneous electrode placements, further enhancing the performance.

After reviewing the previous studies on the SPES for DRE cases, it becomes clear that multiple areas lack comprehensive investigation and need more thorough and effective processing pipelines for analysis. The first topic is the concept of array processing and beamforming, which has been used for a large number of EEG/ magnetoencephalog-

raphy (MEG) related studies for source localisation [112]. Array processing refers to techniques for processing the signals recorded by an array of sensors. These techniques use the spatial information provided by available sensors to improve signal quality and extract meaningful information related to underlying neural sources [4, 81, 113]. In EEG-related studies, array processing involves exploiting the combined signals from multiple electrodes to improve the SNR and spatially resolve the locations of neural activity [4]. The electrode array's spatial information can be used to distinguish signals stemming from different regions in the brain. Beamforming is a spatial filtering technique employed in array processing that is particularly useful for EEG source localisation [114, 115]. It involves steering a beam or focus towards a particular region of interest such as that of abnormal generators in the brain, which leads to enhancing signals from that region. In contrast, the signals from other regions are suppressed.

2.5 CONCLUSION

To alleviate the shortcomings of the previous methods in SPES analysis and identification of the brain responses, there are several areas for research. The first area is identifying the relation between excitatory and inhibitory components of epileptogenic regions using the response to SPES. Considering the critical role of E-I imbalance in epilepsy and seizures, it is necessary to investigate the E-I imbalance and pinpoint the alterations in these regions. It would also be useful to compare the results of depth electrodes from deeper regions to the ones acquired by subdural channels. The investigation of excitatory and inhibitory activities would be helpful in better investigating the brain functional network and monitoring the role of E-I imbalance in the propagation of information between various regions.

The second critical area is employing the responses to SPES for SOZ localisation. A specific approach neglected in previous studies is the concept of spatial filtering and beamforming as a powerful source localisation tool. Beamforming has already proved helpful in EEG and MEG studies as a valuable source localisation tool. Considering the main aim of SPES, which is the identification of abnormal regions, including SOZ for DRE cases and its significant role in patients' diagnostic and assessment period, the thesis also focuses on the benefits of using the iEEG data recorded from the SPES sessions, along with tailored adaptive beamforming methods for identifying the SOZ in the brain.

Signal processing and machine learning methods offer valuable tools for analysing SPES data, especially for DRE cases. By benefiting from these approaches, the researchers can gain deeper insights into the mechanisms underlying epileptogenesis, identify biomarkers for seizure prediction and intervention, and develop targeted treatments for DRE cases. Considering the limitations of the previous studies, this thesis

aims to develop advanced signal processing and machine learning pipelines to investigate some gray areas related to SPES research better and improve the processing algorithms to reach more robust results specifically for DRs, given that, the majority of previous studies focus on ERs. In the following chapters, the aim is to address the ambiguities regarding the E-I imbalance expected in epileptogenic regions associated with DRs using an adaptive subspace single-channel decomposition algorithm. Then, Chapters 4, 5 and 6 focus on developing advanced source localisation pipelines using beamformers as the primary foundation for identifying the source of DRs to SPES, investigating the relation between the source of IEDs and DRs, and ultimately moving towards having an accurate and robust SOZ localisation algorithm for clinical practice.

3

INVESTIGATION OF EXCITATION-INHIBITION IMBALANCE IN EPILEPTIC BRAIN

This chapter aims to investigate the imbalance between E and I in epileptogenic regions of the brain using brain responses to SPES (ERs and DRs). To accurately recognise neuronal excitability in an epileptic brain for modeling or localisation of the epileptic zone, the brain's response to SPES has been decomposed into its components using an adaptive SSA algorithm. Given the neuronal response, these components are expected to be inhibitory and excitatory activities. The primary objective is to thoroughly examine the nature of ERs and DRs. SSA is a useful subspace signal analysis method for separating single-channel iEEG signals into their basic uncorrelated components. The results for both ERs and DRs verify the usability of this approach. Here, the single-channel decomposition approach depends on the fact that the underlying signal components (i.e., E and I) originate from distinct sources within the brain, allowing separability. Following an introduction to the SSA method and the available data, the adaptive SSA algorithm performed on single-channel iEEG signals recorded from SPES sessions is introduced, and the results are reported.

3.1 SINGULAR SPECTRUM ANALYSIS

SSA is a method for analyzing time series data that stands out for its adaptability and ease of use. It excels at breaking down time series information into understandable elements like trends, cyclical patterns and background noise. Originally designed for dynamical systems research SSA has been applied extensively in various fields.

SSA is based on the principles of multivariate statistics and dynamical systems theory. Its objective is to convert a time series into a trajectory matrix by performing eigenvalue decomposition (EVD), and finally reconstruct the original series from a subset of the obtained singular values and vectors. SSA can reconstruct the time series while effectively isolating distinct orthogonal components within it [116]. SSA has found a range of applications across various fields. Some notable uses include:

1. Climate Science: SSA can extract seasonal and long-term trends from temperature and precipitation data, helping in climate modeling and prediction [117]. SSA can also decompose temperature time series into sub-components, which represent annual cycles, multi-decadal trends, and short-term variations, providing insights into climatic changes.

2. Economics and Finance: In financial time series analysis, SSA helps identify and forecast economic cycles, market trends, and volatility patterns [118]. It can decompose stock prices into trends, cyclical components, and noise, facilitating better predicting market behaviours.

3. Engineering: SSA is used in the analysis of physiological signals, such as electrocardiograms (ECG), to detect abnormalities and underlying rhythms. It can separate the ECG signal into components representing the main heartbeat pattern and noise, which enhances the detection of arrhythmias and other cardiac issues [119, 120]. SSA is also used for vibration analysis and fault detection in mechanical and structural engineering [121]. For example, it can decompose the vibration signal of a machine into different frequency components, helping to identify and diagnose faults in machinery.

4. Environmental Science: SSA is used in hydrology and environmental monitoring to analyse water quality data, river flow rates, and other environmental time series [122, 123]. It helps identify trends, seasonal cycles, and anomalies in the data critical for environmental management and planning.

One main advantage of SSA over other subspace analysis methods is its model-free nature. SSA does not require prior assumptions about the data's underlying structure for analysis. This flexibility allows SSA to adapt to different types of time series data, including EEG. Subject to right choice of its parameters, SSA's ability to handle non-stationary data makes it suitable for applications where the data characteristics change over time. It effectively isolates trends and oscillatory components from noise in the data [119]. SSA provides an explicit decomposition of the time series into interpretable components, which can be individually analysed and reconstructed. This facilitates the understanding of complex time series data.

While SSA offers numerous benefits, its use requires careful consideration. The choice of window length (a.k.a embedding dimensions) significantly impacts the results, and there is no universal criterion for selecting the optimal length. However, each windowed time series segment must be stationary and cover at least the longest cycle of the series (i.e. the main harmonic) [4]. The method's computational complexity increases with the length of the time series, making it less efficient for extensive datasets. Applying EVD to large trajectory matrices can be computationally intensive. Grouping the elementary matrices into meaningful components can be subjective and may mandate domain knowledge. Incorrect grouping can lead to misinterpretation of the results.

Apart from using EVD for SSA, ICA can be applied to the covariance of the trajectory matrix. ICA is a statistical method that represents a group of random variables as linear mixtures of statistically independent components. While initially used for multi-channel source separation, it can be used instead of EVD for single channel decompo-

sition considering the independency of the underlying source [4, 124]. These adaptations typically generate multiple copies of the signal (e.g., delayed versions) to create a pseudo-multichannel scenario [124]. ICA is widely used in audio signals, EEG/MEG, and image processing. Its strength is in separating mixed signals into independent sources based on the assumption of statistical independence [124]. One limitation of ICA is its assumption that the observed signal is a linear combination of the sources, which is not always correct particularly for audio signals where the mixtures are convolutive. Also, its performance can degrade significantly in the presence of noise.

Another method for source separation is EMD. EMD is a non-parametric data decomposition technique that has gained considerable attention in various fields, including signal processing and time series analysis. This method, developed in the late 1990s [125], offers an approach for decomposing complex signals into a limited group of components called intrinsic mode functions (IMFs). Unlike decomposition methods like Fourier transform or wavelet analysis, EMD is not based on any predefined basis functions. EMD operates directly on the local characteristics of the signal, making it useful for analysing nonlinear and non-stationary data like EEG. The process iteratively extracts IMFs from the original signal. It starts with the highest-frequency oscillations and progresses to lower-frequency components until a residual trend remains. This data-driven approach allows EMD to uncover inherent patterns within the original data, providing valuable information that might otherwise remain hidden when using conventional processing methods like Fourier transform [126]. A common problem in EMD is where different modes are mixed in a single IMF, leading to ambiguous interpretations. EMD can also be sensitive to the endpoints of the signal, which can affect the decomposition results. At the start and end of a signal, fewer data points are available to estimate the local extrema and measure the envelopes accurately. This lack of data leads to less reliable IMFs near the edges, which can cause distortions. The inaccuracies at the edges can cause different components to get mixed in a single IMF, which complicates the understanding of the results. Techniques like mirroring (reflecting the signal at the boundaries), zero-padding (extending the signal with zeros) or even new correlation based methods to identify the signal pattern are usually employed to mitigate edge effects problem [127]. However, these techniques can introduce artificial artefacts or change the chracteristics of the original signal near the edges.

Another alternative approach is WT. WT is a time-frequency analysis method that decomposes the original signal into different frequency components [128]. WT has been broadly used in signal processing, considering its capability to capture temporal and spectral information. WT has been utilised in image compression, denoising, and biomedical signal processing applications. It is particularly effective in scenarios where signal characteristics vary across time, such as transient signal identification [128]. In WT, selecting an appropriate wavelet function can significantly impact the performance [128]. Like EMD, WT can suffer from edge effects. Like with EMD, techniques such as

padding or periodic extension (where the signal is assumed to repeat beyond its boundaries) are used to reduce the edge effects. However, these can introduce artefacts not present in the original signal. The type of wavelet used can also influence the severity of edge effects. Some wavelets are more localised in time and less prone to edge effects, but the trade-off is often reduced frequency resolution.

SSA, EMD, and WT are well-suited for handling nonlinear and non-stationary signals, making them preferable in scenarios where these characteristics are prominent. However, ICA, on the other hand, assumes linearity of the mixing system, which may limit its applicability in such cases. Also, unlike the EMD approach, SSA decomposes the data (here, recorded iEEG signals using the implanted electrodes) into its orthogonal components. Therefore, SSA is a better option when there is no clear information on which domain or how the underlying components are disjoint. The advantages of SSA method over the other mentioned methods make it suitable for the aim of this chapter.

3.2 DATA DESCRIPTION

The iEEG data was meticulously collected at a sampling rate of 1024 Hz from a cohort of 20 individuals with epilepsy treated at King's College London Hospital. This data acquisition is a crucial component of the clinical assessment process, tailored to each patient's specific condition and medical history. The selection of electrode type, number, and placement is specifically guided by the suspected SOZ, determined through a comprehensive non-invasive assessment process. This evaluation includes various modalities such as clinical history, scalp EEG recordings, anatomical MRI and X-ray images, neuropsychological evaluations, and neuroimaging techniques. Detailed criteria for electrode selection and implantation procedures have been previously outlined, particularly catering to participants suffering from DRE [52].

For the implantation procedure, multi-contact flexible bundles of depth electrodes [129] are precisely positioned stereotactically under the guidance of MRI imaging [130]. These electrodes with platinum contacts, each measuring 2.3 mm in length, are strategically spaced at intervals of 0.5 cm between the centers of adjacent electrodes within the same bundle. Additionally, subdural electrode strips and/or grids from the same manufacturer are utilised. Each strip features a series of platinum disc electrodes, with a spacing of 1 cm between the centers of adjacent electrodes within the same strip. These discs are securely embedded in a 0.7 mm thick polyurethane strip, extended beyond the edges to expose a diameter of 2.3 mm while maintaining a recess of approximately 0.1 mm from the surface plane. Figure 3.2 provides a representative illustration of a post-surgery computed tomography (CT) scan, showcasing the placement of both subdural and depth electrodes in a subject. Grids, on the other hand, are configured

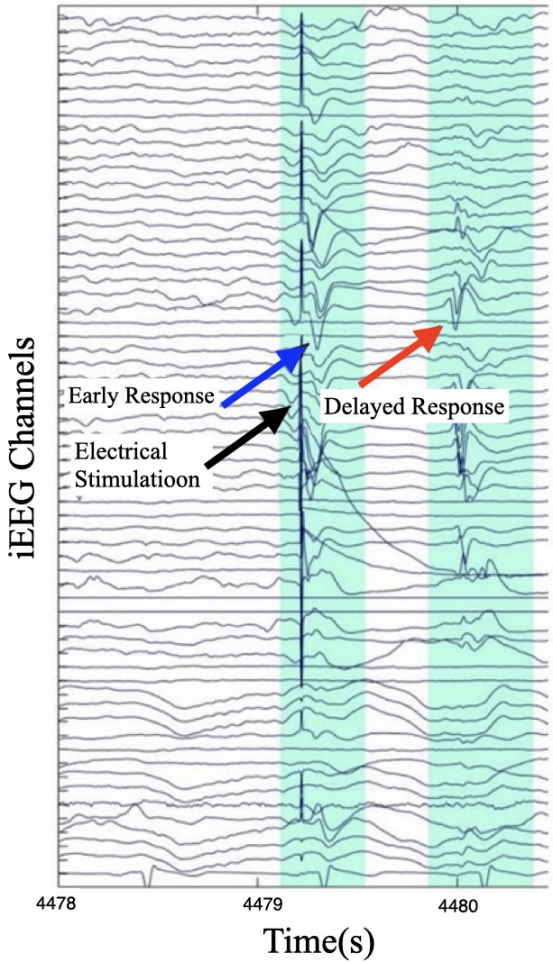

Figure 3.1: The ERs and DRs to the SPES visible in both subdural and depth channels after SPES. The first 32 EEG channels are subdural, and the rest are depth electrodes. The last channel is the ECG signal recorded from the subject.

with similar platinum electrode arrangements, forming rectangular arrays. This meticulous selection and placement of electrodes tries to provide comprehensive coverage of the suspected epileptogenic regions, facilitating accurate monitoring and intervention strategies.

The recording methodology adhered closely to the system and techniques delineated by Kokkinos et al. [52], ensuring consistency across the dataset derived from 20 patients. During the SPES operation, a constant current, typically ranging from 1 to 8 mA and primarily set at five mA, is administered through the neurostimulator. This stimulation involves brief pulses lasting 1 ms at a frequency of 0.4 Hz, with a single monostatic pulse applied every five seconds. Importantly, EEG signals obtained from the electrodes are not utilised for stimulation purposes, maintaining fidelity to the recording process.

Subsequent to data acquisition, 11 out of the 20 cases underwent surgical intervention, the outcomes of which are delineated using the Engel Outcome Scale (EOS) [131]. The EOS is a system used to categorise the outcomes of epilepsy surgery, specifically regarding seizure control. It provides a standardised way to describe how well a patient

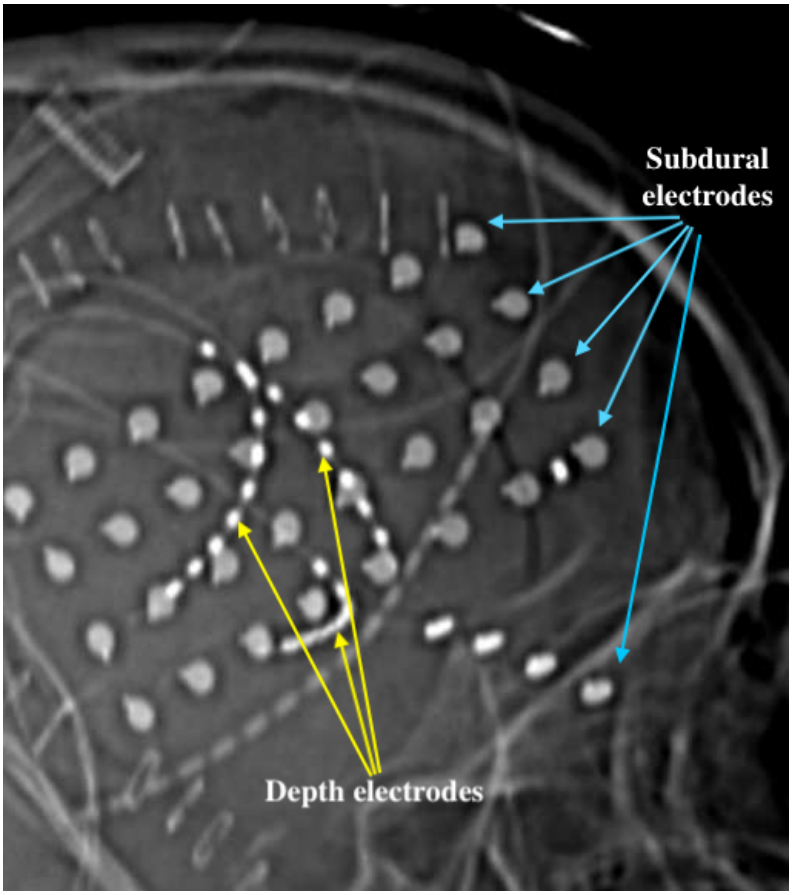

Figure 3.2: Pot-implantation X-ray image showing the implanted subdural (blue arrows) and depth electrodes (yellow arrows) for one subject.

has responded to surgery. The scale is divided into four main categories. Within this scale, Class I signifies achieving freedom from disabling seizures, Class II denotes infrequent disabling seizures, Class III indicates notable improvement or extended seizure-free intervals, and Class IV indicates negligible improvement.

Analysis of the outcomes, as depicted in Table 3.1, underscores the significance of DRs as an effective assessment tool in pinpointing epileptogenic neuronal regions. Approximately 80% of the cases subjected to surgery exhibited improvement, underscoring the pivotal role of DRs in refining surgical interventions and enhancing therapeutic outcomes for DRE cases.

3.3 SEPARATION OF SINGLE CHANNEL EEG INTO EXCITATORY AND INHIBITORY COMPONENTS

In order to investigate the separability of E and I activities and the ratio between them in ERs and DRs, we apply a suitable subspace method to these responses. As mentioned, SSA is a nonparametric method that can be applied to random statistical processes, whether linear or nonlinear, stationary or even mildly non-stationary and Gaussian

Table 3.1: The locations and number of the implanted electrodes alongside the results of the surgery for each case (R=Right, L=Left, T=Temporal, F=Frontal, A=Anterior, P=Posterior, O=Occipital, In=Insular, H=Hippocampus, Ms=Mesial, Par=Parietal).

Case	Locations and number of implanted electrodes	Results of surgery (Engel outcome scale)
1	LT 40, LO 8, LMs 8, LF 8	No Surgery
2	LTA 8, LTP 8, RT 8	I
3	LA 8, LPSubT 8, LF 8, LP 8	III
4	RF 8, RMidT 4, RPost 8, LA 8, LMidT 4, LP 8	IV
5	RT 40, RAT 8, RMsT 8, RPT 8	I
6	RF 8, RT 8, LF 8, LF8, LT 8	No Surgery
7	SubF 8, F 8, TPole 8, AT 8, PT 16, TO 8, Par 8	No Surgery
8	RAH 10, RMidH 10, RH 10, LAH 8, LMidH 10, LPH 10	I
9	RT 32, Tpole 5, MidT 5, PMT 5, AIn 5, MidIn 5, PIn 5	No Surgery
10	RT 32, TPole 5, MidT 5, PMT 5, AIn 5, MidIn 5, PIn 5	II
11	RF 8, RSubT 8, LSubT 8	III
12	RT 32, AT 6, MidT 6	II
13	AF 8, PF 8, SupF 8, AT 8, MsT 8, PT 8	No Surgery
14	RT 8, LT 8	No Surgery
15	LT 20, F 8, IF 8, PF 8, ST 8	IV
16	RT 64, RTPole 5, RMsT 6	No Surgery
17	FIns 4, TIns 4	No Surgery
18	LT 64, LFP 8	I
19	RF 8, RT 8, LF 8, LT 8	No Surgery
20	RMidF 10, RPF 10, LF 10	I

or non-Gaussian, without making prior assumptions about the data [119, 132]. The main purpose of using SSA is its ability to separate the underlying components of single-channel signals belonging to different subspaces. Due to this elegant property, it has found many applications in detection [133, 134], decomposition [135, 136], and forecasting [137, 138]. Given the properties of SSA and its effectiveness with small sample sizes, it appears to be a suitable method for investigating the ERs and DRs and separating each one into its E and I components. This suitability arises from the fact that these components fall into different orthogonal subspaces.

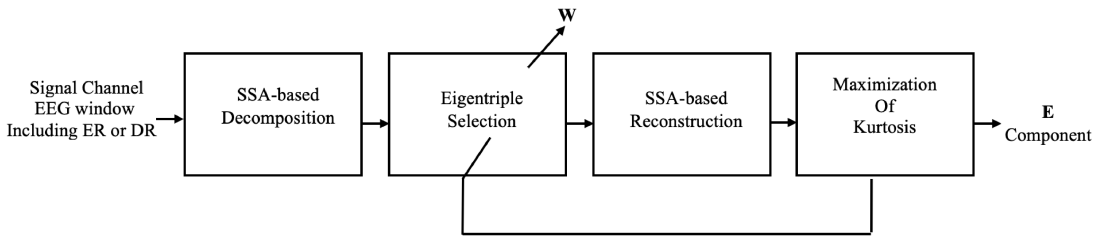

Figure 3.3: Block diagram of adaptive SSA system for E detection from ER or DRs. The I component is obtained by subtraction of E and noise from the original iEEG signal.

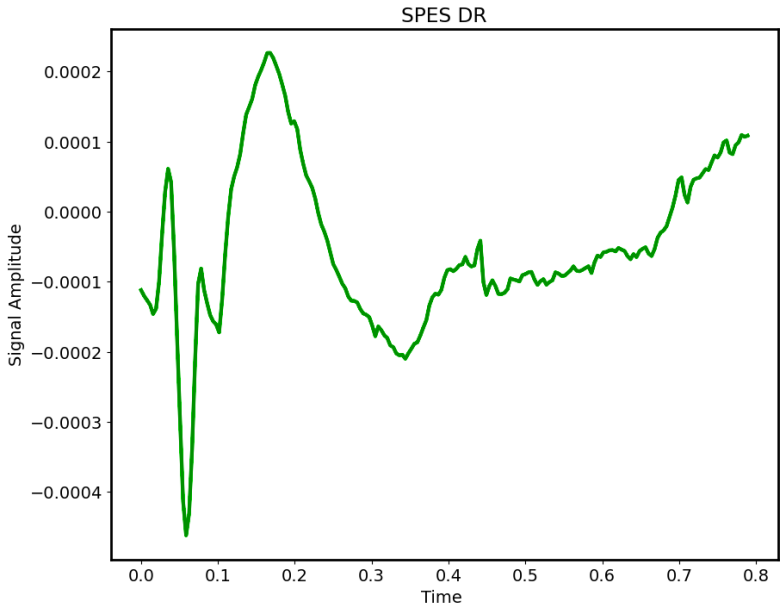

Figure 3.4: A sample segment of data that includes SPES DR

It is important to emphasise that the adaptive SSA pipeline dose not rely on any spectral information in its decomposition process. Here, the intention is not to separate components with different morphologies but those with inherently different statistical distributions. SSA, regularised by the information about statistical distributions, is used to decompose the data into orthogonal subspaces. However, after separating the components using SSA, we examine them in terms of their spectral signatures, and it is clear that they fall perfectly into different frequency ranges. Here, the pipeline based on single-channel SSA has been followed in which, in the reconstruction stage, the eigentriples are adaptively selected. The above SSA stages, together with the mathematical derivations, have been described in the following sections.

3.3.1 *Signal Decomposition*

The decomposition stage includes an embedding process followed by EVD. In the embedding process, after selecting a fixed window length of L, in the first step, the

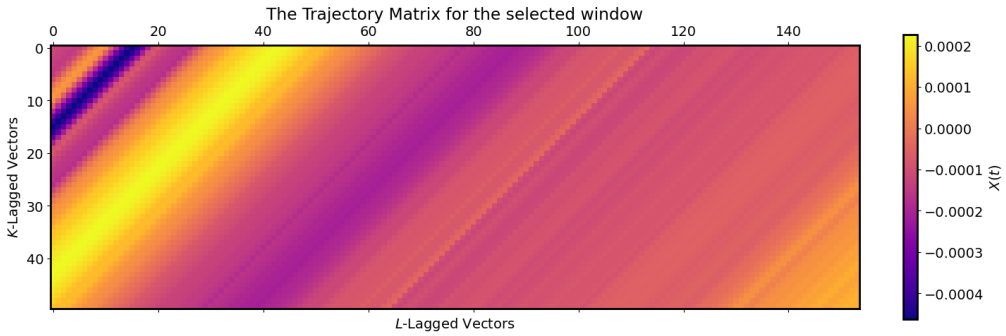

Figure 3.5: Trajectory matrix created from a segment of iEEG data that includes SPES DR during the decomposition stage.

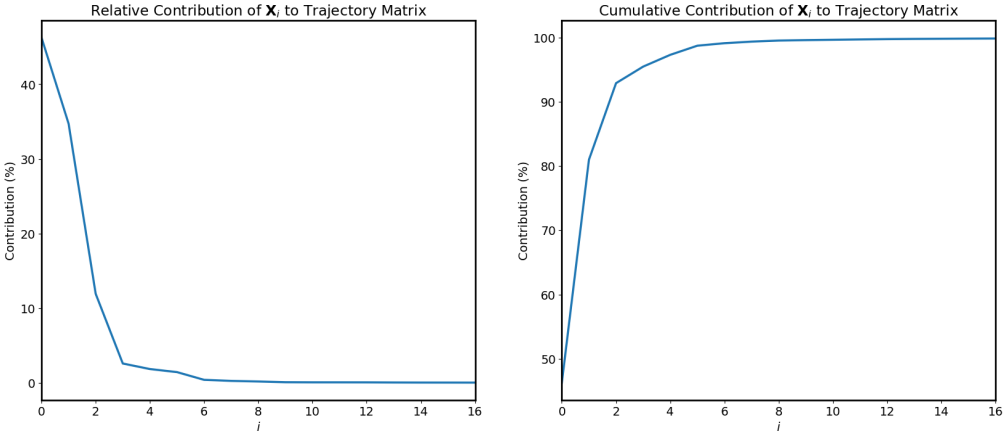

Figure 3.6: The relative contribution and cumulative contribution of extracted components from the original signal to the trajectory component.

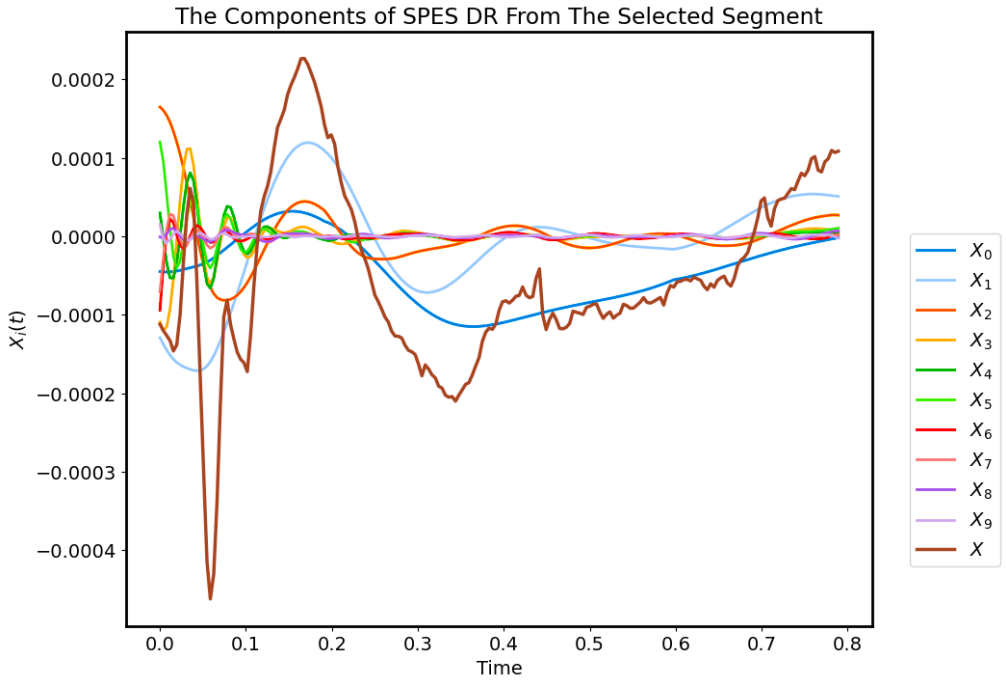

Figure 3.7: The original signal and the extracted components after decomposition stage.

trajectory matrix $\mathbf{X}$ that transfers the one-dimensional signal x of length T into the multi-dimensional series $X_0, \ldots, X_{k-1}$, with vectors $X_i = (x_i, \ldots, x_{i+L-1})^T$ where $K = T - L + 1$ is computed.

$$\mathbf{X} = (x_{i,j})_{i,j=0}^{L-1,K-1} = \begin{pmatrix} x_0 & x_1 & \cdots & x_{K-1} \\ \vdots & & \ddots & \vdots \\ x_{L-1} & x_L & \cdots & x_{T-1} \end{pmatrix}$$

Figures 3.4 and 3.5 show samples of a data segment and the trajectory matrix constructed using that data segment. In the next step, $\mathbf{S} = \mathbf{X}\mathbf{X}^T$ is factorised into its eigenvalues and eigenvectors to decompose trajectory matrix $\mathbf{X}$ into its orthogonal bases, where $\mathbf{S} = \mathbf{U}\mathbf{\Lambda}\mathbf{U}^T$. $\mathbf{\Lambda}$ is the diagonal matrix of eigenvalues ordered so that $\lambda_1 \geq \lambda_2 \geq \ldots \geq \lambda_L \geq 0$, and $\mathbf{U} = (U_1, U_2, \ldots, U_L)$ is the corresponding orthonormal matrix of eigenvectors of $\mathbf{S}$. Here, $\mathbf{X} = X_1 + X_2 + \ldots + X_d$, where $X_i = \sqrt{\lambda_i}\mathbf{u}_i$.
Figure 3.7 demonstrates the original signal shown in figure 3.4 decomposed into its orthogonal components.

3.3.2 *Component Reconstruction*

The reconstruction step corresponds to selection of the eigentriples into groups (eigentriple grouping) for the reconstruction of the one-dimensional time series by splitting the elementary matrices into multiple groups and summing the matrices in each group like $\mathbf{X}_I = X_{I1} + X_{I2} + \cdots + X_{Ip}$. Figures 3.6 show the relative contribution and cumulative contribution of extracted components from the original signal to the trajectory component. Both figures can help better assess if the extracted components can represent the overall original time series. After grouping, diagonal averaging is used to transform the matrices into one-dimensional reconstructed signals like $\tilde{X}_I$. Here, knowing that $x_{ij} \in \mathbf{X}_I$, the $x_k \in \tilde{X}_I$ which is the kth term of the resulting time series $\tilde{x}_I$ is $Mean(x_{ij}|(i+j=k+1))$. Here, for the reconstruction stage and regrouping of the components, an adaptive approach has been developed and used after most of the noise-related eigentriples are removed. Following this method, the remaining components are grouped into two waveforms, which best define the target E and I components. This is performed based on knowing that the E waveform has a spike shape with a peaky distribution, implying high kurtosis. Therefore, during the grouping process, the algorithm tends to separate a component with maximum kurtosis adaptively. To express the reconstruction of the E component mathematically, we employ a diagonal matrix $\mathbf{W}$ with binary diagonal elements, i.e. $w_{jj} = \{0, 1\}$. During the reconstruction process,

$\mathbf{W}$ is iteratively estimated in order to achieve the maximum kurtosis related to the E component, i.e.,

$$\mathbf{W}_{opt} = \max_{\mathbf{W}}(Kurtosis\ (\mathbf{W}\Lambda^{\frac{1}{2}}\mathrm{V})) \tag{3.1}$$

As depicted in Figure 3.3, the SPES ER and DR are first decomposed into N separate components. Often, the first eigentriples represent the overall signal trend, and the rest include low power activities such as noise, spikes, and low-amplitude oscillations. During the presented adaptive process, and after excluding the very last (noise-related) components, the eigentriples related to the E waveform are grouped adaptively to achieve the highest kurtosis. The result is anticipated to be the E waveform. The E component is then subtracted from the refined original signal to obtain the I component. Looking at their temporal, PSD, and time-frequency domain representations, we can conclude that the components are disjoint and belong to orthogonal subspaces. This verifies that the E and I components naturally originate from independent sources and, therefore, are separable.

3.4 EXPERIMENTS AND RESULTS

Overall, 300 annotated segments of iEEG data from 20 DRE cases, each 0.7 second long, containing ERs and DRs, were processed. Considering the length and shape of ERs and DRs in the data, a window length (also known as embedding dimension) of L =20 samples was selected for the SSA algorithm. After plotting the relative contribution and cumulative contribution to the trajectory (Hankel) matrix of base components, the first N=10 components were conisdered within the signal subspace and the rest for the noise subspace. Figure 3.1 demonstrates an example of the ERs and DRs to the SPES in the intracranial EEG from one of the subjects. After separating ERs and DRs, the E and I components and their PSD were inspected. The results show that the I component consists of the overall EEG trend, including lower frequency oscillations with a generally narrow PSD concentrated in low frequencies up to approximately 10 Hz. However, the E component consists of higher frequency oscillations with lower power and a wider PSD, comprising frequencies ranging from 10-20 Hz up to nearly 60 Hz. The frequency ranges for I and E components varied slightly among subjects, reflecting various morphological responses.

Figure 3.8 illustrates the results of the algorithm for a sample ER and DR to SPES recorded by a subdural electrode in the right temporal region. Figure 3.9 shows the PSD plots of E and I components for the sample ER and DR responses, and Figure 3.10 shows the STFT plots for these components, indicating a clear separation in the frequency domain. As shown in the images related to the ERs, the electrical stimulation

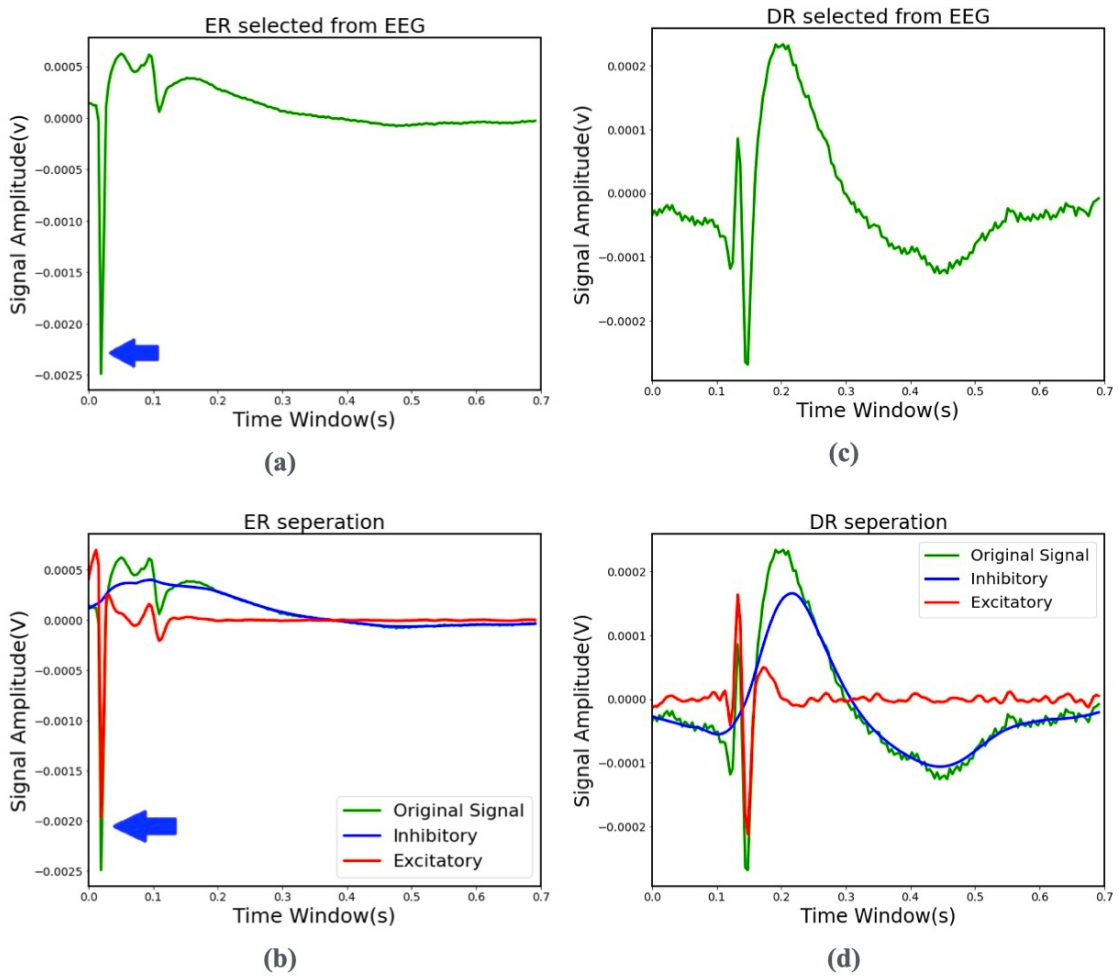

Figure 3.8: (a) An iEEG segment including an ER elicited immediately after SPES, (b) ER automatically decomposed into E and I parts (The arrow shows the stimulus artifact mixed with the E component), (c) An iEEG segment including a DR after SPES, and (d) DR automatically decomposed into E and I components

spike is considered an artefact added to the ER, obscuring the actual excitatory part of the ER. This makes the evaluation of the ER excitatory component difficult.

To ensure that the noise removal process does not significantly alter the morphology of the SPES responses, while the sum of E and I remains similar to the selected overall SPES response, we used the adaptive signed correlation index (ASCI) [139]. The ASCI is a statistical measure used to evaluate the relationship between two variables, considering the direction and the strength of their correlation. It is designed to provide a more nuanced understanding of the relationship between variables, especially in situations where the traditional correlation measures, such as Pearson's correlation coefficient, cannot fully capture the complexity of the data [139].

One of the key components of ASCI is its adaptive nature. The ASCI adapts to the data by considering the variability and distribution of the variables involved. This adaptability allows it to better handle non-linear relationships and varying scales of data. Unlike traditional correlation coefficients that only measure the strength and di-

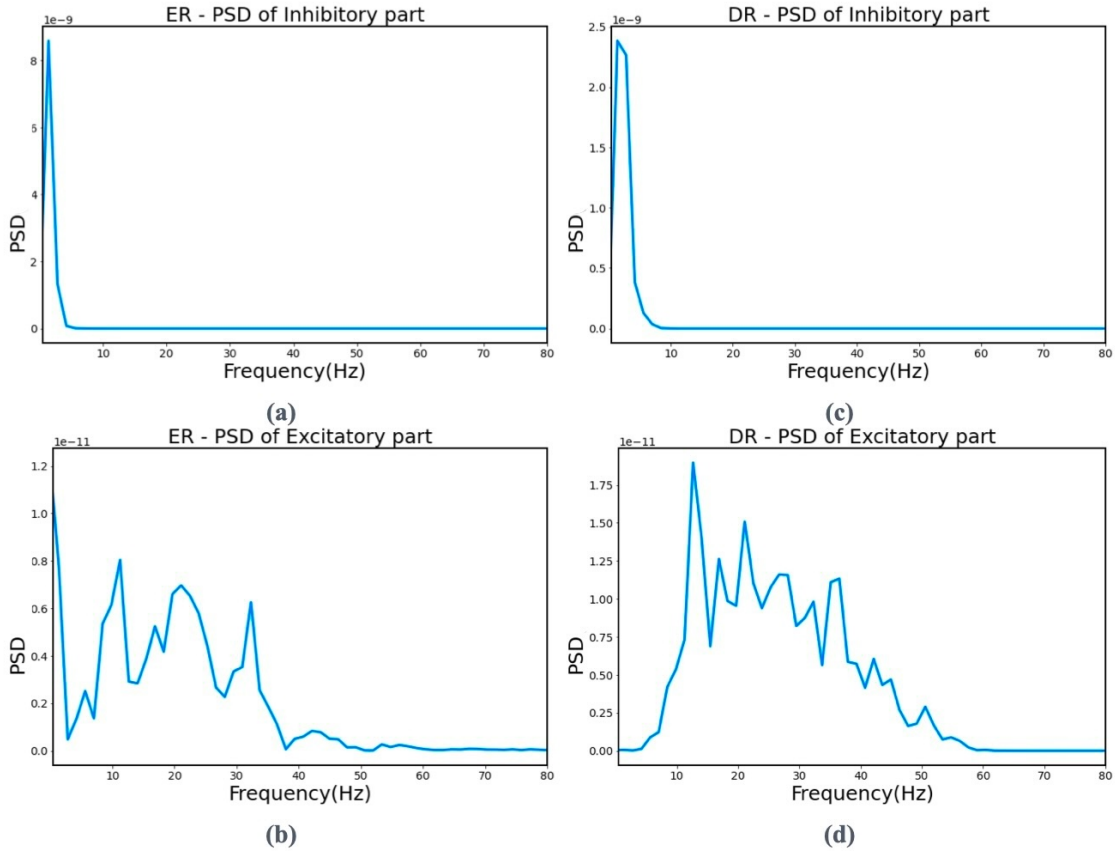

Figure 3.9: (a) PSD of I activity for ER, (b) PSD of E activity for ER (c), PSD of I activity for DR, and (d) PSD of E activity for DR.

rection of a linear relationship, the ASCI explicitly incorporates the sign of the correlation. This means it distinguishes between positive and negative relationships, providing more detailed insight into how the variables interact. Moreover, the ASCI takes into account the magnitude of the correlation, offering a more comprehensive measure that reflects not just whether the variables move together or in opposition but also how strongly they do so [139]. The adaptive nature of ASCI also helps mitigate the impact of outliers, which can significantly distort traditional correlation measures. By adapting to the data distribution, ASCI provides a more robust measure in the presence of outliers. This makes it particularly useful in finance, biology, and social sciences, where the relationships between variables can be complex, nonlinear, and influenced by outliers. Its adaptability and sensitivity make it a valuable tool for researchers and analysts [139].

The exact mathematical formulation of ASCI can vary depending on its specific implementation. Measurment of ASCI involves several steps. First, the data is normalised to ensure comparability across different scales. Then, the weights are assigned to the data points based on their distribution and relevance, which helps emphasise significant correlations while reducing the impact of noise and outliers. The weighted and normalised data is then used to compute the signed correlation, incorporating both di-

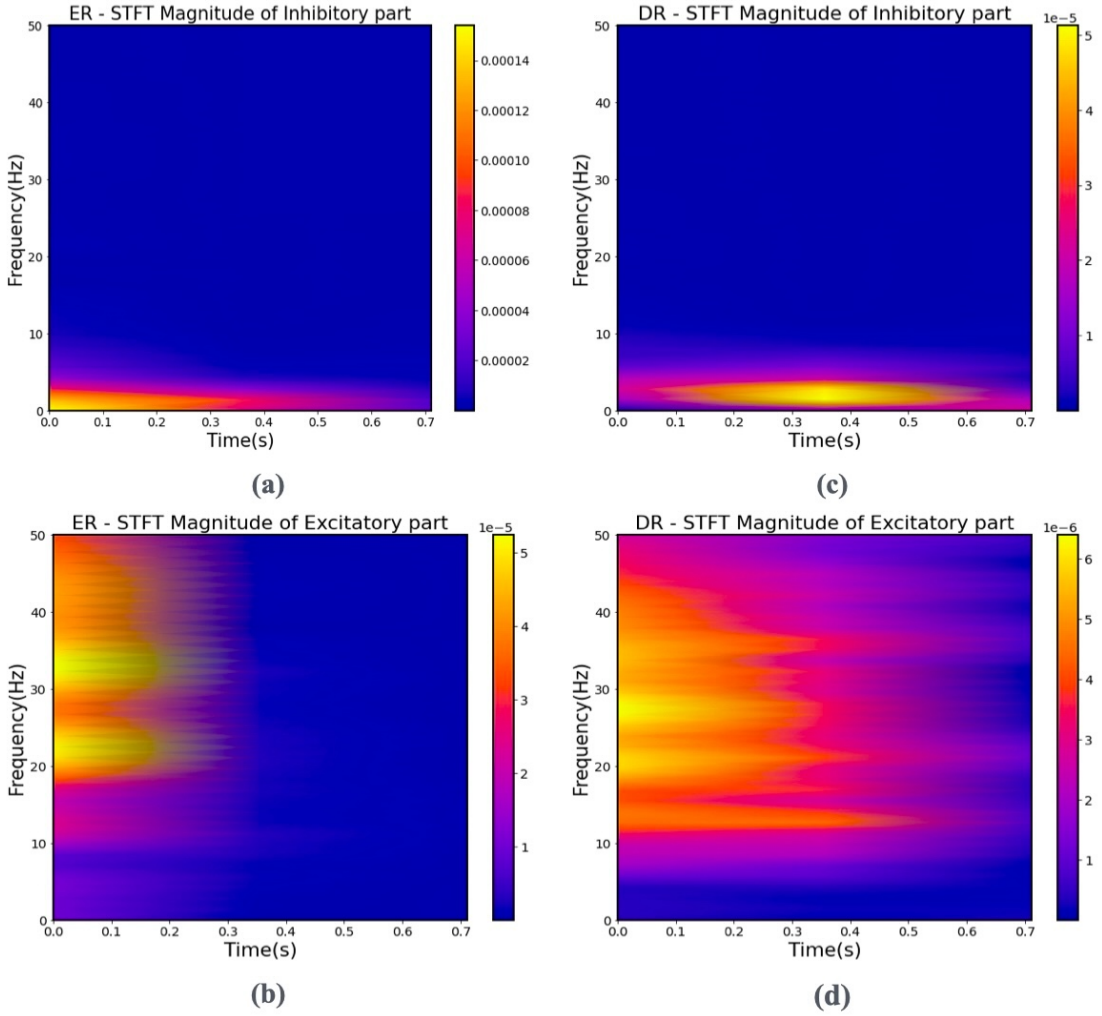

Figure 3.10: (a) STFT magnitude of I component for ER, (b) STFT of E component for ER, (c) STFT magnitude of I component for DR, and (d) STFT magnitude of E component for DR. The plots show how effectively the two components have been separated using SSA.

rection and magnitude. Finally, the individual correlations are aggregated to produce the overall ASCI value, which reflects the adaptive signed correlation between the variables [139].

Interpreting the ASCI is straightforward. An ASCI close to +1 indicates a strong positive correlation, while an ASCI close to -1 indicates a strong negative correlation. An ASCI around 0 suggests little or no correlation. By incorporating both the sign and the magnitude of correlations and adapting to the data distribution, the ASCI provides a richer, more detailed measure of the relationship between variables compared to the traditional correlation coefficient methods. The average ASCI score was 0.85 ± 0.15 for the conducted tests, indicating the close similarity of the two waveforms. Also, $C = (\sum_{j=0}^{N} E_j \times I_j)/L \;\; | \; j$: samples has been measured to check the correlation between the E and I components. The correlation is close to zero for all the tests, illustrating that the E and I components do not share the same subspaces.

From the PSD and STFT magnitudes, the E and I components can be inspected separately. The I-to-E power ratio is plotted for the selected ER and the related DR segments. The I-to-E power ratio plot demonstrates the changes for the selected windows. A consistent observation (approximately 0.75 of overall tests) is that in channels where DRs are present after SPES, there is a considerable increase in the I-to-E power ratio right after ERs and before the appearance of DRs. Figure 3.11 illustrates the ratio for a selected window containing ER and the related DR for a subdural channel implanted in the brain right temporal pole region.

As the E-I imbalance is considered a significant indicator of epilepsy in the epileptic brain and regions associated with seizures [38], investigating the E and I components and the alterations in the I-to-E ratio helps to better understand the underlying information in DRs and consequently, the overall seizure network in future steps. The hypothesis is that the epileptic zones contribute more to the elicitation of I. Therefore, a deeper investigation of the I-to-E power ratio for the DRs could provide more insight into seizure diagnosis and localisation. One possible explanation for the severe and consistent increase in the I-to-E power ratio before DRs in some channels might be their relative location and short distance to the actual SOZ or their association with regions in the seizure network. Previous studies have shown that DRs are generally observed in regions associated with seizure networks. Therefore, after applying SPES to these regions, the role of DRs may be compensatory, preventing further increase of I and synchronisation between various regions, possibly leading to seizure onset.

Also, previous studies have highlighted the similarities between DRs and IEDs [140], suggesting that the occurrence of IEDs might prevent seizures due to their high levels of I indicated by the long suppression periods seen in single-cell activity [56]. Another possible explanation is that the I-to-E ratio might affect the occurrence of DRs, where the I-to-E ratio alteration needs to surpass a limit for elicitation of DRs, even in regions capable of producing such responses after applying electrical stimulation. There is no statistically significant correlation between the location of the selected electrode and the observed changes in the I-to-E ratio in the selected intervals. However, it is worth noting that for all the DRE cases included in this chapter, most of the intracranial electrodes are implanted in the temporal regions based on the preassumptions regarding the SOZ location from the medical history, where most of the DRs are observed.

Findings from a recent study highlight the important relationship between the morphology of the responses to the SPES and the location of the implanted electrodes. According to the results of this study, the local and distant cortical responses to SPES are differentially modulated by specific parameters like the intensity and location of the stimulation point in the brain [141]. Although the differences in the morphology of responses to the SPES (especially DRs), stemming from different SPES setups, make it difficult to perform a direct comparison between these responses, the single channel separation algorithm introduced in this chapter offers the opportunity to investigate

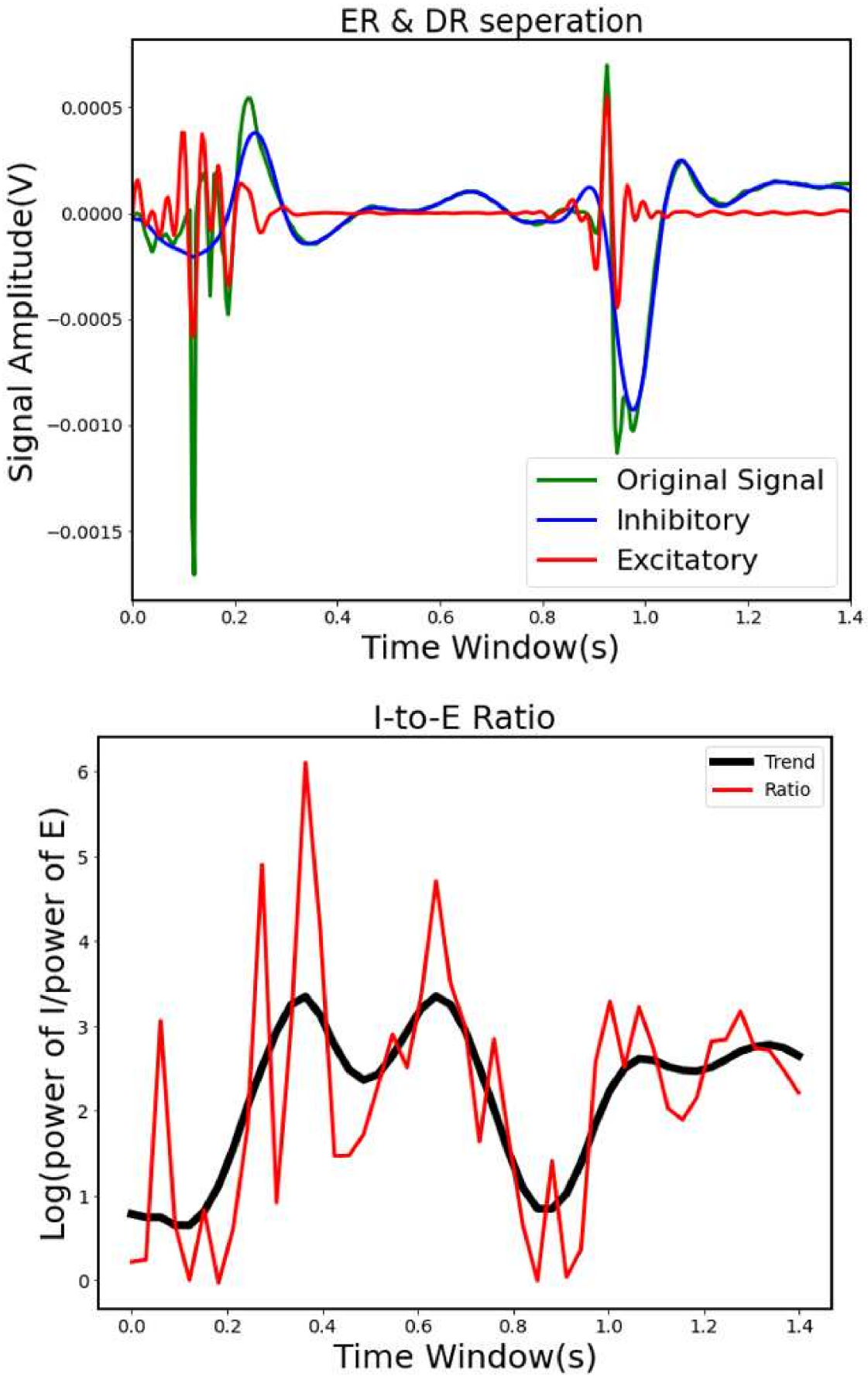

Figure 3.11: Logarithm of I-to-E power ratio for a selected data segment from iEEG channel implanted in the right temporal pole region after SPES. (The black line demonstrates the smoothed trend of I-to-E ratio)

the E-I imbalance for the recorded iEEG data using the implanted electrodes in the epileptogenic region.

Several points need to be considered to ascertain whether the I-to-E ratio measurements explicitly estimated based on our proposed method can elucidate the DRs. Initially, the proposed algorithm was applied to the data recorded from the depth electrodes. However, the method was later applied to the iEEG signals recorded using subdural channels due to the similarity (morphology) of the responses to the SPES recorded from the depth and subdural electrodes. Depth electrodes permit recording the activity from a local and specific region including a much smaller group of neurons. In contrast, subdural channels record a superposition of activities from various sources. Therefore, the decomposed components from subdural channels are more likely the result of synchronised activities for a population of neurons. The E activity is more localised than the I activity, which can affect the observed separated components and I-to-E power ratio in subdural electrodes compared to depth electrodes.

The second point is that the DRs seen in multiple depth electrodes sometimes exhibit different behaviors regarding E and I components and the I-to-E ratio. They have dissimilarities in their morphologies. The DRs or part of them in some depth channels may stem from a propagated signal from a nearby source, causing these differences.

Finally, it must be noted that the adaptive SSA algorithm's performance in separating the input time series into distinguishable orthogonal components differs according to the morphology of the signal and the length of the selected window (L) for computing the trajectory matrix. Therefore, an adaptive approach for selecting SSA parameters like window size instead of having a fixed value for all tested segments is worth exploring in future works.

3.5 CONCLUSION

In this chapter a subspace-based approach based on SSA with an adaptive reconstruction step has been introduced and employed to extract the excitatory and inhibitory components from ER and DRs to SPES in epileptogenic regions where an imbalance between E and I is expected. This approach takes a big step in investigating the separability of E and I activities for ERs and DRs to the SPES for the epileptic brain. Unlike most EEG-based studies that refer to E and I activities solely based on the frequency of the waveforms, the method employed here exploits the waveform morphology and disjoint components using subspace decomposition. However their spectrum show that they are well distinct in their frequency band. This approach can potentially deepen understanding of the excitability of the brain tissue, seizure network, localisation of epileptic regions, and extraction of other valuable information for seizure treatment, mainly through SPES for DRE patients who undergo intracranial electrode implanta-

tion. After showing the imbalance in E-I components expected in epileptogenic regions where the DRs are visible, considering the importance of identifying the SOZ, it is essential to introduce robust algorithms to identify the source of these responses. This topic is discussed in the following chapters.

4

LOCALISATION OF SPES DR SOURCES

SPES DRs in DRE cases, as observed from their intracranial recordings, can assist in identifying regions associated with epileptogenicity. Automatic DR source localisation significantly advances the identification of epileptogenic regions and SOZ. This chapter introduces the concept of spatial filtering and beamforming for source localisation applications, particularly in EEG-related studies. Afterward, the newly developed adaptive iterative linearly constrained minimum variance beamformer (AI-LCMV) is formulated and utilised to localise the DR sources from iEEG recorded using subdural electrodes introduced previously. The primary objective is to accurately localise the regions responsible for the corresponding SPES DRs using a regularised localisation algorithm that leverages the morphology of DRs as the desired sources. The traditional closed-form LCMV (CF-LCMV) solution is designed to track sources with dominating power. By incorporating the morphology of DRs as an additional constraint to an iterative LCMV solution, the array of subdural electrodes can be utilised to localise the low-power DRs, some of which may not even be visible in any of the electrode signals. The results also indicate more distinctive locations than those achievable by conventional beamformers. Most significantly, the proposed AI-LCMV can localise the DRs that are not necessarily visible over the data recorded by subdural electrodes.

4.1 SPATIAL FILTERING AND BEAMFORMING

4.1.1 *EEG Source Localisation*

Source localisation in EEG studies refers to identifying the spatial origins of these signals [4]. This is a challenging task considering the ill-posed nature of the problem, considering that an infinite number of possible sources configurations can lead to the recorded signals. Forward and inverse models localisation problems have been widely researched. The forward model predicts the recorded signals (EEG data) from a given source distribution [142], and the inverse model estimates the source distribution from the observed signals using the EEG electrodes [143].

The forward model describes the relationship between the electrical activity within the brain and the measured EEG signals. It involves computing the potential field generated by a set of neural sources within a head model. The forward problem has a unique solution but needs precise modelling of the head's anatomy and tissue conductivities or having access to the source temporal and spectral properties.

The simplest head model is the spherical model, which assumes the head is composed of concentric spherical layers representing different tissues (like the scalp, the skull, and the brain). While computationally efficient, this model often lacks topological accuracy. More advanced models include the boundary element method (BEM) and the finite element method (FEM) [144].

BEM is widely used in EEG forward modelling. It approximates the head as a set of surfaces (boundaries) between different tissues, reducing the problem to solving boundary integrals rather than volume integrals. This approach is computationally efficient and balances the accuracy and computational cost [145].

FEM involves discretising the entire volume of the head into small elements, allowing for modelling the complex geometries and inhomogeneous conductivities. This method is particularly useful in EEG forward modeling, where the skull's inhomogeneities significantly affect the electrical potential distribution due to different layers of tissue. FEM is more accurate than BEM but it is computationally more expensive [145].

EEG signal sources are commonly modelled as equivalent current dipoles (ECDs), distributed sources, or more complex models like multiple dipoles or cortical patches.

The ECD model considers that a small number of dipoles with fixed locations and orientations can represent neuronal activity. This model is simple and computationally efficient but may not capture the distributed nature of brain activity [146].

Distributed source models assume that the brain's activity is distributed across a grid of dipoles, each with an amplitude and orientation. The distributed approach is more flexible and can represent complex patterns of brain activity. However, it leads to an underdetermined problem, which requires regularisation methods in the inverse modelling process [147].

Cortical patch models constrain the sources to the cortical surface, aligning them with the brain's anatomy. Cortical patch models reduce the dimensionality of the source space and improve the interpretability of the results where the primary sources are tangentially oriented [148].

The inverse problem in EEG source localisation aims to estimate the distribution of neural sources from the recorded signals [149]. As mentioned earlier, unlike the forward problem, the inverse problem is ill-posed. Inverse methods can be classified into various approaches.

Dipole fitting methods estimate the location, orientation, and strength of a small number of dipoles that best explain the recorded signals. The most common approach is the least-squares fitting, where the parameters of the dipoles are iteratively adjusted to reach the minimum difference between the measured and predicted sensor data [150]. Single dipole models assume that the neural activity can be represented by a single dipole, which is effective for well-localised sources but inadequate for multiple isolated distributed or complex source configurations. Multiple dipole models allow for localisation of multiple dipoles, providing greater flexibility in representing complex

brain activity. However, the increased number of parameters requires more sophisticated optimisation algorithms and can lead to overfitting if not adequately regularised [150].

Distributed source imaging methods estimate the activity of a large number of dipoles distributed throughout the brain. These methods often employ regularisation techniques to constrain the solution, addressing the ill-posed nature of the inverse problem.

Minimum norm estimation (MNE) is a widely used method that estimates the source distribution by minimising the L2-norm of the source amplitudes, subject to the constraint that the forward model explains the measured data [151]. While computationally efficient, the MNE produces smeared or biased solutions, especially for deep sources. Low-resolution electromagnetic tomography (LORETA) extends MNE by imposing an additional smoothness constraint, encouraging neighbouring sources to have similar activity [152]. Beamforming techniques estimate source activity by constructing spatial filters that pass signals from a specific location while attenuating signals from other locations. Beamforming is particularly effective for localising oscillatory sources but may suffer from localisation errors in the presence of correlated sources [153].

The precision of EEG sources relies on a range of factors, like the head model's quality and the source model's selection, in addition to the regularisation methods applied to solve the inverse problem. Enhancements in imaging technologies like combining EEG with MRI or fMRI can enhance the accuracy of pinpointed sources by offering more precise head models. Balancing resolution and resistance to noise pose key obstacles in pinpointed source determination. Techniques like conventional beamforming algorithms can offer estimations of sources but are prone to noise and model errors compared to the more reliable yet less detailed approach of low-resolution methods, such as LORETA, for source localisation.

Lately, there has been a lot of interest in merging inverse methods with machine learning techniques. Methods like learning have shown potential in enhancing source localisation by recognizing intricate patterns from large datasets [154, 155]. As an example, a recent research paper introduced a neural network structure for identifying and monitoring the spread of seizure activity in multichannel EEG data by combining a convolutional neural network encoder for each EEG channel using recurrent neural networks to track seizure progression over time [156].

In another recent study, the researchers introduced a machine learning methodology aimed at localising SOZ with a new approach that involves representing brain states as functional networks derived from iEEG recordings, using correlation and phase-locking values to measure the interactions between different brain regions [157]. The methodology is built on the foundations of graph neural networks and the attention mechanism, two major advancements in artificial intelligence studies. The study demonstrates that the regions identified by the network align closely with those pinpointed by experts as the SOZ. The approach was validated with both human patients and brain activity

simulators. It also showed the network's ability to express uncertainty in those cases where the clinical localisation was unsuccessful, underscoring the robustness of this method.

Deep learning techniques have also been recently applied to SPES responses to identify the SOZ. In a recent study by Johnson et al. [110], authors explored the use of machine learning methods to aid in the localisation of the SOZ in DRE cases with temporal lobe epilepsy. The study involved training a multichannel convolutional neural network on CCEPs recorded via sEEG to identify SOZs. The authors utilised 500,000 unique poststimulation sEEG segments to train the network to determine whether an SOZ had been stimulated. Based on leave-one-patient-out testing, the results showed that the model could classify SOZs with a mean sensitivity of 78.1% and specificity of 74.6%. The optimal classification accuracy was achieved within a 0- to 350-millisecond poststimulation window. Further analysis revealed that the model could accurately distinguish between different SOZs. This study represents the first demonstration of a deep learning framework effectively classifying SOZs using SPES responses.

In another study by Norris et al. [111], authors try to address the challenge of precisely localising the SOZ. Firstly, the authors executed an existing deep learning model to compare two SPES analysis paradigms: divergent and convergent. These paradigms evaluate outward and inward effective connections, respectively. The study evaluated the generalisability of these models to new patients and electrode placements using held-out test sets. The results showed notable improvement when shifting from the divergent to the convergent approach. This study demonstrated the effectiveness of convolutional transformers with cross-channel attention in managing heterogeneous electrode placements, further increasing the performance.

Although deep learning methods show promising advancement in EEG source localisation, employing techniques like deep neural networks for source localisation requires considerable amount of annotated information, which is not frequently accessible in medical or research environments.

4.1.2 *Spatial Filtering*

The spatial filtering objective is to create a directional array of signal energy, or in other words, manipulate the spatial characteristics of signals to enable the localisation of sources within a particular area or volume [158, 159]. Spatial filtering has various applications in various fields, like neuroscience and wireless communications. Spatial filtering entails employing an array of sensors to record signals at different spatial locations and then applying mathematical operations to enhance certain components and suppress others based on their spatial properties. Some of the key concepts of spatial filtering are:

1. Spatial filtering focuses on the spatial domain (location), analysing how signal properties change across different locations.

2. An essential component of spatial filtering is an array of sensors (such as microphones, antennas, or electrodes). These sensors capture signals from different spatial positions, providing data that encompasses spatial information for the filter.

3. Spatial signals can be analysed in terms of spatial frequencies. Spatial filtering can then be performed in the spatial frequency domain.

4.1.3 *Beamforming*

Beamforming is a signal processing technique that falls within the adaptive array processing and spatial filtering domain used to direct the reception or transmission of signals in specific directions using an array of sensors, such as microphones, antennas, sonar transducers, or EEG electrodes [153]. By manipulating the signals received by each sensor in the array, the beamformer enhances the signal from a desired direction while suppressing signals from other directions [160, 161]. This technique is widely used in applications such as wireless communications, radar, sonar, and audio processing [162, 163].

Conventional beamforming involves an array of sensors arranged in specific geometries, such as linear, circular, or planar, to capture the signals received from different spatial locations. The fundamental idea of beamforming is to modify the phase and amplitude of the signals recorded by each sensor, allowing for a constructive combination of signals from the desired direction and rejecting those which come from other directions. A critical aspect of beamforming is the estimation of direction of arrival (DOA), which helps in aligning the beam toward the desired source. The radiation or reception pattern of a beamformer includes a main lobe, which is the primary direction of signal enhancement, and side lobes, which are secondary, often unwanted, directions of signal reception. The goal for an optimum beamformer is to maximise the main lobe toward the desired direction and minimise the side lobes to exclude unwanted activity. Minimising side lobes relative to the main lobe in an optimum beamformer is important for several reasons. It improves the SNR by enhancing the desired signal while suppressing unwanted noise and interference from other directions. This also aids in better interference suppression, as smaller side lobes reduce the impact of signals from unwanted directions, thereby improving system performance. Additionally, smaller side lobes enhance spatial resolution, enabling the system to distinguish closely spaced sources more accurately and reducing the likelihood of false alarms. Finally, minimising side lobes increases energy efficiency by concentrating more energy in the desired direction.

The Minimum Variance Distortionless Response (MVDR) beamformer, also known as the Capon beamformer, is a popular adaptive beamforming technique used in array signal processing. The primary goal of the MVDR beamformer is to minimise the total output power of an array while ensuring that the signal coming from a desired direction is received without distortion [164]. One main disadvantage of the conventional MVDR beamformer is that it can have a high side lobe, which is notably not ideal for low sample inputs. This characteristic can lead to a significant performance drop in the presence of unexpected interference [165].

One strategy to overcome the shortcomings of the conventional MVDR beamformer is to introduce side lobe pattern control. In work by Liu et al. [165], the authors present a method for an adaptive beamformer that improves upon the standard MVDR beamformer and control the high side lobe effect. The authors introduce a second-order cone programming approach that includes additional constraints to control sidelobe levels, ensuring they remain below a preselected threshold. This helps to move towards the optimum beamforming solution. This method is computationally efficient and capable of detecting infeasibility in the optimisation problem, providing a robust solution for maintaining performance in the presence of interferers. Simulation results demonstrate its effectiveness compared to the traditional MVDR solution.

The beamforming process generally consists of various steps, including:

1. Signal Collection: Signals are collected from the array of sensors (here, subdural electrodes). Each sensor receives the signal with a different phase and amplitude depending on the signal's direction and electrod's relative location to the source location.

2. Weight Calculation: Appropriate weights (amplitude and phase adjustments) are calculated for each sensor to steer the beam toward the desired direction. In fixed beamforming, these weights are predetermined. In adaptive beamforming, the weights are dynamically adjusted based on the signal environment or source characteristics.

3. Signal Combining: The weighted signals from each sensor are aligned and combined. For reception, this means summing the weighted signals to enhance the desired signal and suppress others. For transmission, this means distributing the signal to the array elements with the appropriate weights to form a directional beam.

4. Beam Pattern Formation: The combined signal forms a beam pattern with a main lobe pointing towards the desired direction and minimised side lobes.

In addition to beamforming, there are other methods available for source localisation. Multiple Signal Classification (MUSIC) [166] decomposes the signal covariance matrix into signal and noise subspaces, identifying DOA from the peaks of a pseudo-spectrum.

MUSIC offers high resolution and can resolve closely spaced sources, whereas adaptive beamforming provides good interference rejection and higher resolution than provided by the conventional beamformers. However, MUSIC is computationally intensive and requires a large number of sensors. An extenstion of MUSIC method is recursively applied and projected (RAP) MUSIC. It is an advanced algorithm for estimating the DOA of signals in array signal processing. It enhances the standard MUSIC algorithm for detection of closely spaced multiple source, by iteratively projecting the signal subspace onto a noise subspace, refining the estimation of signal sources in scenarios with closely spaced or correlated signals [167]. RAP MUSIC is particularly useful in situations where the traditional MUSIC algorithm may struggle due to signal correlation or insufficient resolution. [167, 168].

Estimation of signal parameters via rotational invariance techniques (ESPRIT) [169] leverages the rotational invariance of signal subspaces for DOA estimation. Beamforming, in contrast, manipulates the phase and amplitude of received signals to focus on desired directions. ESPRIT offers high resolution and is less computationally intensive than MUSIC. Adaptive beamforming excels in interference rejection and offers good resolution. However, ESPRIT requires a significant number of snapshots.

Regarding computational complexity, MUSIC, and adaptive beamforming are highly complex, while the ESPRIT method is moderately complex, and conventional beamforming is relatively low in complexity. For robustness to noise and interference, the adaptive beamforming method is highly robust, MUSIC and ESPRIT offer moderate robustness, and conventional are less robust. Sensitivity to model errors and array imperfections is high for adaptive beamforming, moderate for MUSIC and ESPRIT, and low for conventional beamforming and ICA. Finally, ease of implementation is greatest for conventional beamforming, moderate for ICA, and most complex for adaptive beamforming, MUSIC, and ESPRIT.

Adaptive (regularised) beamforming has been successfully used in EEG source localisation studies. In a study by Spyrou et al., [112], an algorithm for the localisation of ERP sources within the brain is proposed. In this spatial filtering algorithm, spatial notch filters are developed to exploit the EEG data with a model of ERP with variable parameters to accurately localise the corresponding ERP signal sources. The results indicated the algorithm's robustness in the presence of noise and superior performance compared to conventional LCMV beamformer, indicating the benefits of regularised beamforming for EEG source localisation.

4.1.4 *Linearly Constraint Minimum Variance Beamformer*

A popular and effective beamforming method used for various applications is the LCMV beamformer [170]. The LCMV beamformer is a more generalised version of the

MVDR beamformer. While the MVDR beamformer sets a single constraint to preserve a distortionless response in the direction of the desired signal, the LCMV beamformer can impose multiple linear constraints. These constraints can be utilised to control the response in several directions or to shape the beam pattern in distinctive ways.

The conventional LCMV beamformer, although flexible, might not consistently acquire the optimal beam pattern (high main lobe, low side lobes). This suboptimality arises due to multiple reasons. First, the multiple constraints in the solution might conflict, which can compromise beam pattern performance. Also, while the LCMV beamformer allows for the regulation of multiple aspects of the beam pattern, it does not inherently optimise the sidelobe levels. Finally, the complexity introduced by multiple constraints might make it more challenging to achieve the most efficient solution, especially compared to approaches specifically developed to minimise sidelobes [153, 171].

The LCMV beamformer is a method that has been used extensively in the context of neuroimaging and signal processing. In neuroimaging, the LCMV beamformer was first applied to MEG data by Van Veen et al. [171]. This groundbreaking step demonstrated the beamformer's ability to localise neural sources with high spatial resolution, while effectively suppressing interference from other brain regions and external noise sources. The LCMV beamformer has since found widespread use in various applications, particularly in the analysis of MEG and EEG data. LCMV algorithm's primary function is to estimate the activity of neural sources by scanning through a predefined grid of source locations and constructing spatial filters for each point [172]. This approach allows for the reconstruction of source activity without the need for averaging across trials, making it particularly useful for studying ongoing brain activity and temporary events.

One of the key advantages of the LCMV beamformer is its ability to provide focal reconstructions of neural activity, even for deep brain sources. In addition to source localisation, the LCMV beamformer has been extensively used to study functional connectivity. By applying the beamformer to time series data, the researchers can investigate the temporal dynamics of neural networks and assess the interactions between different brain regions [173]. Also, the versatility of the conventional LCMV beamformer has led to its availability in various open-source neuroimaging toolboxes, including FieldTrip [174], SPM12 [175], Brainstorm [176], and MNE-Python [177].

A conventional form of the LCMV beamformer is CF-LCMV, in which the weights are determined through covariance minimisation [171, 178, 179]. The CF-LCMV minimises the output power (with a narrow main lobe) while maintaining a constant response in the direction of the signal of interest. Key concepts and equations related to the conventional form of the LCMV beamformer are presented here.

In the context of the LCMV beamformer, several key concepts are fundamental to understand its operation. An array signal model describes an array of M sensors re-

ceiving signals, where the received signal vector $\mathbf{X}(t)$ at time t consists of a desired signal component $\mathbf{S}(t)$ and noise plus interference $\mathbf{n}(t)$. The beamformer output $Y(t)$ is computed as a weighted sum of sensor outputs, given by $Y(t) = \mathbf{W}^H\mathbf{X}(t)$, where $\mathbf{W}$ is the beamforming weight vector and $\mathbf{W}^H$ denotes its conjugate transpose. The objective of beamforming is to minimise the output power, typically formulated as $\min_{\mathbf{W}} \mathbb{E}[|Y(t)|^2] = \min_{\mathbf{W}} \mathbf{W}^H\mathbf{R}\mathbf{W}$, where $\mathbf{R}$ is the covariance matrix of $\mathbf{X}(t)$. Constraints are imposed to preserve the desired signal, often expressed as linear constraints. One constraint here is $\mathbf{G}^H\mathbf{W} = \mathbf{f}$, where $\mathbf{G}$ is a constraint matrix (leadfield matrix based on head model estimation for EEG source localisation) and $\mathbf{f}$ is a vector of desired responses. To reach the solution for the CF-LCMV beamformer, the Lagrange multipliers method can be employed. This technique allows the incorporation of the constraints directly into the optimisation problem. By doing so, the original constrained optimisation problem can be transformed into an unconstrained format, which makes it easier to solve analytically [180]. The Lagrange multipliers method introduces additional variables for each constraint. These multipliers enable us to construct a new objective function called the Lagrangian, which combines the original objective function and the constraints. Solving the Lagrangian yields the optimal solution for the beamformer that satisfies the given constraints. Here, the Lagrangian function for the constrained optimisation problem is:

$$\mathcal{L}(\mathbf{W}, \boldsymbol{\lambda}) = \mathbf{W}^H\mathbf{R}\mathbf{W} + \boldsymbol{\lambda}^H(\mathbf{f} - \mathbf{G}^H\mathbf{W}) + (\mathbf{f} - \mathbf{G}^H\mathbf{W})^H\boldsymbol{\lambda} \tag{4.1}$$

where $\boldsymbol{\lambda}$ is the vector of Lagrange multipliers. Taking the derivative of $\mathcal{L}$ with respect to $\mathbf{W}$ and setting the value eqaul to zero leads to:

$$\frac{\partial \mathcal{L}}{\partial \mathbf{W}} = \mathbf{R}\mathbf{W} - \mathbf{G}\boldsymbol{\lambda} = 0 \quad \Rightarrow \quad \mathbf{R}\mathbf{W} = \mathbf{G}\boldsymbol{\lambda} \tag{4.2}$$

Taking the derivative of $\mathcal{L}$ with respect to $\boldsymbol{\lambda}$ and setting the value equal to zero gives:

$$\frac{\partial \mathcal{L}}{\partial \boldsymbol{\lambda}} = \mathbf{f} - \mathbf{G}^H\mathbf{W} = 0 \quad \Rightarrow \quad \mathbf{G}^H\mathbf{W} = \mathbf{f} \tag{4.3}$$

From $\mathbf{R}\mathbf{W} = \mathbf{G}\boldsymbol{\lambda}$, $\mathbf{W}$ can be measured as:

$$\mathbf{W} = \mathbf{R}^{-1}\mathbf{G}\boldsymbol{\lambda} \tag{4.4}$$

Substitute this into the constraint $\mathbf{G}^H\mathbf{W} = \mathbf{f}$:

$$\mathbf{G}^H\mathbf{R}^{-1}\mathbf{G}\boldsymbol{\lambda} = \mathbf{f} \quad \Rightarrow \quad \boldsymbol{\lambda} = (\mathbf{G}^H\mathbf{R}^{-1}\mathbf{G})^{-1}\mathbf{f} \tag{4.5}$$

Finally, substitute $\boldsymbol{\lambda}$ back into the expression for $\mathbf{W}$:

$$\mathbf{W} = \mathbf{R}^{-1}\mathbf{G}(\mathbf{G}^H\mathbf{R}^{-1}\mathbf{G})^{-1}\mathbf{f} \tag{4.6}$$

This approach allows us to determine the optimal beamforming weights $\mathbf{W}$ that satisfy the given constraints using the LCMV beamformer. The CF-LCMV beamformer weight vector $\mathbf{W}$ is given by:

$$\mathbf{W} = \mathbf{R}^{-1}\mathbf{G}(\mathbf{G}^H\mathbf{R}^{-1}\mathbf{G})^{-1}\mathbf{f} \tag{4.7}$$

This solution ensures that the beamformer minimises the output power while satisfying the linear constraints imposed to preserve the desired signal.

Although conventional LCMV beamformer has proven useful for various applications, including EEG-MEG source localisation [181], its robustness is poor when the target signal is sparse or with low power, such as spike type waveforms, or the SNR is low [153, 171]. A typical approach to compensate for the beamformer's sensitivity to the power of the recorded signal and to increase the SNR is averaging the signals over a large number of segments [182]. However, averaging overlooks the variability in time and source power and diminishes the algorithm's sensitivity to localising multiple nearby sources. Moreover, unlike some ERPs, DRs are inconsistent in latency and exhibit differences in morphology even for the same subject, stimulation region, and parameters. Therefore, averaging over various segments can be deceitful.

To address the limitations of conventional LCMV beamformer, numerous methods have been introduced previously, including LCMV with stochastic gradient (LCMV-SG) [183], LCMV with recursive least squares (LCMV-RLS) [184], and robust adaptive iterative suboptimal solution for LCMV (RAIS-LCMV) [185]. For example, in [185], the authors derive a low-complexity RAIS-LCMV using the conjugate gradient (CG) optimisation method. The steepest descent weight update strategy is adopted for this simple iterative process. The main contributions of the RAIS-LCMV approach are (1) lower computational complexity compared to CF-LCMV, achieved by using a CG optimisation method, (2) adaptive output adjusted to the measurements with convergence speed comparable to existing methods and (3) robust performance in challenging conditions, including low SNR and small numbers of snapshots (samples in a selected segment of input data). In RAIS-LCMV, the authors employ the steepest descent weight update strategy to create a simple iteration process. This approach differs from some other

recent methods that use more complex recursive least squares techniques for weight updates [185]. The simulation results reveal the superiority of this algorithm. However, although the mentioned iterative methods achieve better results than the conventional CF-LCMV, they are still sensitive to the overall power of the input signal. Therefore, these methods cannot fully differentiate between sources with similar power ranges that differ in morphology or detect low-power sparse events, in our cases sources responsible for the generation of SPES DRs.

4.2 AI-LCMV BEAMFORMER

Here, the aim is to develop an iterative adaptive beamformer that employs the DR morphology as an additional target for the beamformer output. This beamformer considers a dipole assumption of the source in three-dimensional space, and the considered template ensures a unique solution for the beamformer. In the conventional LCMV beamformer design, the main objective is to detect the source location by steering the beamformer toward maximum received power. In the closed-form solution of the LCMV beamformer [186], the weight vector $\mathbf{W}$ can be obtained from the solution to the multiple linearly constrained optimisation problem of minimising:

$$\frac{1}{2}\mathbf{W}^T\mathbf{R}\mathbf{W} \text{ subject to } \mathbf{G}^T\mathbf{W} = \mathbf{f}$$

where $\mathbf{R}_{xx}$ is the covariance matrix $(M \times M,\ M:$ number of channels$)$ of the recorded signal $\mathbf{X}$, $\mathbf{G}$ is the leadfield vector, and $\mathbf{f}$ is the vector indicating the unit gains in the considered directions of arrival. The optimal weight for the CF-LCMV beamformer is

$$\mathbf{W}_{\text{Optimal}} = \mathbf{R}^{-1}\mathbf{G}\left(\mathbf{G}^T\mathbf{R}^{-1}\mathbf{G}\right)^{-1}\mathbf{f} \tag{4.8}$$

and indicates the high sensitivity of the beamformer to the covariance and power of the input signal.

Previous studies have introduced various approaches, including RAIS-LCMV [187], to reduce computational complexity and achieve better performance for smaller sample sizes and higher robustness for low SNR recorded signals. Although previously established iterative methods can offer better performance compared to CF-LCMV, they remain sensitive to the covariance and power of the recorded activity and are, therefore, not ideal for identifying DR sources, which are generally spike-type with low power. To further improve the performance of the iterative form of the LCMV beamformer for such sources, a new adaptive approach is employed by adding a second constraint to the iterative LCMV formulation. This second constraint matches the output of the beamformer to the morphology of DRs as the source of interest. After each iteration,

the algorithm adjusts the weighting coefficients to minimise the output signal variance, similar to the main objective of the conventional LCMV beamformer, while adhering to the linear constraint related to the desired source due to the availability of information about the approximate shape of the DRs. After a sufficient number of iterations, the algorithm converges to the beamformer's optimal weighting coefficient, which helps identify the desired source.

Considering the general aim similar to the LCMV beamformer for minimising the output power, the weight vector $\mathbf{W}$ for each of the directions in the three-dimensional space, which can be used to measure the source activity is the solution to the following multiple linearly constrained optimisation problem:

$$\text{Minimise } \frac{1}{2}\mathbf{W}^T\mathbf{R}\mathbf{W} \quad \text{subject to} \quad \mathbf{G}^T\mathbf{W} = \mathbf{f} \quad \& \quad \mathbf{W}^T\mathbf{X} = \mathbf{U} \tag{4.9}$$

where $\mathbf{R} = \mathbb{E}\{\mathbf{X}(n)\mathbf{X}^T(n)\}$ is the covariance matrix of the recorded signal $\mathbf{X}$ and $\mathbf{U}$ in the second constraint ($\mathbf{W}^T\mathbf{X} = \mathbf{U}$) refers to the template as the desired source for the beamformer output with the same length as $\mathbf{X}$. Here $\mathbf{U} = \mathbf{Q}/\|\mathbf{G}\|$ where $\mathbf{Q}$ is a visible DR template selected from the SPES recordings as the desired source (output for the beamformer). Considering the objective optimisation of (4.9) and rewriting $\mathbf{W}^T\mathbf{X} = \mathbf{U}$ in the form of $\mathbf{X}^T\mathbf{W} = \mathbf{U}^T$, $\mathbf{W}$ can be obtained iteratively after converting the constrained problem to an unconstrained format using Lagrange multipliers:

$$J(\mathbf{W}) = \text{Min}\left(\frac{1}{2}\mathbf{W}^T\mathbf{R}\mathbf{W} + \lambda_1(\mathbf{f} - \mathbf{G}^T\mathbf{W}) + \lambda_2\|\mathbf{U}^T - \mathbf{X}^T\mathbf{W}\|^2\right) \tag{4.10}$$

where λ_1 and λ_2 are the Lagrange multipliers. By taking the gradient with respect to $\mathbf{W}$, the following equation can be reached:

$$\mathbf{W}(n+1) = \mathbf{W}(n) - \nabla_{\mathbf{W}}J(\mathbf{W}(n)) \tag{4.11}$$

where

$$\nabla_{\mathbf{W}}J(\mathbf{W}(n)) = \mathbf{R}\mathbf{W}(n) - \lambda_1\mathbf{G} - 2\lambda_2\mathbf{X}(\mathbf{X}^T\mathbf{W}(n) - \mathbf{U}^T) \tag{4.12}$$

Therefore, the following iterative equation is used to estimate $\mathbf{W}$:

$$\mathbf{W}(n+1) = \mathbf{W}(n) - \alpha(\mathbf{R}\mathbf{W}(n) - \lambda_1\mathbf{G} - 2\lambda_2\mathbf{X}(\mathbf{X}^T\mathbf{W}(n) - \mathbf{U}^T)) \tag{4.13}$$

where α is the non-negative step size considered for optimisation in each iteration that can alter the convergence rate. Considering the constraint $\mathbf{G}^T\mathbf{W} = \mathbf{f}$, pre-multiplying both sides of (4.13) by $\mathbf{G}^T$ yields:

$$\mathbf{f} = \mathbf{G}^T\mathbf{W}(n) - \alpha(\mathbf{G}^T\mathbf{R}\mathbf{W}(n) - \lambda_1\mathbf{G}^T\mathbf{G} - 2\lambda_2\mathbf{G}^T\mathbf{X}(\mathbf{X}^T\mathbf{W}(n) - \mathbf{U}^T)) \tag{4.14}$$

By considering λ_2 as $\lambda_2 = P\lambda_1$, λ_1 can be obtained from (4.14) as:

$$\lambda_1(n) = \frac{\mathbf{f} - \mathbf{G}^T\mathbf{W}(n) + \alpha\mathbf{G}^T\mathbf{R}\mathbf{W}(n)}{\alpha\mathbf{G}^T\mathbf{G} + 2\alpha P\mathbf{G}^T\mathbf{X}(\mathbf{X}^T\mathbf{W}(n) - \mathbf{U}^T)} \tag{4.15}$$

Therefore, by substituting the values for λ_1 and λ_2 in (4.13), $\mathbf{W}(n+1)$ can be estimated for each iteration. Finally, for equation (4.13) to be fully adaptive, $\mathbf{R}$ should also be estimated recursively. To do that, we adopt the iterative $\mathbf{R}$ estimation used in the RAIS-LCMV approach to reduce the estimation error [187].

$$\tilde{\mathbf{R}}(n) = \beta\tilde{\mathbf{R}}(n-1) + (1-\beta)\mathbf{X}(n)\mathbf{X}^T(n) \tag{4.16}$$

where $\tilde{\mathbf{R}}(n)$ is the estimate of the covariance matrix in the nth observation with β as a forgetting factor which determines a trade-off between adaptability and stability for the algorithm. By substituting $\tilde{\mathbf{R}}(n)$ in equation (4.13), the beamformer weight vector can be estimated in each iteration as:

$$\mathbf{W}(n+1) = \mathbf{W}(n) - \alpha(\tilde{\mathbf{R}}(n)\mathbf{W}(n) - \lambda_1\mathbf{G} - \lambda_2\mathbf{X}(\mathbf{X}^T\mathbf{W}(n) - \mathbf{U}^T)) \tag{4.17}$$

Here, the template selected for the AI-LCMV is a waveform with similar morphology to the DRs recorded by the intracranial channels, normalised by dividing it by the norm of the leadfield vector for each DOA. A smoother DR waveform is used as the template to enhance the overall beamformer performance and ensure the beamformer captures the constraint. This increases the likelihood of overlap between the template and the actual DRs. Figure 4.1 shows a sample template for the adaptive beamformer.

The initial weight vector for the beamformer is set to an $M \times 1$ vector of zero values. The initial covariance matrix $\tilde{\mathbf{R}}(0)$ is set to an $M \times M$ identity matrix while the forgetting factor β is set to a constant close to one (0.95) so that the model is stable while still reasonably adaptable to the changes in the input signal. The value of step size (α) and the ratio between λ_1 and λ_2 are empirically adjusted considering the convergence rate for $\frac{1}{2}\mathbf{W}^T\mathbf{R}\mathbf{W}$ and $\|\mathbf{W}(n+1) - \mathbf{W}(n)\|$ in order to find the best possible values. If the ratio of λ_1 to λ_2 (P) is too low, the weight for the second constraint related to the desired

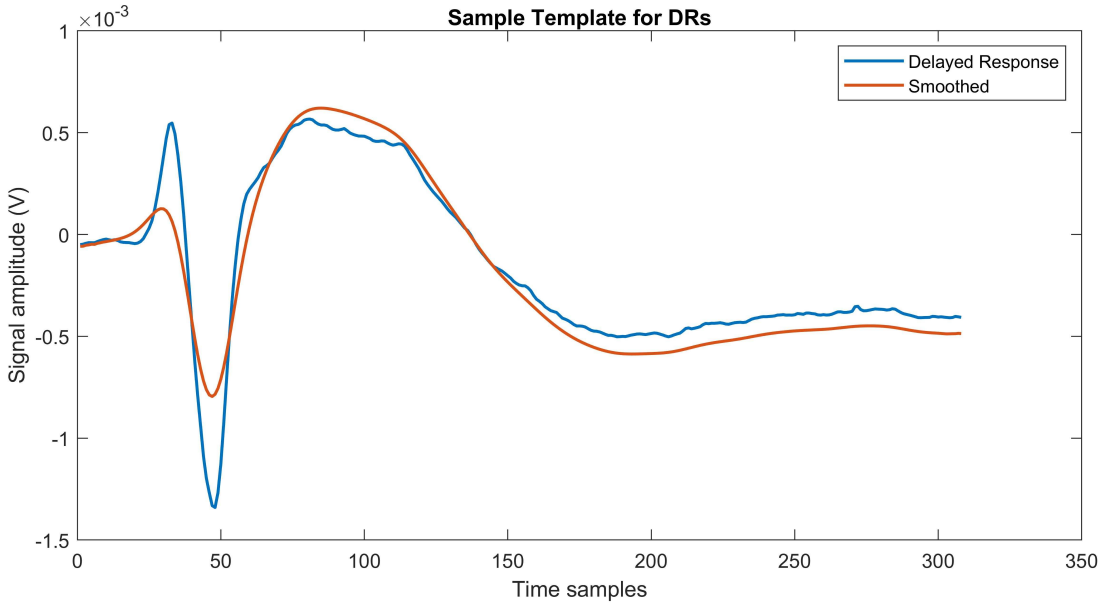

Figure 4.1: A sample DR selected from the recorded data and its smoothed version with similar morphology which is used as template in the AI-LCMV algorithm (variable Q).

template for the AI-LCMV becomes negligible, and therefore the results become similar to those of the conventional RAIS-LCMV beamformer. Increasing the value of P up to a specific threshold for each segment causes the $\frac{1}{2}\mathbf{W}^T\mathbf{R}\mathbf{W}$ and $\|\mathbf{W}(n+1)-\mathbf{W}(n)\|$ not to converge, in which case the optimal value for the weight cannot be reached. Figure 4.2 demonstrates the values of $\frac{1}{2}\mathbf{W}^T\mathbf{R}\mathbf{W}$ and $\|\mathbf{W}(n+1)-\mathbf{W}(n)\|$ for a selected segment.

4.3 DATASET AND HEAD MODEL ESTIMATION

The data used in this chapter (SPES procedure and parameters) has already been described in chapter 3. Figure 4.3 shows the brain X-ray scan after implantation of the intracranial electrodes (including the 32 electrodes in the subdural mat) for the SPES session, in addition to a window of recorded iEEG signals where SPES DRs are visible after stimulation artefact. As depicted in Figure 4.3, DRs do not necessarily appear after each stimulation of the same region (same SPES setup) and are not visible in all intracranial electrodes. For all cases included in this chapter, a 32-contact subdural array (mat) is placed on the cortex. Each subject's rectangular subdural mat contains a 32 platinum electrode array with 10 mm center-to-center intervals. The iEEG signals recorded using this array are used as the input sensor array for the adaptive beamformer, while the recorded data from the rest of the electrodes, in addition to ictal recordings, are used to identify the SOZ and assess the performance of the developed beamformer.

Overall, 76 data segments annotated by clinical experts with visible SPES DRs and 47 consecutive segments recorded using the same setup but with DRs invisible on the recording electrodes are employed as input data for the AI-LCMV algorithm. Table

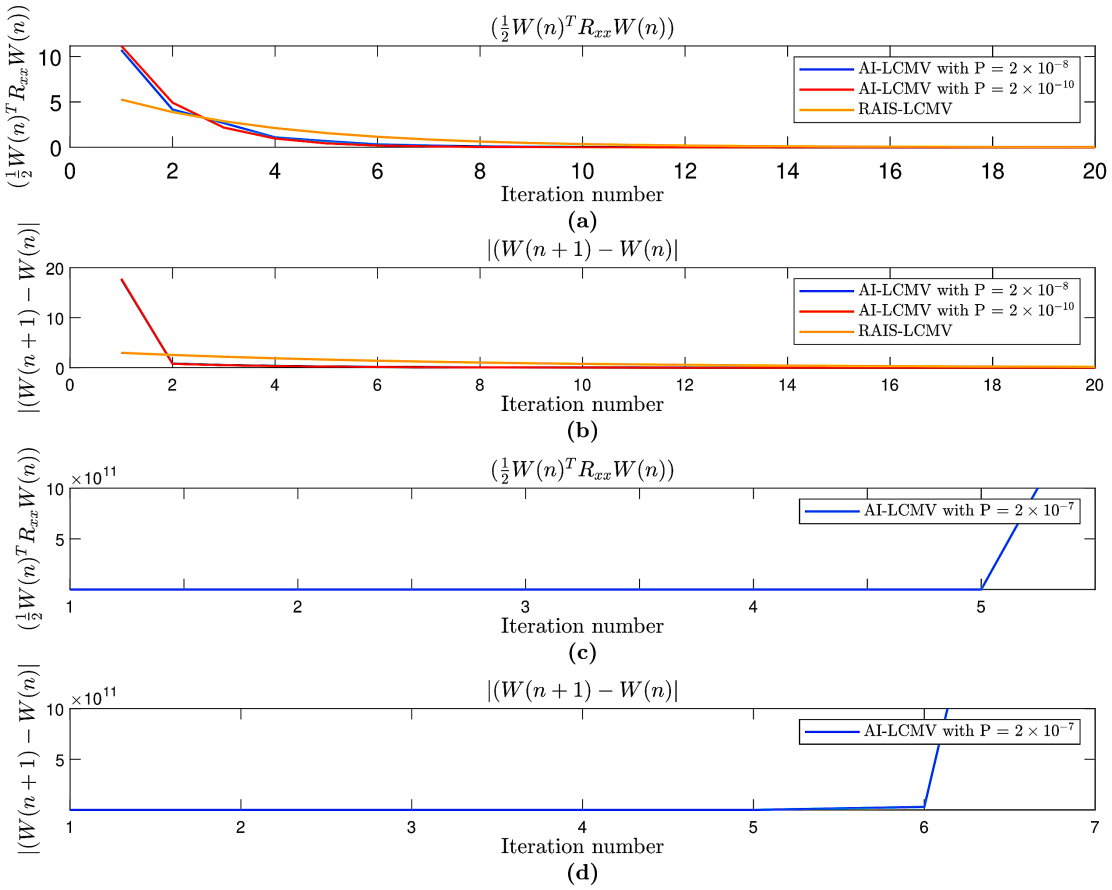

Figure 4.2: (a) Values of $\frac{1}{2}\mathbf{W}^T\mathbf{R}_{xx}\mathbf{W}$, and (b) $\|\mathbf{W}(n+1) - \mathbf{W}(n)\|$ for the same segment for both AI-LCMV with different P values and RAIS-LCMV with the same step size for a number of iterations averaged over all grid points. Plots (c) and (d) indicate an example of a wrong P value for the AI-LCMV beamformer which causes $\frac{1}{2}\mathbf{W}^T\mathbf{R}_{xx}\mathbf{W}$ and $\|\mathbf{W}(n+1) - \mathbf{W}(n)\|$ not to converge.

4.1 provides the information related to the cases involved in this study, including the surgical operation outcomes using the EOS [188].

In addition to the intracranial recordings, pre-operation MRI and post-operation CT scans are used to identify the anatomical positions of the implanted electrodes. These images are used to measure the head model and the leadfield matrix, which acts as the linear operator that links brain activity to the signals recorded by the intracranial electrodes. To estimate the leadfield matrix and localise the intracranial electrodes for each case, the subjects' pre-surgery MRI and post-surgery (after electrode implantation) CT images are co-registered using the anterior commissure-posterior commissure (ACPC) coordinate system. In ACPC, the origin is the anterior commissure, the negative y-axis passes through the posterior commissure, and the z-axis passes through a mid-hemispheric point in the superior direction. After identifying electrode locations, the leadfield matrix is measured for each subject to be used for the beamformer estimation. Various pairs of electrodes are used for stimulation during SPES recordings for each subject, necessitating multiple measurements of the leadfield matrix for each case

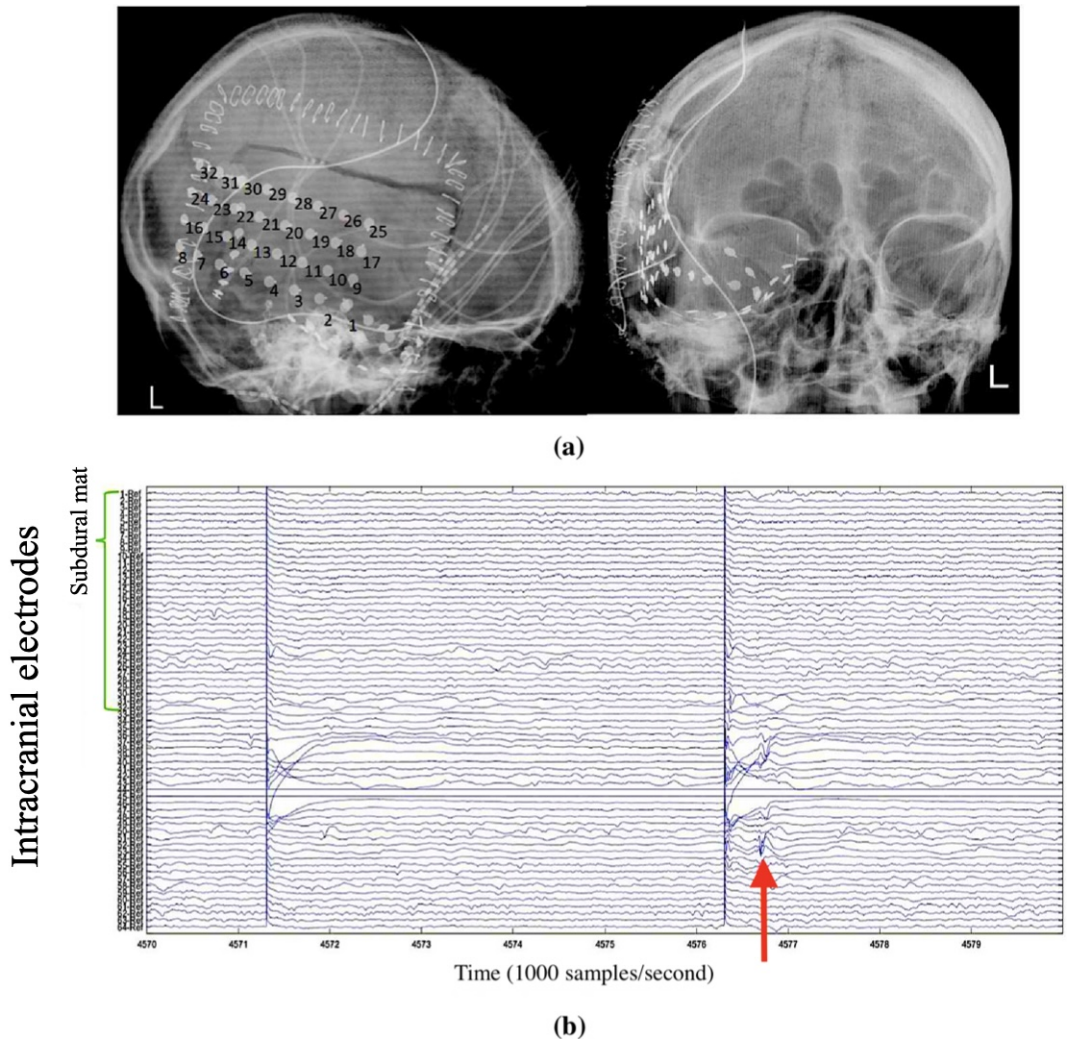

Figure 4.3: The X-Ray (a) shows the intracranial EEG channels implanted in the head of one DRE case included in this study with the electrode labels in the subdural mat alongside, (b) the data recorded using these channels during a SPES session. The red arrow indicates examples of observed DRs after SPES. Evidently, DRs are not necessarily visible in the data recorded using the subdural mat placed over the cortex (channels 1-32). For this segment of data, channels 44 and 45 have been used for stimulation and, therefore, are not used for data recording.

accordingly. The coregistration of CT-MRI images and the measurement of the leadfield matrix is conducted using the Fieldtrip toolbox [189].

4.4 EXPERIMENTS AND RESULTS

The AI-LCMV beamformer is applied to the annotated segments of 0.3 seconds that contain SPES DRs. To compare the performance, the RAIS-LCMV is also tried on the same segments. After DR source localisation, the Euclidean distance between the identified location with the maximum power and the electrodes closest to the SOZ for each case is calculated to monitor the relevant distance between the localised primary source and the SOZ. Figure 4.4 shows the results for both RAIS-LCMV and AI-LCMV algo-

Table 4.1: The number and locations of implanted electrodes alongside the result of surgery for each case (R=Right, L=Left, T=Temporal, F=Frontal, A=Anterior, P=Posterior, O=Occipital, In=Insular, H=Hippocampus, M=Mesial).

Case	Number and locations of electrodes	EOS
1	32 RT, 8 ROF, 8 RAT, 6 RMT, 6 RPT	I
2	32 RT, 5 Tpole, 5 MT, 5PMT, 5 AIn, 5 MIn, 5 PIn	I
3	32 RT, 8 RATP, 8 RAT, 8 RMT, 8 RPT	II
4	32 LT, 8 AF, 8 Motor, 8 PF, 8 O	No surgery

rithms for a sample data segment with DRs visible in iEEG data. The results from the tested segments suggest that the source identified using AI-LCMV is much more distinctive than that obtained by RAIS-LCMV, pointing to the possible region responsible for causing the SPES DRs. As expected, the subdural array captures the information related to the DR sources and can help identify them even if they are not visible at the subdural electrode positions.

Estimating the distance between the identified source using the beamformers and the SOZ reveals that the source identified using the AI-LCMV is, on average, 2.66 cm closer to the channel which is closest to the SOZ, compared to that identified by the RAIS-LCMV algorithm. This indicates that the source identified by AI-LCMV is closer to the SOZ in the brain and, therefore, more suited for clinical assessment. Figure 4.5 displays the localised DR source using AI-LCMV laid on pre-operation MRI slices for one case with the SOZ located at the right mesial-temporal region. The localised sources are highlighted over MRI slices using Fieldtrip toolbox [189]. The difference in the distance between the SOZ and the source identified using the RAIS-LCMV method was greater when the amplitude of the observed DRs was lower, confirming the advantage of AI-LCMV compared to the conventional iterative form in these cases.

In addition to the segments where the DRs were visible, both AI-LCMV and RAIS-LCMV were used for consecutive data segments where the SPES was applied using the same setup with similar parameters. However, the DRs were not visible in the data. Figure 4.6 shows the results of AI-LCMV and RAIS-LCMV beamformers for a segment where SPES DRs were not visible after the stimulation artefact. Here, the results of RAIS-LCMV show no distinctive source. In contrast, the AI-LCMV algorithm results reveal similar sources to the segments with visible DRs alongside other sources with comparable power levels. For the segments where the DRs were not visible, the AI-LCMV algorithm shows multiple active regions with notable power compared to the

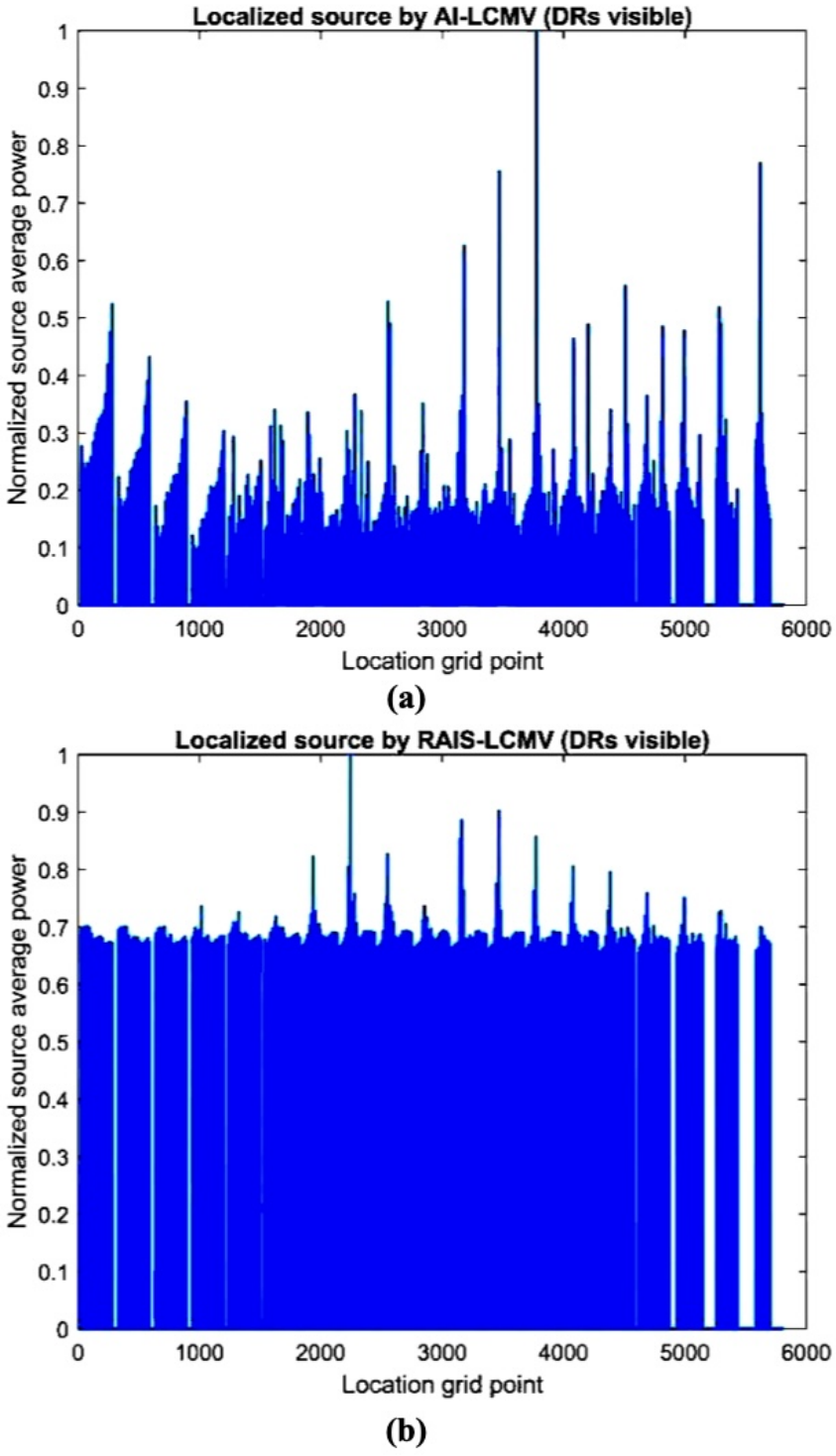

Figure 4.4: The normalised power for (a) the sources localised by the AI-LCMV and (b) RAIS-LCMV beamformers for each location in the head model for a single data segment where DRs are visible in multiple channels (not necessarily subdural mat used as input). As shown here, the main source (identified source with maximum power) using AI-LCMV is much more distinctive compared to that of the RAIS-LCMV method. Although the peaks are distanced from each other in number, they point towards the neighborhood of the same seizure generator depicted in the corresponding MRI.

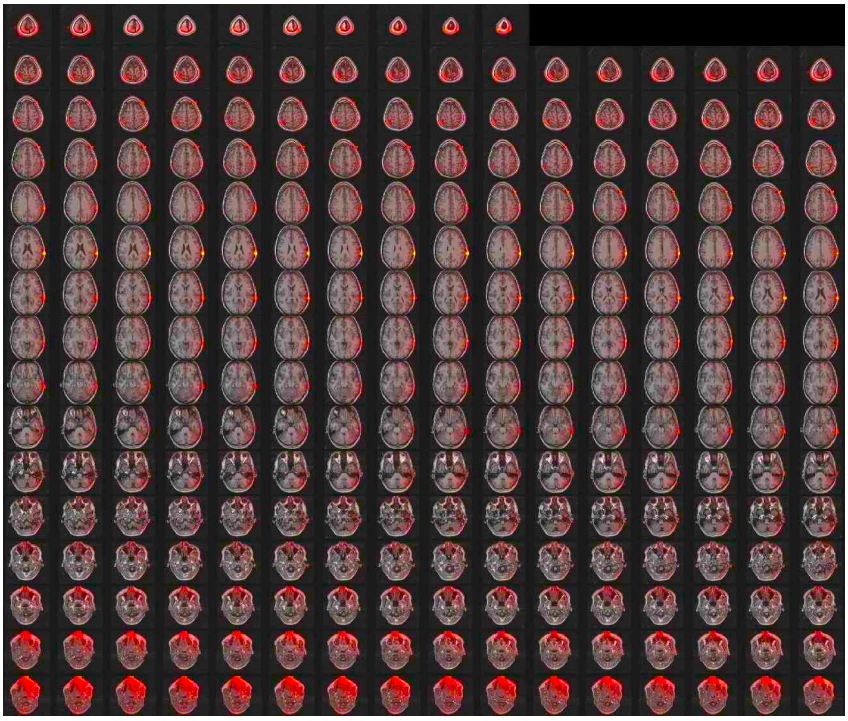

Figure 4.5: The locations of the DR sources in the brain via AI-LCMV beamformer. The identified source with the maximum power in the right temporal region is very close to the location SOZ for this case which according to the ictal recordings, is expected to be in the same region.

segments where DRs were visible in the iEEG data. Figure 4.7 illustrates the sources for the segments where DRs were not visible using AI-LCMV over MRI slices. The localised sources are highlighted over pre-operation MRI slices [189]. Similar to the segments where the DRs were visible, the localised primary source using AI-LCMV was closer (on average, 3.32 cm) to the location of the closest electrode to the SOZ compared to that achived by the RAIS-LCMV method. Finally, both algorithms were tested for 30 segments with no stimulation. The overall results for these segments did not indicate a clear pattern for the identified primary source. The results of AI-LCMV and RAIS-LCMV methods for the tested segments are shown in Table 4.2.

Identifying SPES DR sources is crucial to make the SPES recording sessions effective for the clinical examination of DRE cases. Previous research suggests that deep regions such as the amygdala, hippocampus, frontal cortex, temporal cortex, and olfactory cortex are frequently noted as potentially epileptogenic [190]. The DRs generated in these areas can be located very deep in the brain, making some DRs invisible to the implanted electrodes. This highlights the necessity for a method to identify DRs that are invisible to the subdural channels.

Current clinical practice identifies DRs when the source is close to an implanted intracranial electrode. However, the proposed method allows for the localisation of these sources even when they are not detected by any individual electrode, which can also compensate for possible errors during the electrode implantation process. This is possi-

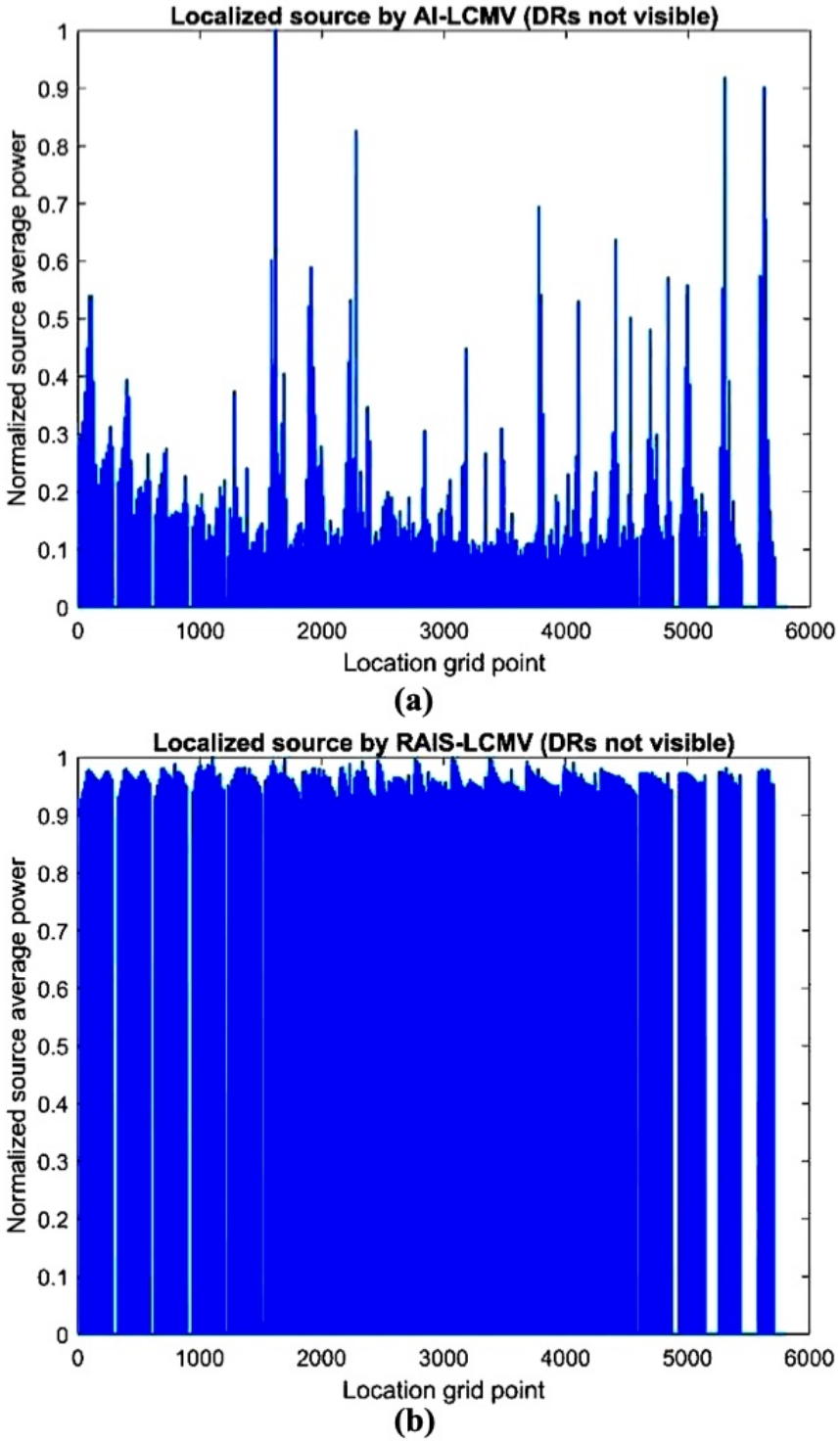

Figure 4.6: The normalised power for (a) the sources localised by the AI-LCMV and (b) RAIS-LCMV beamformers for each location in the head model for a single data segment where DRs were not visible in any channels while stimulation is applied using the same pair of channels (same SPES setup). As shown here, the primary source via AI-LCMV is much more distinctive than the RAIS-LCMV method. The average power of the secondary sources is closer to the maximum value than the segments where DRs are visible.

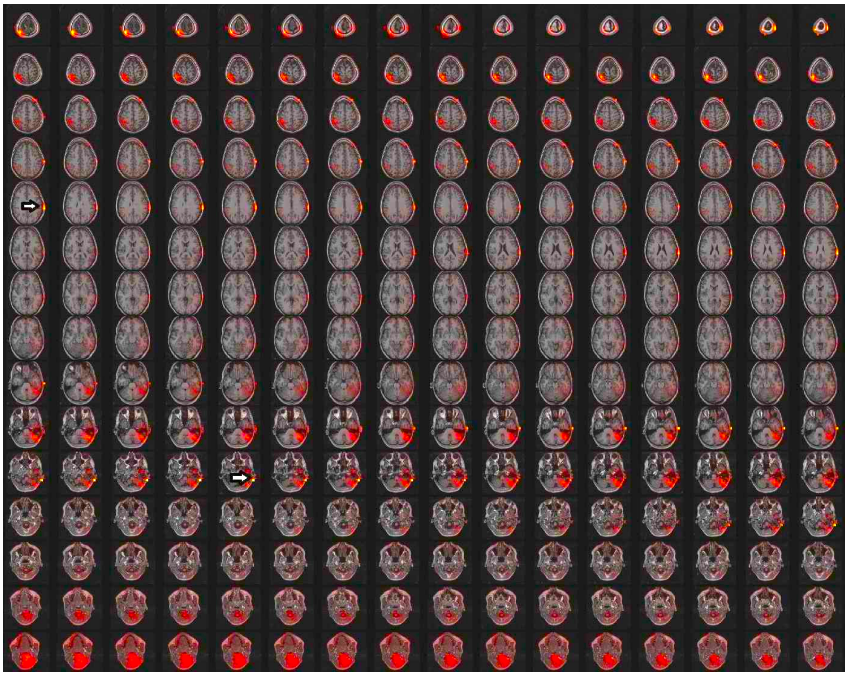

Figure 4.7: The locations of identified brain source via AI-LCMV beamformer. Compared to the segments where DRs are visible, here, with invisible DRs, the secondary sources close to the primary source are shown with the white arrow.

Table 4.2: The number of tested segments for each case where DRs were visible (not necessarily in subdural mat used as input) alongside the Euclidean distance between the estimated location and SOZ using AI-LCMV and RAIS-LCMV methods. The same numbers are also reported for the consecutive segments with the same SPES setup where DRs were not visible in any channels. (N: number of tested segments, D: average distance between the primary source and SOZ, (v): DRs visible in multiple channels, (inv): DRs not visible in any of the implanted channels).

	RAIS-LCMV				AI-LCMV			
Case	N(v)	D (cm)	N(inv)	D (cm)	N(v)	D (cm)	N(inv)	D (cm)
1	23	4.5 ± 0.36	12	5.9 ± 0.4	23	1.8 ± 0.56	12	2.9 ± 0.62
2	18	5.21 ± 0.22	15	6.52 ± 0.52	18	1.4 ± 0.37	15	2.6 ± 0.4
3	20	4.35 ± 0.51	10	6.95 ± 0.81	20	2.5 ± 0.33	10	3.5 ± 0.45
4	15	3.8 ± 0.31	10	5.5 ± 0.68	15	1.5 ± 0.4	10	2.8 ± 0.78

ble due to propagating such sources over the subdural sensor array, which captures the relevant information. Consequently, the subdural sensor array improves the ability to detect DR sources, including those that are not visible at any of the individual electrode locations, thereby improving the overall effectiveness of SPES sessions.

Some researchers have discussed the possible benefits of a probabilistic interpretation of responses to brain stimulation and their variabilities, even within an individual [191]. Although recent studies have shown the capability of conventional beamforming methods like the LCMV beamformer in seizure localisation [192], these methods are

not suitable for low-power, spike-like events like DRs. The alterations in the amplitude and morphology of DRs present a challenge for the conventional beamforming methods, which are sensitive to the power of recorded signals. A more robust beamformer has been proposed and applied in this study to address this sensitivity and guide the beamformer in localising sources with specific characteristics. The existing cortical sensor array (subdural mat) allows us to best exploit the footprints of visible and invisible sources across all channels to localise the source of DRs. It also allows us to identify IEDs due to their similar morphology, often coexisting with DRs in epileptic brains [193].

In addition to the segments where DRs are visible, both AI-LCMV and RAIS-LCMV were applied to consecutive segments where stimulation was conducted using the same pair of channels, but DRs were not visible in any of the intracranial EEG channels implanted in the brain. In contrast to the conventional method, which was unsuccessful in identifying the primary active source in the brain after stimulation, the AI-LCMV revealed secondary active sources in these segments in addition to the primary source with comparable power. The additional active regions identified for the segments where DRs were invisible are close to the region with the maximum power and the seizure onset zone, without a clear pattern among the subjects in this study. These results are encouraging, as previous research indicates that one key difference between evoked responses (ERs) and DRs is that DRs are less consistent in appearance [194]. Given that DRs and IEDs are sparse and low-power in nature, traditional power-based beamformers often fail in their localisation. Therefore, the proposed AI-LCMV outperforms such beamformers by considering the expected shape of the targets.

In addition to localising DRs to SPES and similar epileptiform activities, the AI-LCMV method developed in this study can enhance our understanding of brain synchronisation [54, 195]. This offers an excellent opportunity for a more comprehensive examination of the E-I imbalance and seizure generation and propagation models. Considering that the excitatory activity is more localised than inhibitory activity, having a robust method to monitor and localise these components using subdural channels is highly valuable. Finally, it has been suggested that the brain responses to electrical stimulation can be recorded using high-density EEG (EEG setup with a large number of electrodes), capturing the shape and location of brain responses more accurately than what can be achived using normal sEEG [196]. The use of proposed AI-LCMV beamformer in better localisation of DR sources is the major practical contribution of this chapter. This achievement is a significant step towards the localisation of SOZ in the epileptic brain.

While the findings and advantages of the established method in this chapter are significant, there are a few points worth considering for further improvement. First, a more accurate pipeline for identifying the locations of intracranial electrodes through more precise coregistration of CT-MRI images to estimate the leadfield matrix can fur-

ther improve the beamformer's accuracy, overcoming the problem of anatomical brain shift after the surgical operation. Secondly, the DR template here is considered similar to the DRs visible in other available implanted electrodes for each subject. A dictionary of DR templates can be used instead to account for variability in DR morphology. This is expected to improve the accuracy of the algorithm. Finally, the geometry of the subdural mat has been the same for all the subjects included in this chapter (a standard size commonly used in operation). Therefore, the developed AI-LCMV method was not tested with subdural mats of different geometries. In general, the sensor array geometry and the spacing between sensors determine the resolution and beamwidth of the beamformer. Smaller inter-sensor spacing allows for higher spatial resolution and narrower beamwidth. Larger spacing provides broader beamwidth with lower resolution.

4.5 CONCLUSION

The objective of this chapter is to establish the groundwork for DR source localisation highly applicable to DRE cases by analysing the brain's SPES DRs. The DR sources in DRE patients with subdural mat are identified, enabling the localisation of hyperexcitable and potentially epileptogenic regions in the brain that are not close to the intracranial electrodes. A regularised iterative LCMV beamformer called AI-LCMV has been designed and used to identify the DR primary sources to achieve a more accurate and robust localisation solution. This is accomplished using an array of electrodes arranged in a mat-like structure placed on the cortex. This new pipeline allows for a more comprehensive and accurate mapping of the brain's electrical activity. Compared to conventional localisation methods, the approach used here better suits the characteristics of the recorded responses to SPES and IEDs, overcoming the general spatial limitations of intracranial recordings. The AI-LCMV algorithm introduced and examined in this chapter has the potential to greatly impact the assessment stage in clinical practice for DRE cases prior to resection surgery for possible candidates. Moreover, detecting DRs that are invisible to the recording electrodes can considerably improve the certainty in localising SOZ following comprehensive statistical validation. Although AI-LCMV and RAIS-LCMV algorithms have been tested on numerous segments from four DRE subjects, and the results indicate the better performance of AI-LCMV, there is still room for improvement particularly on spatial side lobe supression. The AI-LCMV, like other LCMV approaches, is fairly sensitive to possible highly correlated sources near each other, and the additional constraint in the algorithm makes the beamformer vulnerable to possible temporal delay mismatch between the selected template and the beamformer's output. Additionally, incorporating a dictionary of desired templates, more accurate head models for subjects undergoing surgery, and even customised subdural mats with specific geometry can help improve the accuracy and practicality of the

established AI-LCMV method. The following chapters aim to improve the AI-LCMV algorithm and solve the shortcomings of this method.

5

INVESTIGATING THE COMMONALITY OF DR AND IED SOURCES

IEDs are distinctive electrical patterns observed in the EEG of individuals with epilepsy [197]. These abnormal waveforms typically manifest as sharp waves or spikes that stand out from the background brain activity, characterised by their high amplitude and brief duration [197]. IEDs are considered a hallmark of epilepsy, occurring between seizures (interictal periods) and reflecting the underlying epileptogenic potential of the brain. They result from the synchronous firing of a population of neurons, producing a summation of excitatory and inhibitory postsynaptic potentials [198]. The presence of IEDs can significantly increase the probability of a seizure happening and can provide useful information about the location of SOZ [197, 199]. Accurately identifying the IEDs requires expertise in EEG interpretation, as normal variants and artefacts can sometimes be mistaken for epileptiform activity [197]. IEDs [200], which may or may not be frequent in the data recorded during interictal periods, are considered a meaningful biomarker for epilepsy.

In case DRs and IEDs originate from common locations and the DRs can be accurately localised, there will be a significant step in SOZ identification. The solution to this critical question has been investigated in this chapter. For this, the morphology of DRs and IEDs as spike-type events and their variability in the temporal domain has been exploited to develop new constraints for an adaptive Bayesian beamformer that outperforms the conventional and proposed beamformer in Chapter 4 (AI-LCMV). Similar to chapter 4, this algorithm is applied to a subdural iEEG electrode array (subdural mat). The significant outcome of applying this beamformer reveals that the IEDs and DRs associated with seizure for a DRE case originate from the same primary location in the brain.

As mentioned previously, the conventional form of LCMV beamformer is not robust when the SNR for the input signal is low. To solve this problem, in the previous chapter, the AI-LCMV algorithm was developed and employed to identify the DR sources where the use of a template as the desired source in the form of an additional constraint improved the localisation accuracy. It also solved the problem of conventional LCMV beamformer sensitivity to low SNR input to a degree [55]. Although the AI-LCMV beamformer in its regularised format demonstrated significant refinement over the conventional algorithm, especially when the DRs are not visible to the implanted intracranial electrodes, the performance is still questionable due to the possible temporal mismatch between the selected template and the algorithm output. This is mainly

due to using Euclidean distance as the similarity measure between the chosen template as the desired source and the beamformer output at each iteration. Moreover, another limitation of the AI-LCMV algorithm, like the conventional format, is the beamformer's low sensitivity to multiple nearby sources when trying to distinguish them from each other, mainly when they are temporally correlated [201]. To exclude the likely effect of nearby correlated sources, a model data covariance estimation by sparse Bayesian learning (SBL) has been incorporated into a localisation algorithm recently [202]. As a result, compared to conventional LCMV beamformer for identifying multiple correlated sources the performance has been improved [202].

In this chapter, a new regularised beamforming pipeline named adaptive Bayesian with multiple constraints (ABMC) employs the cross-correlation between the selected template as the desired target source and the beamformer output for each iteration as the additional constraint to the LCMV. It also incorporates sparse Bayesian learning to the covariance estimation [203] in which possible correlation between active sources is exploited and excluded from the input data fed to the beamforming algorithm. In the cases where the source of DRs or IEDs are spatially close to each other and correlated in time domain, this approach enhances the localisation performance. The ABMC algorithm developed here considers the morphology of IEDs and DRs as the desired target source and mitigates the effects of correlated sources exploiting the covariance of input signals.

5.1 DATASET AND HEAD MODEL ESTIMATION

The iEEG signals recorded from five DRE cases have been included in this chapter. Similar to the data included in the previous chapters, for each subject, the unique SPES setup, including the type, number, and location of the electrodes, is chosen based on the presumed location of epileptogenic regions using the medical history and other relevant clinical information and inspecting potential brain cortical functions. The SPES setup has already been explained in previous chapters. Table 5.1 displays the information for each case, including the number and locations of the intracranial electrodes and the EOS score after resection operation[204].

Here, pre-operation MRI and post-operation CT scans are used to identify the anatomical positions of the intracranial electrodes and to estimate the head model used to estimate the leadfield matrix, which is used as the linear operator linking brain activity sources to the recorded iEEG signals. The coregistration of pre-operation MRI and post-operation CT is performed through a pipeline implemented in Lead-DBS [205]. In this process, the CT images are first registered to the MRIs, then the volumes are normalised, and finally, any potential brain shift due to the surgery is compensated for [206–208]. The co-registration outcomes are utilised to localise the electrodes using

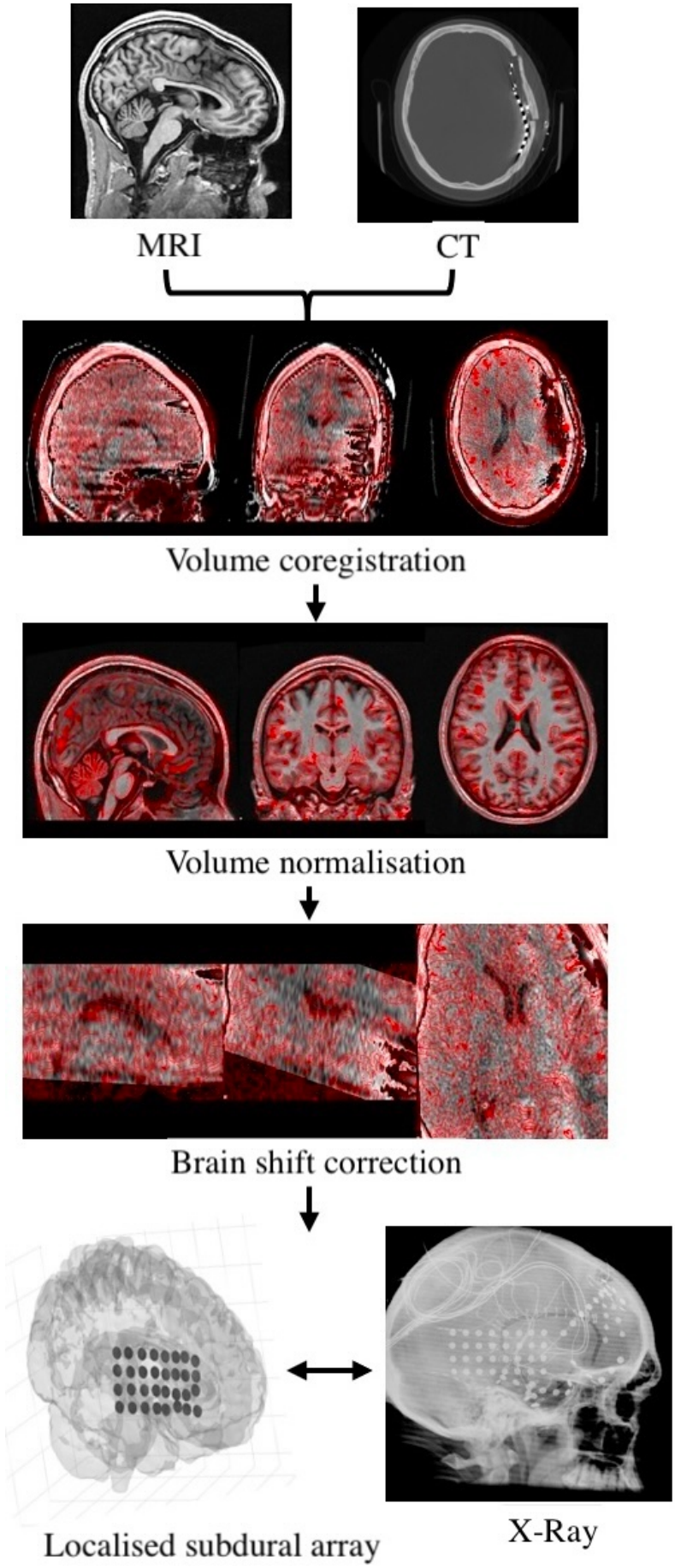

Figure 5.1: The pipeline for coregistration of pre- and post-operation MRI and CT images and localisation of intracranial electrodes (including the subdural mat used as the input array of signals for the beamformer).

Table 5.1: The number and locations of implanted intracranial electrodes alongside the result of surgery for each case (R=Right, L=Left, T=Temporal, F=Frontal, A=Anterior, P=Posterior, O=Occipital, In=Insular, H=Hippocampus, M=Mesial).

Case	Number and locations of electrodes	EOS
1	20 LT, 4 Posterior Superior Parietal, 8 Mid Parietal, 8 Inferior Parietal	No surgery
2	32 RT, 8 RF, 8 Central	II
3	20 RT, 8 RF, 8 AT, 8 SubT	No surgery
4	32 RT, 5 Tpole, 5 MT, 5 PMT, 5 AIn, 5 MIn, 5 PIn	I
5	32 RT, 8 RATP, 8 RAT, 8 RMT, 8 RPT	II

Fieldtrip [174], and LeGUI [209] independently. These results are then compared by professionals to make sure the process is as accurate as possible. The final co-registered images and electrode positions are used to measure the leadfield matrix for the ABMC beamformer. Similar to the procdure in Chapter 4, since various pairs of electrodes are used for stimulation during the SPES session for each case, the leadfield matrix is measured multiple times for each subject accordingly. Figure 5.1 displays the pipeline for coregistration of pre- and post-implantation MRI and CT scan images.

5.2 ABMC ALGORITHM

Considering the LCMV beamformer's sensitivity to the SNR for the input signal and its deficiency in distinguishing nearby correlated sources, the ABMC beamformer is developed and employed here. The ABMC beamformer mitigates the potential effects of correlated sources by employing a sparse Bayesian algorithm for covariance estimation. Also, the cross-correlation between the beamformer output and the selected template is used as an additional constraint. In each iteration, the algorithm adjusts the weights to minimise the output signal variance, similar to the primary objective of the LCMV and AI-LCMV beamformers, while adhering to the additional constraint. This constraint exploits the maximum cross-correlation between the beamformer's output and the chosen DR or IED template for the desired source at the right time lag. After sufficient iterations, the ABMC algorithm converges to the beamformer's optimal parameters, which can be used to identify the primary source. The formulations for the ABMC beamformer are presented below.

Consider the brain source activity $\mathbf{s}(t) = [s_1(t), \ldots, s_N(t)]^\intercal$ at time instant t ($t = 1, \ldots, T$), and the leadfield matrix $\mathbf{G} = [\mathbf{g}_1 \ldots \mathbf{g}_N] \in \mathbb{R}^{M \times N}$ where M is the number of

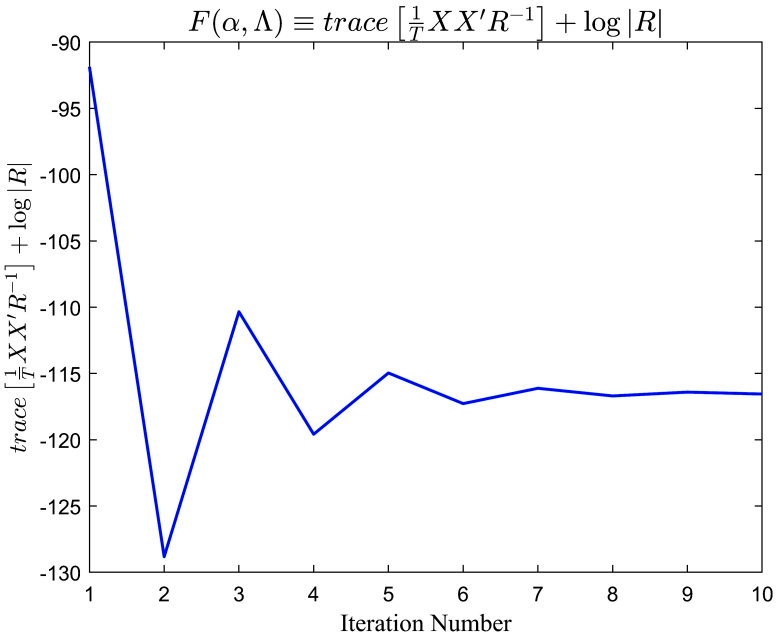

Figure 5.2: Convergence plot for trace $\left[\frac{1}{T}\mathbf{X}\mathbf{X}^{\intercal}\mathbf{R}^{-1}\right] + \log|\mathbf{R}|$ for a selected segment of data.

electrodes in the subdural mat and N is the number of grid points in the head model. Then, the linear model for brain activity can be presented as:

$$\mathbf{x}(t) = \sum_{n=1}^{N} s_n(t)\mathbf{g}_n + \boldsymbol{\varepsilon}(t) \tag{5.1}$$

where $\mathbf{x}(t) = [x_1(t), \ldots, x_M(t)]^{\intercal}$ is the recorded signal using the subdural mat and $\varepsilon(t)$ represents noise. This equation is initially presented for scalar values, but an extension to vector leadfields that considers source orientation in a three-dimensional head model is utilised in the calculations. Additionally, for simplicity, we define $\mathbf{X} = [\mathbf{x}(1), \ldots, \mathbf{x}(T)]$ and $\mathbf{S} = [\mathbf{s}(1), \ldots, \mathbf{s}(T)]$.

To derive an estimation for the input signal array covariance via sparse Bayesian learning, equation (5.1) is converted into its probabilistic form. This conversion involves defining prior distributions for the unknown variables, outlined as follows:

$$(\mathbf{x}(t) \mid \mathbf{s}(t)) = N(\mathbf{x}(t) \mid \mathbf{G}\mathbf{s}(t), \boldsymbol{\Lambda}) \tag{5.2}$$

The diagonal noise covariance is denoted as $\boldsymbol{\Lambda} = \text{diag}(\lambda_1, \ldots, \lambda_M)$. The noise is assumed to have a zero-mean Gaussian distribution. The source prior distribution is represented as:

$$p\left(\mathbf{s}(t) \mid \boldsymbol{\alpha}\right) = \prod_{n=1}^{N} N(s_n(t) \mid 0, \alpha_n) \tag{5.3}$$

where $\boldsymbol{\alpha} = \text{diag}(\alpha_1, \ldots, \alpha_N)$ and α_n is the prior variance for the activity of the n-th grid location in the head model. The process of estimating the hyperparameters and noise covariance for each grid point is linked to the maximisation of the marginal likelihood $p(\mathbf{X} \mid \boldsymbol{\alpha}, \boldsymbol{\Lambda})$.

$$p(\mathbf{X} \mid \boldsymbol{\alpha}, \boldsymbol{\Lambda}) = \prod_{t=1}^{T} N(\mathbf{x}(t) \mid 0, \mathbf{R}) \tag{5.4}$$

The input signal covariance $\mathbf{R}$ can be expressed as a matrix in which the sources are assumed to be uncorrelated, and $\boldsymbol{\alpha}$ is considered as an uncorrelated source covariance matrix where:

$$\mathbf{R} = \mathbf{G}\boldsymbol{\alpha}\mathbf{G}^{\mathsf{T}} + \boldsymbol{\Lambda} \tag{5.5}$$

The estimation of hyperparameters and data covariance can be achieved through type-II maximum likelihood or by minimising the cost function [202]:

$$F(\boldsymbol{\alpha}, \boldsymbol{\Lambda}) \triangleq -2 \log p(\mathbf{X} \mid \boldsymbol{\alpha}, \boldsymbol{\Lambda}) \quad \equiv \text{tr}\left[\frac{1}{T}\mathbf{X}\mathbf{X}^{\mathsf{T}}\mathbf{R}^{-1}\right] + \log|\mathbf{R}| \tag{5.6}$$

To minimise the non-convex cost function in (5.6), a majorisation-minimisation approach [210] is followed, providing a convex upper-bound limit as an alternative cost function for optimisation. Here, $\mathbf{z} = \text{diag}(z_1, \ldots, z_N)$ and $\mathbf{h} = \text{diag}(h_1, \ldots, h_M)$ are auxiliary parameters, with z_0 and h_0 being scalar terms dependent only on $\mathbf{z}$ and $\mathbf{h}$ [211, 212].

$$\begin{aligned} F(\boldsymbol{\alpha}) =& \frac{1}{T}\sum_{t=1}^{T} \mathbf{x}^{\mathsf{T}}(t)\mathbf{R}^{-1}\mathbf{x}(t) + \log|\mathbf{R}| \\ &\leq \frac{1}{T}\sum_{t=1}^{T}\left[\left(\mathbf{x}(t) - \mathbf{G}\bar{\mathbf{s}}(t)\right)^{\mathsf{T}}\boldsymbol{\Lambda}^{-1}\left(\mathbf{x}(t) - \mathbf{G}\bar{\mathbf{s}}(t)\right)\right] \\ &+ \frac{1}{T}\sum_{t=1}^{T}\left[\bar{\mathbf{s}}^{\mathsf{T}}(t)\boldsymbol{\alpha}^{-1}\bar{\mathbf{s}}(t)\right] + \text{tr}(\mathbf{z}^{\mathsf{T}}\boldsymbol{\alpha}) - z_0 \end{aligned} \tag{5.7}$$

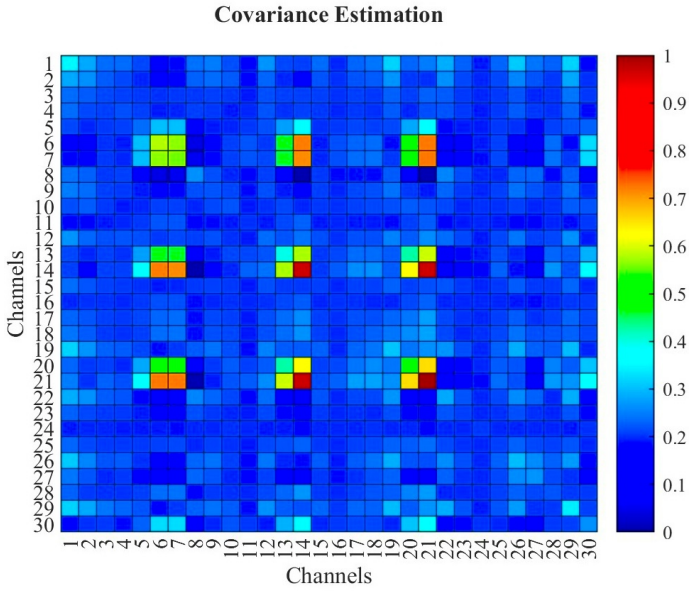

(a)

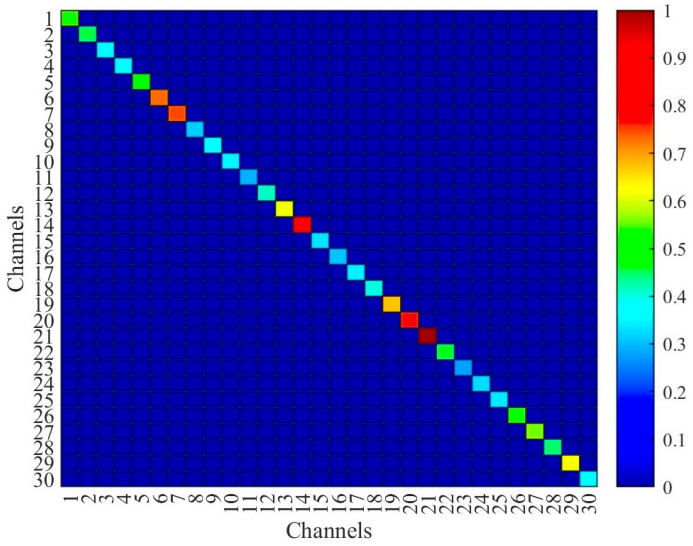

(b)

Figure 5.3: The covariance of (a) input signal $\mathbf{X}$ (i.e., $\frac{1}{T}\mathbf{X}\mathbf{X}^\intercal$) and (b) the estimated covariance using the sparse Bayesian learning algorithm after sufficient iterations.

$$
\begin{aligned}
F(\mathbf{\Lambda}) =& \frac{1}{T}\sum_{t=1}^{T}\mathbf{x}^\intercal(t)\mathbf{R}^{-1}\mathbf{x}(t) + \log|\mathbf{R}| \\
&\leq \frac{1}{T}\sum_{t=1}^{T}\left[(\mathbf{x}(t)-\mathbf{G}\bar{\mathbf{s}}(t))^\intercal\,\mathbf{\Lambda}^{-1}\,(\mathbf{x}(t)-\mathbf{G}\bar{\mathbf{s}}(t))\right] \\
&+ \frac{1}{T}\sum_{t=1}^{T}\left[\bar{\mathbf{s}}^\intercal(t)\boldsymbol{\alpha}^{-1}\bar{\mathbf{s}}(t)\right] + \mathrm{tr}(\mathbf{g}^\intercal\mathbf{\Lambda}) - g_0
\end{aligned}
\tag{5.8}
$$

The convex bounding update rule for the n-th grid position variance and m-th channel noise variance is derived by equalling the derivatives of $F(\boldsymbol{\alpha})$ and $F(\boldsymbol{\Lambda})$ with respect to α_n and λ_m to zero, resulting in:

$$\widehat{\alpha}_n = \sqrt{\frac{\frac{1}{T}\sum_{t=1}^{T} \bar{s}_n^2(t)}{\hat{z}_n}} \tag{5.9}$$

$$\widehat{\lambda}_m = \sqrt{\frac{\left[\sum_{t=1}^{T} \left(\mathbf{x}\left(t\right) - \mathbf{G}\bar{\mathbf{s}}(t)\right)\left(\mathbf{x}\left(t\right) - \mathbf{G}\bar{\mathbf{s}}(t)\right)^{\mathsf{T}}\right]_{mm}}{T\hat{h}_m}} \tag{5.10}$$

The update rule for $\mathbf{z}$ and $\mathbf{h}$ involves finding two hyperplanes $\mathbf{z}^{\mathsf{T}}\boldsymbol{\alpha} - z_0$ and $\mathbf{h}^{\mathsf{T}}\boldsymbol{\Lambda} - h_0$ that tightly bound $\mathbf{R}$ given $\boldsymbol{\alpha}$ and $\boldsymbol{\Lambda}$. These hyperplanes, tangential to $\mathbf{R}$, lead to updated values for $\mathbf{z}$ and $\mathbf{g}$ given by [213]:

$$\hat{z}_n = \mathbf{g}_n^{\mathsf{T}}\mathbf{R}\mathbf{g}_n \tag{5.11}$$

$$\hat{g}_m = \mathbf{R}_{mm} \tag{5.12}$$

The update rule for $\bar{s}_n\left(t\right)$ is presented in:

$$\bar{s}_n\left(t\right) = \widehat{\alpha}_n \mathbf{g}_n^{\mathsf{T}}\mathbf{R}\mathbf{x}(t) \tag{5.13}$$

The iterative estimation process for the covariance of the input signals, while excluding the effect of correlated sources, involves iterating across equations (5.9) to (5.13) and substituting $\boldsymbol{\alpha}$ and $\boldsymbol{\Lambda}$ in equation (5.5). Figure 5.2 illustrates the convergence plot for equation (5.6) after ten iterations. After sufficient iterations, the estimated covariance is then used adaptively to estimate the weights for the beamformer. Figure 5.3 shows the estimated covariance for a segment of data after a sufficient number of iterations.

Considering that the aim of ABMC beamformer is to minimise the output power while matching the output to the desired target template, the weight vector $\mathbf{W}$ for each of the x, y, and z directions in the three-dimensional space is the solution to the following multiple linearly constrained optimisation problem:

$$\min_{\mathbf{W}} \left(\frac{1}{2}\mathbf{W}^{\mathsf{T}}\mathbf{R}\mathbf{W}\right) \quad \text{subject to} \quad \mathbf{G}^{\mathsf{T}}\mathbf{W} = \mathbf{f} \quad \& \quad \max_{\mathbf{W}} \left(\mathbf{W}^{\mathsf{T}}\mathbf{X} \cdot \mathbf{u}\right)$$

where **R** is the estimated covariance matrix, **W** is the weight vector for the beamformer, and **u** (a visible IED or DR template selected from the recordings) in the additional constraint refers to the selected template as the desired source (beamformer's output) with the same length as **X**. Figure 5.4 demonstrates examples of different IEDs observed in the intracranial data for a single case. This optimisation can be iteratively executed after converting the constrained problem to an unconstrained one using Lagrange multipliers:

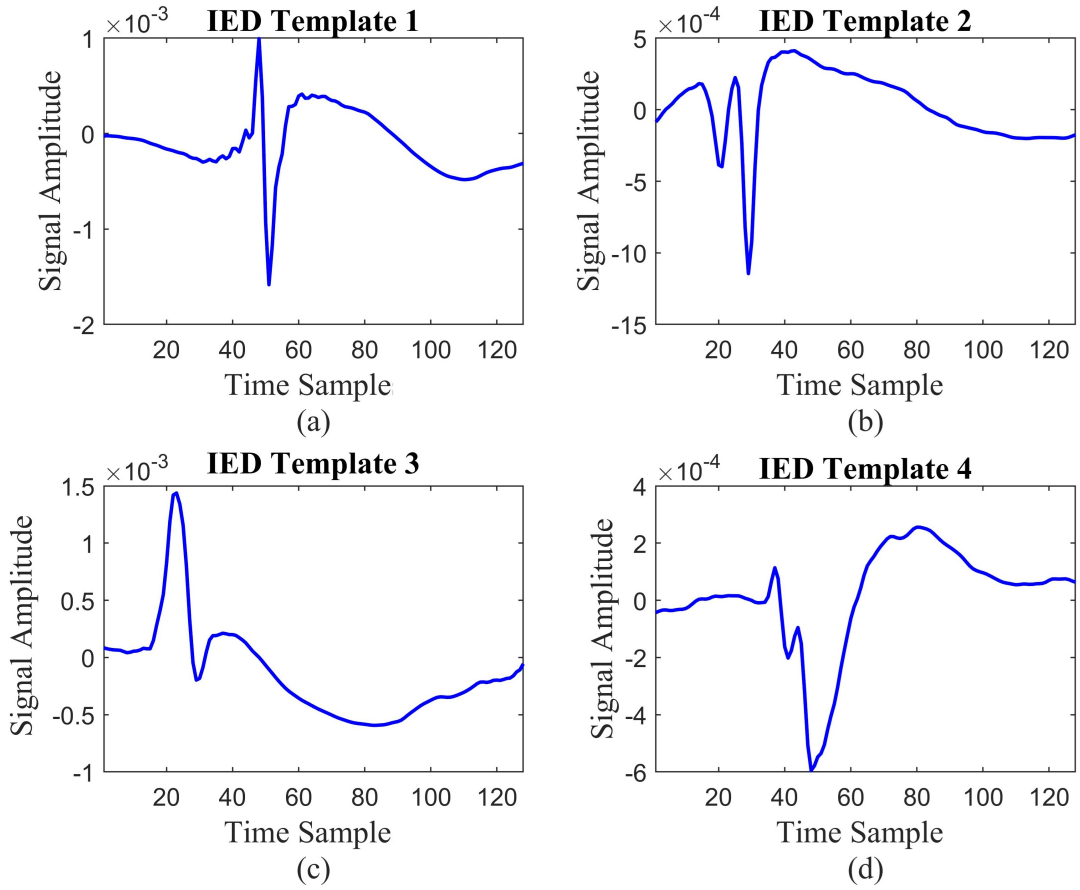

Figure 5.4: Various templates (a)-(d) selected as the desired source for identification of the IED source for a single case.

$$J(\mathbf{W}) = \text{Min}\left(\frac{1}{2}\mathbf{W}^{\intercal}\mathbf{R}\mathbf{W} + \beta_1(\mathbf{f} - \mathbf{G}^{\intercal}\mathbf{W}) - \beta_2(\mathbf{W}^{\intercal}\mathbf{X} \cdot \mathbf{u})\right) \tag{5.14}$$

where β_1 and β_2 are the Lagrange multipliers. By measuring the gradient with respect to **W**, the following equation can be reached:

$$\mathbf{W}(n+1) = \mathbf{W}(n) - \mu\nabla_{\mathbf{W}}J(\mathbf{W}(n)) \tag{5.15}$$

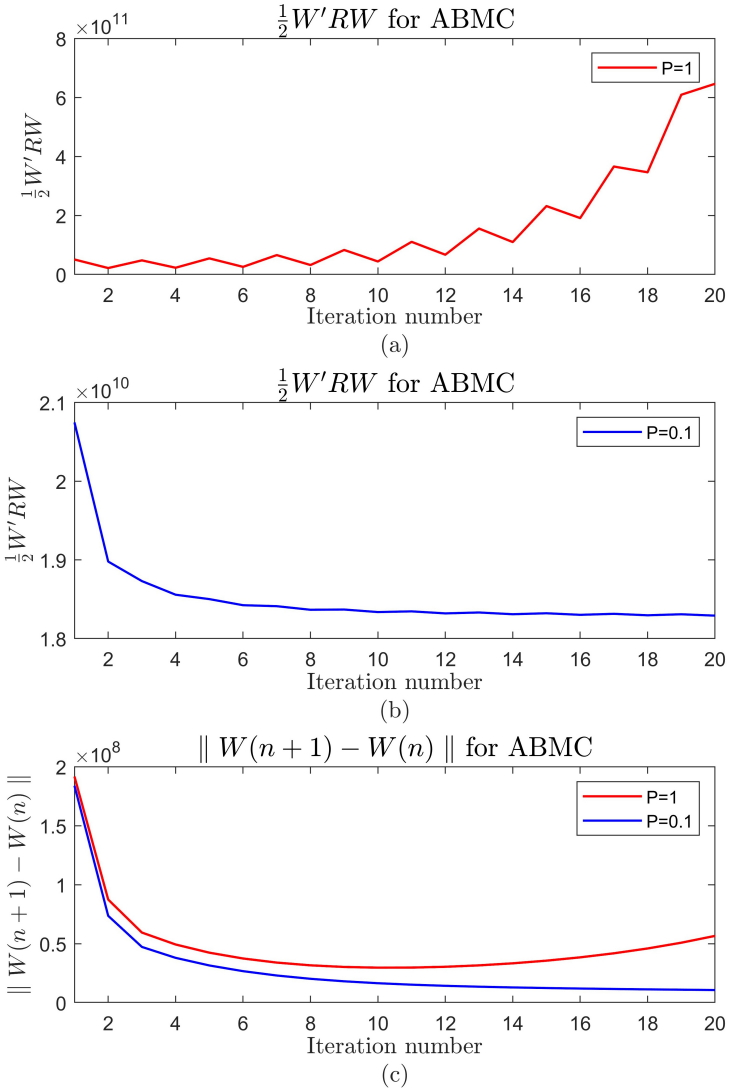

Figure 5.5: The convergence plot for $\frac{1}{2}W^{\intercal}RW$ and $\| W(n+1) - W(n) \|$ for various P values over 20 iterations.

where

$$\nabla_{\mathbf{W}} J(\mathbf{W}(n)) = \mathbf{R}\mathbf{W}(n) - \beta_1 \mathbf{G} - \beta_2 \mathbf{X}\mathbf{u}^{\intercal} \tag{5.16}$$

with $\mathbf{U}^{\intercal}$ at lag j ($\mathbf{U}^{\intercal}(m+j)$). The following iterative process is used to estimate $\mathbf{W}$:

$$\mathbf{W}(n+1) = \mathbf{W}(n) - \mu(\mathbf{R}\mathbf{W}(n) - \beta_1 \mathbf{G} - \beta_2 \mathbf{X}\mathbf{u}^{\intercal}) \tag{5.17}$$

where μ is the non-negative step size for each iteration. Considering the constraint $\mathbf{G}^{\intercal}\mathbf{W} = \mathbf{f}$, pre-multiplying both sides of (5.17) by $\mathbf{G}^{\intercal}$ yields:

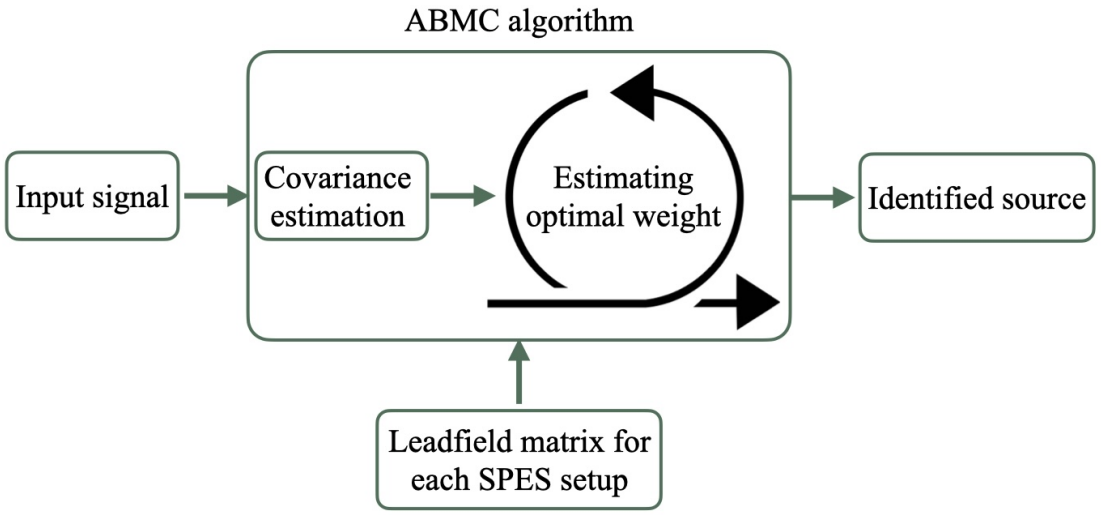

Figure 5.6: Pipeline for the ABMC beamformer.

$$\mathbf{f} = \mathbf{G}^{\intercal}\mathbf{W}(n) - \mu(\mathbf{G}^{\intercal}\mathbf{R}\mathbf{W}(n) - \beta_1\mathbf{G}^{\intercal}\mathbf{G} - \beta_2\mathbf{G}^{\intercal}\mathbf{X}\mathbf{u}^{\intercal}) \tag{5.18}$$

By considering β_2 as $\beta_2 = P\beta_1$, β_1 can be obtained from 5.18 as:

$$\beta_1 = \frac{\mathbf{f} - \mathbf{G}^{\intercal}\mathbf{W}(n) + \mu\mathbf{G}^{\intercal}\mathbf{R}\mathbf{W}(n)}{\mu\mathbf{G}^{\intercal}\mathbf{G} + \mu P\mathbf{G}^{\intercal}\mathbf{X}\mathbf{u}^{\intercal}} \tag{5.19}$$

By replacing the values for β_1 and β_2 in equation (5.17), $\mathbf{W}(n+1)$ is calculated in each iteration. The initial $\mathbf{W}$ is set to an $M \times 1$ vector of zero values. The step size μ and the ratio between β_1 and β_2 (P) are empirically adjusted according to the convergence rate for $\frac{1}{2}\mathbf{W}^{\intercal}\mathbf{R}\mathbf{W}$ and $\parallel \mathbf{W}(n+1) - \mathbf{W}(n) \parallel$. If P is too low, the weight for the second constraint related to the template matching with the desired source becomes negligible, and the output becomes similar to that of conventional iterative LCMV beamformer. Conversely, increasing the value of P up to a specific threshold for each segment causes $\frac{1}{2}\mathbf{W}^{\intercal}\mathbf{R}\mathbf{W}$ and $\parallel \mathbf{W}(n+1) - \mathbf{W}(n) \parallel$ not to converge, and therefore, the optimal value for the ABMC beamformer weight cannot be reached. Figure 5.5 shows the values of $\frac{1}{2}\mathbf{W}^{\intercal}\mathbf{R}\mathbf{W}$ and $\parallel \mathbf{W}(n+1) - \mathbf{W}(n) \parallel$ for a single segment of data over 20 iterations. Figure 5.6 shows the overal pipeline for the ABMC beamformer.

5.3 EXPERIMENTS AND RESULTS

Throughout the following experiments, this chapter aimed to demonstrate the performance of the ABMC and investigate if IEDs and DRs originate from the same location for each DRE case. The ABMC beamformer developed in this study has been employed

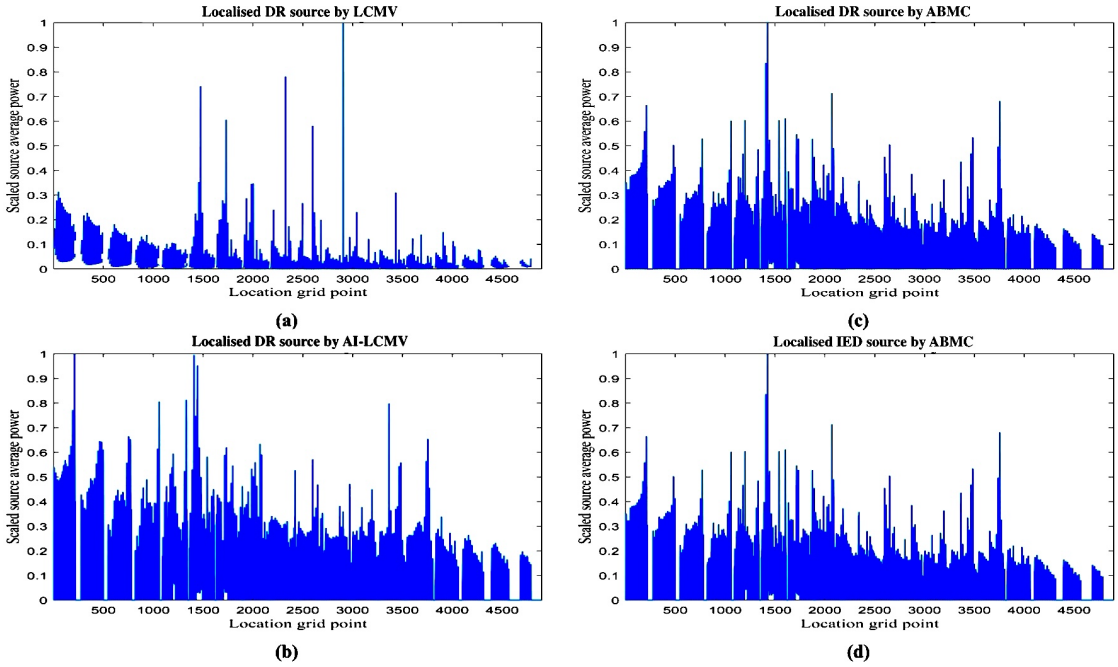

Figure 5.7: Localised DR source from a sample segment using (a) conventional LCMV, (b) AI-LCMV, and (c) ABMC approaches for one subject. Plot (d) indicates the localised IEDs using the ABMC approach for the same case. As shown in this figure, the conventional LCMV approach identifies a different region as the source compared to the adaptive methods. The ABMC demonstrates the highest accuracy and consistency in localisation. Most importantly, ABMC localises DRs and IEDs of a subject at the same position in the brain morphology.

for 300 data segments, each 0.5 seconds long. These include 93 segments with visible SPES DRs and 57 from the same sessions with a similar setup where DRs were not visible to the implanted electrodes. Initially, the segments containing DRs were fed as input to ABMC and AI-LCMV algorithms. The general results from the subjects included in this chapter revealed that, although the identified sources using both pipelines were close to the closest electrode to the SOZ, the identified primary source using the ABMC beamformer was, on average, 0.82 cm closer to the SOZ and more consistent compared to those achieved by AI-LCMV for the tested segments with visible DRs. Also, in the tested segments where no DRs were visible to the implanted electrodes, the identified primary source using the ABMC was, on average, 1.35 cm closer to the closest electrode to the SOZ compared to those achieved by the AI-LCMV algorithm. The detailed results for each case are reported in Table 5.2.

Figure 5.7 shows the localised source for a selected segment of visible DRs using conventional LCMV, AI-LCMV, and ABMC approaches. Figure 5.8 also shows the results of ABMC and AI-LCMV algorithms for another DRE case with the clinical report of suspected SOZ in the right temporal region with notable improvement in symptoms after resection operation. These Figures clearly show the improved accuracy of the ABMC beamformer compared to the AI-LCMV approach for the tested segment.

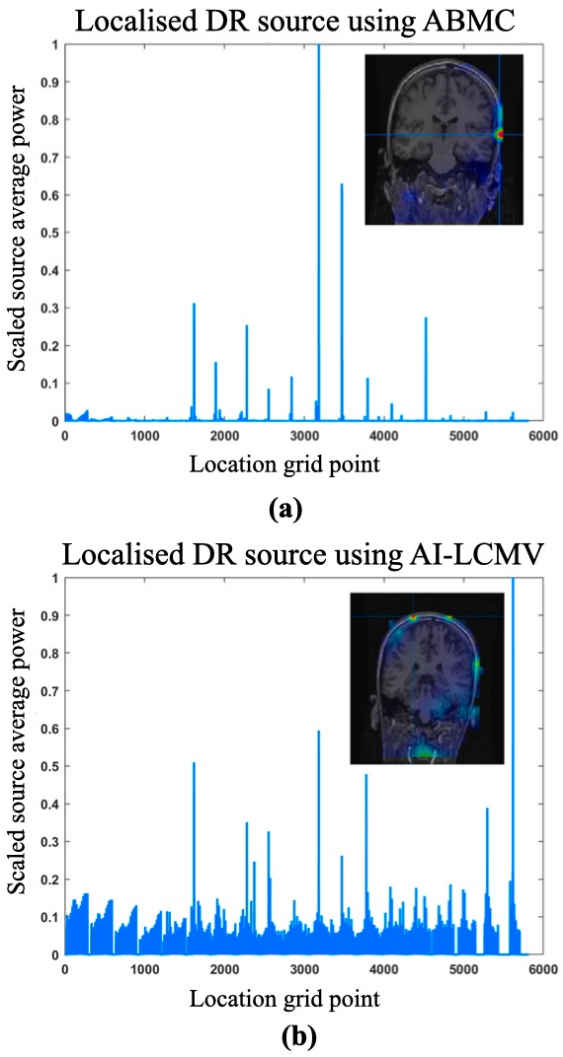

Figure 5.8: The localised DRs using (a) ABMC, and (B) AI-LCMV approaches for a DRE case with the clinical report of suspected SOZ in the right temporal region.

In addition to DRs, 145 data segments with visible IEDs were fed to the ABMC beamformer. For each case, multiple IED templates observed and annotated by the experts were used as the desired template for the beamformer. Using the ABMC beamformer, the localised sources for these segments were compared to the primary identified source for DRs selected from the SPES sessions and the lead electrode at seizure onset (hyperexcitable region). The source localisation results for IEDs show similar regions to those achieved from DRs, with a considerably higher average distance between the primary source and the seizure onset in general. The details related to the average distance between the identified source for each specific IED template and the lead channel at the seizure source, alongside the similarity of the selected template with the selected template for DRs for the same subject, are presented in Table 5.2. The similarity between the templates is measured using an adaptive signed correlation index [214]. Figure 5.9 compares the locations identified as the primary source of DRs and

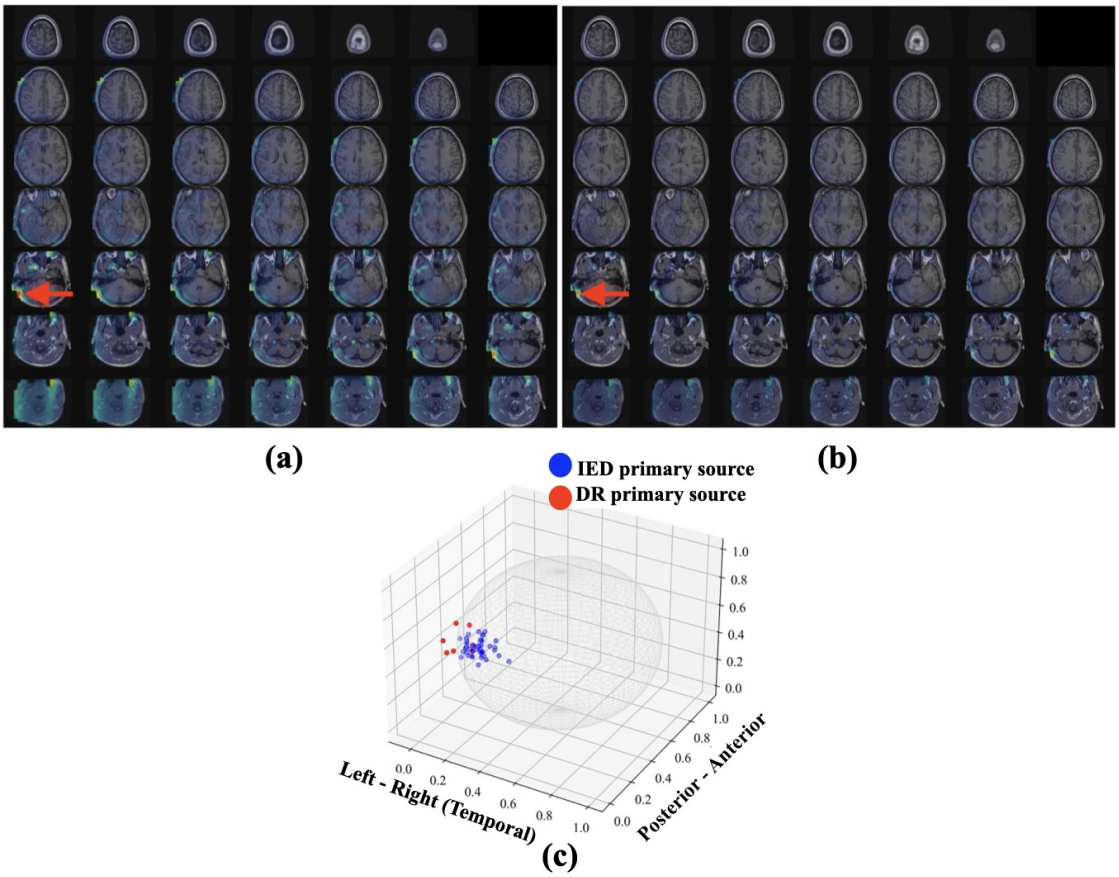

Figure 5.9: The identified source locations (pointed to with red arrow) for (a) DRs and (b) IEDs via ABMC beamformer for a DRE case with clinical report of regional abnormal responses to SPES, in the posterior and lateral aspect of the left temporal lobe suggesting that this region is hyperexcitable and potentially epileptogenic. (c) shows the normalised locations of IED (blue) and DR (red) sources for various tested iEEG segments.

IEDs for one subject. The results from the selected segments indicate that in overall, for 90% of the segments, the sources responsible for IEDs are in the same hemisphere and in proximity to the closest electrode to the SOZ. However, for 10% of the segments, including IEDs, the source was in the opposite hemisphere, far from the location of the DR source and SOZ. This is likely to be an estimation error due to the spurious sources and the head model estimation. Figure 5.10 shows the ABMC output for the identified grid point as the primary source of SPES DRs.

The advantage of the proposed ABMC method compared to those of the conventional methods becomes more evident when the power of DRs and IEDs is low. This advantage is clear when comparing the results of the developed approach here with those achieved using conventional methods [55]. Compared to the AI-LCMV introduced in Chapter 4, the results achieved using the ABMC algorithm are more accurate (considering the distance between the identified primary source and the SOZ confirmed using other available implanted electrodes) and more consistent across the tested segments. The ABMC beamforming employed here not only alleviates the sensitivity of

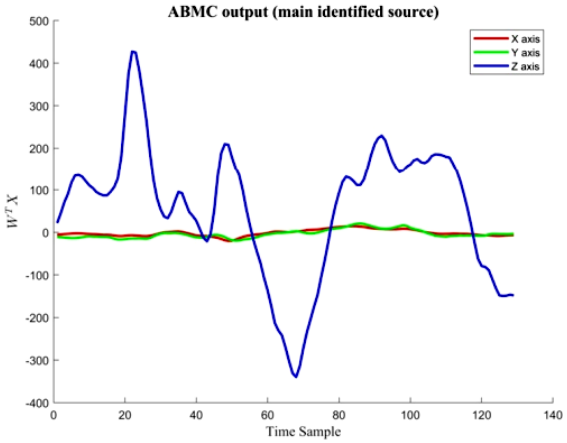

(a)

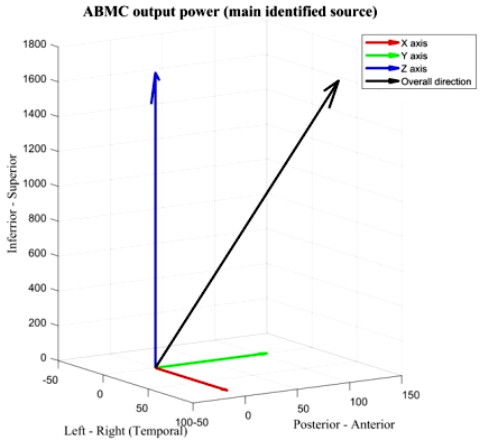

(b)

Figure 5.10: (a) The output of ABMC beamformer for the grid point (location) identified as the main source along each axis in three dimensional space and (b) the overall direction of source acitivity based on the received power along each axis.

the conventional LCMV beamformer to the power of the recorded signals but also can exploit the sparsity and temporal location variation of the DRs and IEDs. Although the iterative process can be time-consuming and computationally expensive, the clinical benefits of a robust localisation pipeline are invaluable. Considering the results of recent research indicating the capability of high-density EEG setups compared to stereo EEG [215], the ABMC beamformer developed here can significantly contribute to the non-invasive localisation of seizure generators within the epileptic brain.

Having mentioned the benefits of the ABMC, it is important to note that, like for AI-LCMV, although the head model and leadfield vectors are measured multiple times according to the SPES setup for each case using the available software, improving the electrode localisation and head model estimation can greatly improve the accuracy and reliability of the results. Another point is that, the geometry of the input array

Table 5.2: The number of tested segments for each case where DRs were visible and not visible after stimulation alongside the Euclidean distance (in cm) between the localised SOZ using AI-LCMV and ABMC methods (N: number of tested segments).

	AI-LCMV				ABMC			
Case	N (Visible)	Distance (cm)	N (Invisible)	Distance (cm)	N (Visible)	Distance (cm)	N (Invisible)	Distance (cm)
1	15	1.5± 0.4	10	2.8 ± 0.78	15	0.62± 0.21	10	1.1 ± 0.16
2	15	1.4 ± 0.37	10	2.6 ± 0.4	15	0.87 ± 0.1	10	1.8 ± 0.14
3	20	2.5 ± 0.33	10	3.5 ± 0.45	20	1.4 ± 0.24	10	1.7 ± 0.33
4	23	1.8 ± 0.56	12	2.9 ± 0.62	23	1.1 ± 0.17	12	2.2 ± 0.21
5	20	1.4 ± 0.37	15	2.6 ± 0.4	20	0.75 ± 0.16	15	1.4 ± 0.15

Table 5.3: The relative distance between the location of the main identified source for DRs or IEDs and the SOZ (closest channel to SOZ) and the average ASCI index between the IED and DR templates.

Case	DR segments	IED segments	Source distance DR	Source distance IED	Hyperexcitable region	Average ASCI
1	20	30	0.62± 0.21	0.65± 0.18	Posterior & lateral aspects of the left temporal lobe	0.84
2	15	25	0.87 ± 0.1	1.23 ± 0.14	Posterior medial & lateral aspects of the frontal lobe	0.81
3	20	30	1.3 ± 0.24	1.14 ± 0.33	Anterior temporal pole right	0.83
4	23	35	1.1 ± 0.17	1.2 ± 0.11	Tpole & mesiotemporal right	0.80
5	20	25	0.87 ± 0.16	1.24 ± 0.31	Mid-temporal lobe right	0.75

is restricted to the gold-standard clinical assessment equipment available for all the cases (standard sizes commonly used in operation). Due to this limitation, the ABMC approach was not tested with different input array geometries for the same subject. Generally, the arrangement of the sensor array and the distance between the individual sensors play a crucial role in defining the resolution and beamwidth of the beamformer. The sensor array geometry and the spacing between sensors determine the resolution and beamwidth of the beamformer.

5.4 CONCLUSION

The ABMC localisation algorithm introduced in this chapter not only advances the general understanding of the sources responsible for SPES DRs and IEDs but also can provide clinicians with a practical tool for identifying the source of epileptic activities like DRs and IEDs. The results from applying the ABMC algorithm suggest that for the pool of cases included in this chapter and over multiple tested segments, these sources are highly likely to be in the same anatomical location. Clinicians can consider this information to better manage DRE patients during the assessment stage. The ABMC robustness and accuracy have been investigated and compared with the AI-LCMV and the previously established algorithms, and its clear superior performance has been demonstrated. Having addressed the key challenges of the conventional beamformers, the following chapter aims to further improve the consistency of the beamforming algorithm for SPES DR and IED source localisation using a temporally distributed approach.

6

TEMPORALLY-DISTRIBUTED BEAMFORMER

A distributed system includes a network of agents (nodes). A distributed network exploits the data transferred to each agent from its neighboring nodes. In a single-objective adaptive cooperative network, the agents in a neighborhood cooperate to achieve their objectives. This chapter exploits the similarity in the leadfield matrices of consecutive IEDs and DRs (same SPES setup) by designing a temporally distributed beamformer. Such a beamformer is expected to enhance the robustness of the solution against IED/DR shape variability and the inherent noise. After introducing the ABMC algorithm for localising the source of IEDs and DRs, the primary objective of this chapter is to further enhance the accuracy and robustness of the localisation pipeline. Based on previous findings, DRs are anticipated to originate from the same location as IED sources associated with SOZ. Consequently, before localising the DRs, the similarity between consecutive DRs or IEDs is utilised to design a robust time distributed localisation system to identify the epileptogenic brain zone more precisely. Like the ABMC approach introduced in Chapter 5, the proposed beamformer leverages the morphology of IEDs and DRs as a constraint in its formulation as the template for the desired source. Additionally, the algorithm benefits from a tensor decomposition approach to improve the SNR of the input signal recorded using the intracranial subdural mat to the adaptive beamformer, thereby refining the localisation pipeline. The results indicate an enhancement in localisation accuracy and consistency compared to the methods introduced in the previous chapters (AI-LCMV in Chapter 4 and ABMC in Chapter 5).

6.1 DATA AND HEAD MODEL ESTIMATION

The description of SPES setup, interictal recordings, along with the data and preprocessing stages for the DRE cases included for this part, has already been detailed in Chapter 5.

6.2 TENSOR FACTORISATION - DISTRIBUTED BEAMFORMING

6.2.1 *Tensor Factorisation*

Tensor factorisation is a mathematical technique to decompose a high-dimensional array, known as a tensor, into a sum of simpler, often lower-dimensional components.

There are different tensor factorisation methods [216]. This technique is beneficial in signal processing, data mining, machine learning, and neuroscience, where the meaningful information often naturally lies within multiple dimensions. A tensor is a generalisation of matrices to higher dimensions. While a matrix is a two-dimensional array of numbers, a tensor can have three, four, or even more dimensions. For instance, a three-dimensional tensor might be used to represent a series of images (considering height, width, and time). Similarly, a four-dimensional tensor could represent a dataset with dimensions such as time, location, frequency, and type. The most common models include:

1. Canonical polyadic decomposition (CPD), also known as CANDECOMP/PARAFAC, aims to express a tensor as a sum of rank-one tensors [217]. A rank-one tensor in three dimensions can be visualised as an outer product of three vectors. For a tensor $\mathcal{X} \in \mathbb{R}^{I \times J \times K}$, CPD attempts to find vectors $\mathbf{a}_r \in \mathbb{R}^I$, $\mathbf{b}_r \in \mathbb{R}^J$, and $\mathbf{c}_r \in \mathbb{R}^K$ such that:

$$\mathcal{X} \approx \sum_{r=1}^{R} \mathbf{a}_r \circ \mathbf{b}_r \circ \mathbf{c}_r \tag{6.1}$$

   This decomposition is unique under mild condition of disjointedness of sources, meaning that the components are identifiable without ambiguity, which is beneficial for interpretability. CPD is particularly useful when the data is expected to have an underlying structure that can be captured by a small number of components.

2. Tucker decomposition is a more flexible model compared to CPD. It decomposes a tensor into a core tensor, which captures interactions among different components and factor matrices that represent the modes. For a three dimensional tensor, the decomposition can be written as:

$$\mathcal{X} \approx \mathcal{G} \times_1 \mathbf{A} \times_2 \mathbf{B} \times_3 \mathbf{C}$$

   Here, $\mathcal{G} \in \mathbb{R}^{R_1 \times R_2 \times R_3}$ is the core tensor, and $\mathbf{A} \in \mathbb{R}^{I \times R_1}$, $\mathbf{B} \in \mathbb{R}^{J \times R_2}$, and $\mathbf{C} \in \mathbb{R}^{K \times R_3}$ are the factor matrices. The core tensor $\mathcal{G}$ represents the interactions between the factors in each mode, allowing for more complex data structures to be captured. However Tucker decomposition dose not lead to unique results unless properly regularised.

3. Nonnegative tensor factorisation (NTF) is a variant of tensor factorisation where the factor matrices are constrained to be no-nnegative. This is useful for data

that is inherently non-negative, such as pixel values in images or counts in text analysis. NTF is particularly useful for data that are non-negative by nature, such as counts or intensities. By constraining the factor matrices to be non-negative, NTF ensures that the resulting factors are interpretable in contexts where negative values do not make sense. The NTF model can be formulated as:

$$\mathcal{X} \approx \sum_{r=1}^{R} \mathbf{a}_r \circ \mathbf{b}_r \circ \mathbf{c}_r, \quad \mathbf{a}_r, \mathbf{b}_r, \mathbf{c}_r \geq 0$$

This constraint aids in interpretability, making NTF popular in areas like image processing and text mining. The non-negativity constraint makes the factorisation output unique.

The tensor factorisation has a wide range of applications across various fields including but not limited to:

1. Recommender systems: Tensor factorisation is used to model user-item interactions over time, improving recommendation accuracy [218].
2. Social network analysis: It helps in analysing dynamic interactions and community detection within social networks [219].
3. Neuroscience: In brain imaging, tensor factorisation aids in identifying patterns and anomalies in multi-dimensional brain activity data [219].
4. Chemometrics: It assists in decomposing complex chemical data into interpretable components [219].
5. Computer vision: Tensors are used to represent and process multi-dimensional visual data like videos or 3D scans [219].

Tensor factorisation provides an opportunity to analyse multi-dimensional data [216]. It reduces the dimensionality of data, making it easier to handle and analyse. By decomposing the data into a few significant components, tensor factorisation can effectively filter out noise, resulting in more robust data representations [218–220]. The resulting factors often have meaningful interpretations, making it easier to understand the underlying structure of the data [218, 220]. Furthermore, tensor factorisation methods can be scaled to handle large datasets, especially with advancements in computational power and algorithms [218–220]. The flexibility of tensor structure allows for various models to be chosen based on the specific nature and requirements of the data. It has widespread application in EEG signal processing, particularly in IED detection [221–223]. Here, the aim is to use tensor factorisation to extract the dominant latent factors from IED and DR segments to improve the accuracy of seizure source localisation.

However, tensor factorisation also has some weaknesses. It can be computationally expensive, particularly for large and high-dimensional tensors, posing a barrier to real-time or large-scale applications. Many tensor factorisation algorithms are iterative and may suffer from slow convergence or getting stuck in local minima, leading to suboptimal solutions [219]. Choosing the right tensor factorisation model and the appropriate rank (number of components) is not always straightforward and often requires domain knowledge and experimentation [218–220]. Additionally, the outcome of tensor factorisation can be sensitive to the initial values of the factor matrices or vectors, potentially affecting the reproducibility and stability of results. In cases of sparse data, tensor factorisation may struggle to find meaningful patterns due to the low signal energy or lack of sufficient information in certain parts of the tensor [218, 220].

The CPD captures essential patterns, reducing data dimensionality and improving subsequent beamforming performance. By preserving signal characteristics and eliminating noise, CPD ensures accurate source localisation. Moreover, it enhances generalisation to handle complex EEG signals with varying noise sources and subject variability, which is crucial for dynamic activities like IEDs and DRs.

Consider a scenario where N segments, each comprising L time samples and recorded across M channels, are available. We consolidate the temporal, spatial, and segmental aspects into a three-dimensional tensor $\boldsymbol{\mathcal{X}} \in \mathbb{R}^{L\times M\times N}$. To decompose this tensor, we use CPD, breaking it down into a series of rank-one components. These components possess not only orthogonality but also independence. CPD is defined in (6.1). It is generally useful to consider that the components are normalised to length one with the associated weights represented by the vector $\boldsymbol{\lambda} \in \mathbb{R}^{R}$. Therefore, (6.1) is reformulated to:

$$\boldsymbol{\mathcal{X}} \approx \sum_{r=1}^{R} \lambda_r \, \mathbf{a}_r \circ \mathbf{b}_r \circ \mathbf{c}_r. \tag{6.2}$$

The factor matrices are formed by combining the rank-one tensors, i.e., $\mathbf{A} = [\mathbf{a}_1 \dots \mathbf{a}_R]$. Following the Kruskal operator [224], (6.2) can be represented as:

$$\boldsymbol{\mathcal{X}} \approx [\![\boldsymbol{\lambda}; \mathbf{A}, \mathbf{B}, \mathbf{C}]\!] \equiv \sum_{r=1}^{R} \lambda_r \, \mathbf{a}_r \circ \mathbf{b}_r \circ \mathbf{c}_r, \tag{6.3}$$

where $\mathbf{A} \in \mathbb{R}^{L\times R}$, $\mathbf{B} \in \mathbb{R}^{M\times R}$, and $\mathbf{C} \in \mathbb{R}^{N\times R}$ are factor matrices. Figure 6.1 demonstrates a diagram of CPD of a 3-way tensor. To optimise the factor matrices with R components that best approximates $\boldsymbol{\mathcal{X}}$, (6.3) can be formulated as a least-square optimisation problem:

$$\min_{\mathbf{A},\mathbf{B},\mathbf{C}} \quad f \equiv \frac{1}{2} \left\| \boldsymbol{\mathcal{X}} - [\![\boldsymbol{\lambda}; \mathbf{A}, \mathbf{B}, \mathbf{C}]\!] \right\|^2. \tag{6.4}$$

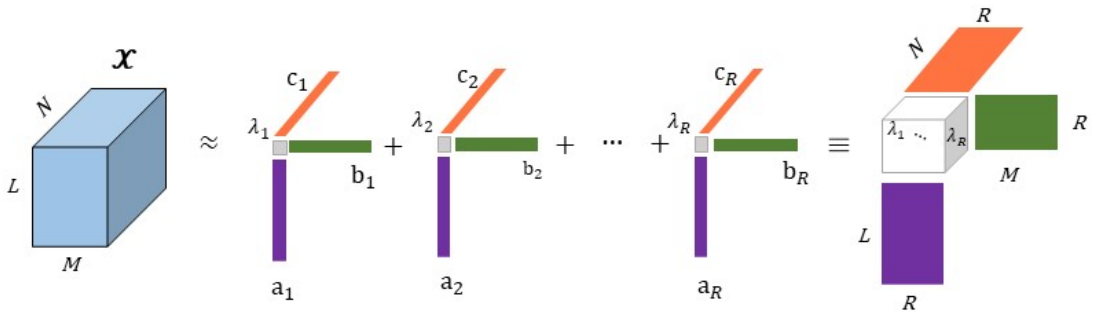

Figure 6.1: L and M correspond to time samples and recording electrodes. N is either the IED or DR segments, depending on the input. The tensor is decomposed to R rank-one tensors, which are orthogonal and independent. a, b, and c include temporal, spatial, and segmental components, respectively.

There are different algorithms to optimise the objective function (6.4). We employ a gradient-based algorithm for optimisation. For more details, the reader is referred to [217]. After estimating the factors, the first J components assuming to have the most informative content are selected and reconstructed as follows:

$$\bar{\boldsymbol{\mathcal{X}}} \approx \sum_{j=1}^{J} \lambda_j \, \mathbf{a}_j \circ \mathbf{b}_j \circ \mathbf{c}_j, \tag{6.5}$$

where $\bar{\boldsymbol{\mathcal{X}}}$ contains the denoised mat data.

As a result of their similar morphology and common origin, DRs (or IEDs) may share some temporal and spatial characteristics. We aim to merge the time, channel, and segment dimensions of data (IEDs or DRs) into a 3D tensor. Subsequently, we decompose the tensor into temporal, spatial, and segmental factors, allowing for the extraction of more physiologically informative components. These selected components are then reconstructed to generate more informative data. This is used as input to an adaptive array processing algorithm introduced in Chapter 5 to improve SOZ localisation. The mathematical formulation is detailed in the following sections.

6.2.2 *Temporally Distributed Beamforming*

Despite the promising results from the AI-LCMV and ABMC methods, enhancing the precision and consistency of localisation during the pre-surgical assessment phase remains a significant challenge that directly impacts patient treatment. Therefore, having a consistent and reliable localisation algorithm is critical. A crucial aspect of addressing this challenge lies in the effective exploitation and adaptation to temporal variations in recorded signals, particularly during SPES sessions. These sessions often present DRs that exhibit morphological and latency inconsistencies, even across consecutive stimulations using the same SPES setup.

Temporally distributed beamforming offers several significant advantages. By adapting to time-varying conditions of the recorded signals, this method can enhance the accuracy and consistency of signal localisation [225, 226]. It leverages temporal diversity by capitalising on variations in the signal over time, which can lead to improved detection of relevant features despite inconsistencies. Additionally, temporally distributed beamforming can better suppress interference by adjusting to the dynamic nature of the signals, thereby enhancing overall robustness in signal processing [225, 226].

This method helps improve the accuracy of neural activity locations even when dealing with changes in shape or delays over time. The system can sustain decent performance despite the temporal variability inherent in SPES sessions by adjusting the beamforming weights. Moreover, it can easily adjust to signal or channel failures on the fly, ensuring dependable performance [225, 226].

The use of temporally distributed beamforming can be very important in enhancing the dependability and efficiency of localisation algorithms in medical environments. Especially in situations, like pre-operation evaluations where accuracy is extremely important.

In the time distributed approach employed in this chapter, the weights estimated for the selected segments are averaged following each iteration, serving as the weight vector's current value for the subsequent iteration. Through sufficient iterations, the algorithm converges toward the optimal weighting coefficients for the beamformer while mitigating any irregularities (e.g., spurious IEDs). In this approach, according to a number of consecetive stimulations using the same SPES setup (ten stimulations using the same pair of channels) and also the initial localisation results after manually adjusting the number of considered consecutive segments for the algorithm, three data segments were utilised to estimate the distributed weight of the beamformer, striking a balance between adaptability to signal variabilities and specificity in localisation.

The formulations for the beamforming algorithm are detailed below. Similar to the previous algorithms, the preliminary objective of the beamformer is to minimise output power while aligning the output with the selected template for each data segment. The

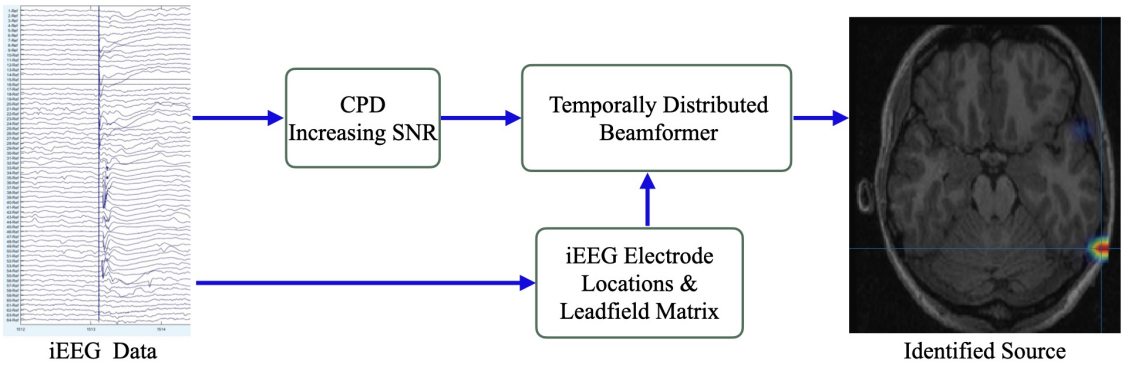

Figure 6.2: Pipeline for temporally distributed beamformer.

weight vector ϕ for each of the x, y, and z directions is reached using the solution to a constrained optimisation problem similar to **??** in Chapter 5.

Here again, **u** (a visible IED or DR template selected from the recordings) in the additional constraint refers to the desired template with the same length as the input signal. The optimisation problem can be executed iteratively after converting the via Lagrange multipliers.

Unlike Chapter 5, here for each iteration, after estimating the weight vector for the k^{th} segment, the value is averaged over neighbouring consecutive segments. Therefore, the current weight vector for the weight vector in the next iteration is derived by the following combination step:

$$\mathbf{W}_k(n+1) = \frac{1}{3}\sum_{l=k-m}^{k+m} \phi_l(n+1) \tag{6.6}$$

where m is the neighbourhood radius. Therefore, in the adaptation step, the following iterative process is used to estimate ϕ:

$$\phi_k(n+m) = \phi_k(n) - \mu(\mathbf{R}\phi_k(n) - \beta_1\mathbf{G} - \beta_2\mathbf{X}\mathbf{u}^\intercal) \tag{6.7}$$

where μ is the non-negative step size for each iteration. Considering the constraint $\mathbf{G}^\intercal\phi_k = \mathbf{f}$, pre-multiplying both sides of (6.7) by $\mathbf{G}^\intercal$ yields:

$$\mathbf{f} = \mathbf{G}^\intercal\phi_k(n) - \mu(\mathbf{G}^\intercal\mathbf{R}\phi_k(n) - \beta_1\mathbf{G}^\intercal\mathbf{G} - \beta_2\mathbf{G}^\intercal\mathbf{X}\mathbf{u}^\intercal) \tag{6.8}$$

By considering β_2 as $\beta_2 = \beta_1$, β_1 can be obtained from (6.8) as:

$$\beta_1(n) = \frac{\mathbf{f} - \mathbf{G}^\intercal\phi_k(n) + \mu\mathbf{G}^\intercal\mathbf{R}\phi_k(n)}{\mu\mathbf{G}^\intercal\mathbf{G} + \mu P\mathbf{G}^\intercal\mathbf{X}\mathbf{u}^\intercal} \tag{6.9}$$

By replacing the values for β_1 and β_2 in (6.7) $\phi_k(n+1)$ is calculated in each iteration. The initial ϕ is set to an $M \times 1$ vector of zero values. The value of step size μ and the ratio between β_1 and β_2 (P) are empirically adjusted according to the convergence rate for $\frac{1}{2}\mathbf{W}_k^\intercal\mathbf{R}\mathbf{W}_k$ and $\parallel \mathbf{W}_k(n+1) - \mathbf{W}_k(n) \parallel$. With the value of P too low, the weight for the second constraint related to the desired template for the beamformer becomes negligible, and the output becomes similar to those of the conventional iterative LCMV beamformer. Also, increasing the value of P up to a specific threshold for each segment causes $\frac{1}{2}\mathbf{W}_k^\intercal\mathbf{R}\mathbf{W}_k$ and $\parallel \mathbf{W}_k(n+1) - \mathbf{W}_k(n) \parallel$ not to converge, and therefore, the optimal value for the weight cannot be reached. Figure 6.2 shows the implemented pipeline for source localisation.

Table 6.1: The measured distance between the location of the main identified sources for DRs or IEDs and the SOZ using the hybrid time-distributed beamformer, and the average ASCI number between the IED and DR templates.

Case	DR segments	IED segments	Source distance DR	Source distance IED	SOZ	ASCI
1	20	30	0.47± 0.13	0.56± 0.08	Posterior & lateral aspects of the left temporal lobe	0.86
2	10	25	0.83± 0.11	1.1 ± 0.1	Posterior medial & lateral aspects of the frontal lobe	0.85
3	20	30	1.15 ± 0.15	1.1 ± 0.23	Anterior temporal pole right	0.83
4	20	35	0.8 ± 0.12	0.54 ± 0.17	Tpole & mesiotemporal right	0.80
5	20	25	0.81 ± 0.15	1.14 ± 0.22	Mid-temporal lobe right	0.8

6.3 RESULTS AND EXPERIMENTS

The temporally distributed adaptive beamformer has been used to analyse 235 data segments, each lasting 0.5 seconds, and annotated by experts as either SPES DR or IED segments (90 segments for DRs and 145 segments for IEDs) after applying the CPD algorithm to the data to increase the SNR. The source identification in each segment was followed by measuring the Euclidean distance between the localised primary source (source with the maximum power) and the electrode closest to SOZ, identified from seizure recordings. In the implemented experiments the m was emperically set to 1 as the neighbourhood radius which is sufficients for obtaining favourable results.

The results of analysed segments reveal that the distributed algorithm has higher consistency and accuracy than the previously introduced ABMC across the DRE cases included in this chapter. On average, the source identified using the distributed algorithm for DR segments is 0.13 cm closer to the closest electrode to the SOZ than that determined by the ABMC. Similarly, for the IED segments, the source identified using the distributed algorithm is, on average, 0.27 cm closer to the closest electrode to the SOZ. Table 6.1 presents the outcomes of applying the distributed algorithm developed here for localising the sources of DRs and IEDs. Figure 6.3 shows the output of the employed algorithm for identifying the source of sample DR and IED segments alongside the identified source overlaid on the anatomical MRI image. Figure 6.4 shows the nor-

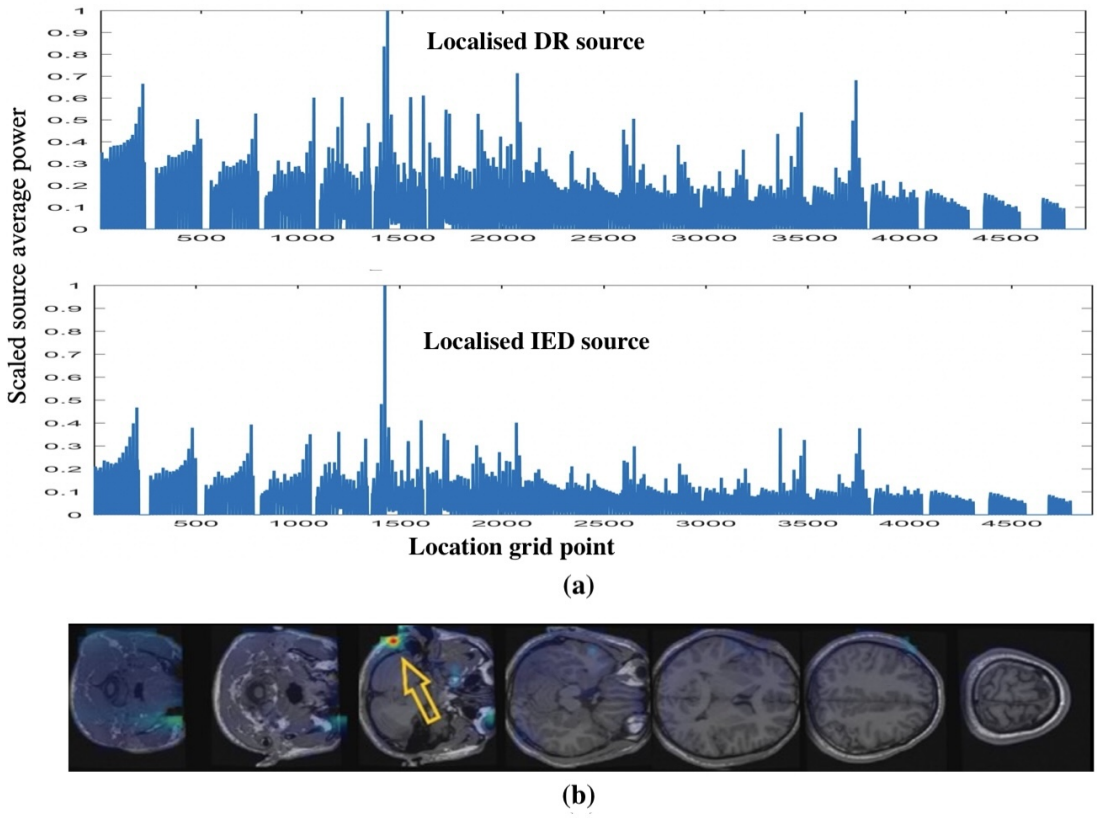

Figure 6.3: (a) The identified location of IED and DR primary sources for sample segments via the temporally distributed approach. (b) the identified source overlaid on the MRI brain image (pointed by the yellow arrow) for a DRE case with a clinical report of clear regional abnormal responses to SPES in the posterior and lateral aspect of the left temporal lobe.

malised location of the identified primary source for IEDs and DRs for the same subject using the ABMC and the temporally distributed algorithm. The results of the analysed segments suggest that the temporally distributed approach developed in this chapter exhibits superior consistency and accuracy compared to the ABMC for the tested DRE cases. The use of tensor factorisation prior to source localisation, further influences the results towards higher accuracy.

6.4 CONCLUSION

This chapter aimed to enhance the accuracy and robustness of localising SPES DR and IED sources. Building on the speculation that DRs and IEDs often originate from the same primary regions in the brain, a temporally distributed beamformer was developed and tested. This approach was integrated into an adaptive beamformer, similar to the ABMC method discussed in Chapter 5, with additional constraints based on the morphology of IED and DR signals. To improve the SNR of the input to the adaptive beamformer, we incorporated a tensor decomposition approach. Specifically, we em-

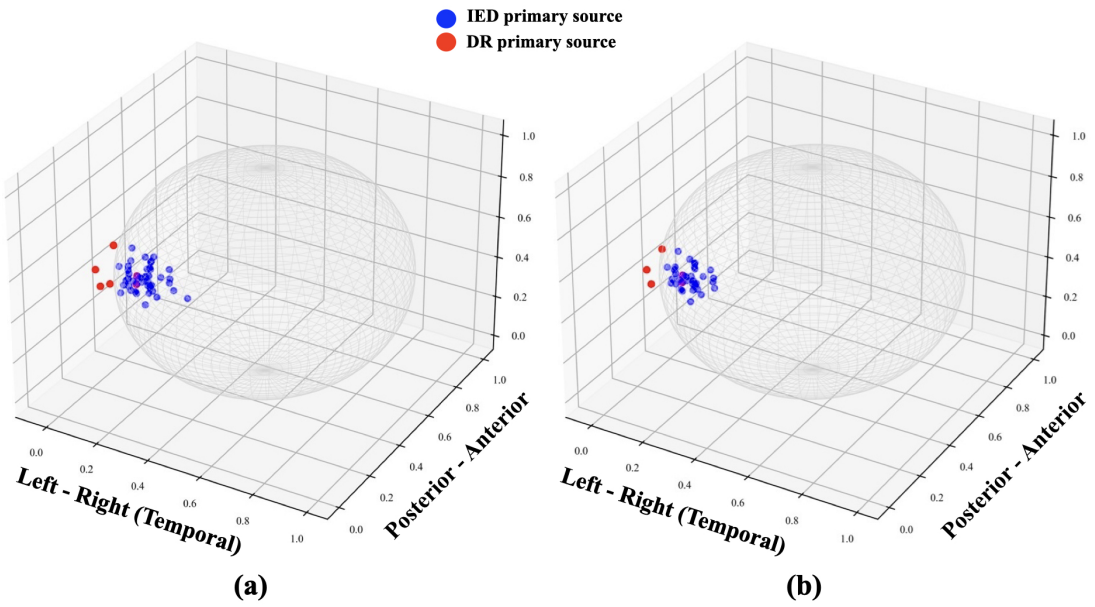

Figure 6.4: The identified normalised locations of IED (blue) and DR (red) primary sources for various intracranial EEG segments using (a) the ABMC and (b) the temporally distributed approach developed here for a subject with a clinical report of clear regional abnormal responses to SPES in the posterior and lateral aspect of the left temporal lobe implying that this region is hyperexcitable and epileptogenic.

ployed CPD to effectively capture essential patterns in the data, reducing dimensionality and enhancing the beamformer's performance by preserving signal characteristics and eliminating noise.

The experimental results demonstrated a significant improvement in localisation accuracy. Analysing data segments showed that the proposed distributed algorithm outperformed the ABMC approach. The improved precision and consistency of the method highlight its potential for more accurate identification of SOZ, which is crucial for effective pre-operation evaluation and treatment of epilepsy.

7

SUMMARY, CONCLUSION, AND FUTURE RESEARCH

7.1 CLINICAL IMPACT AND EXPLOITATION

SPES has emerged as a promising technique in the context of drug-resistant epilepsy. This method offers a controlled approach to probing the excitability and connectivity of neural circuits involved in epilepsy, thereby facilitating the identification of regions associated with seizure in the brain. Existing methods for processing, assessing, and treating epilepsy fall short of precisely identifying SOZ and understanding the underlying neurophysiological mechanisms. The data recorded using intracranial electrodes during SPES sessions present significant challenges due to the complex morphology and inconsistent behaviour of the responses, even within a fixed setup for a patient. These complexities render conventional processing algorithms inadequate, often resulting in misleading or inaccurate conclusions. This PhD thesis aimed to enhance the efficiency of SPES sessions by developing advanced signal processing and machine learning pipelines. To enable that the E-I imbalance was investigated and the sources responsible for generating DRs and IEDs were identified.

In this thesis, after introducing the current challenges for the SPES sessions, an adaptive single-channel EEG separation pipeline based on SSA was developed and employed to investigate the E-I imbalance in regions associated with seizures. The developed and employed algorithm separates the E-I components verified by a clear separation in the frequency domain. The results revealed an increase in the I-to-E ratio in majority of the tested segments from recordings collected from regions associated with seizures immediately after ERs and before DRs, implying that the DRs can be a brain compensatory reaction aiming to reset the E-I balance and avoid an increase in I and synchronisation between different channels leading to seizure.

Next, identification of the regions responsible for generating DRs, IEDs, and consequently seizures in the brain was researched. The main aim of SPES, as an assessment tool, is to better identify the regions responsible for DR and seizure generation. Recognising the importance and significance of having an accurate and robust method to identify the DR and IED sources, we developed several adaptive source localisation methods. Considering the specific nature of the brain responses to SPES, we aimed to introduce regularised methods that perform better than those sensitive to signal power only. Using the concept of beamforming as a powerful source localisation tool, we first developed AI-LCMV, which aims to adjust the beamformer weights in an iterative fash-

ion while trying to match the output of the beamformer to a selected template as the desired source. After showing a significant improvement in DR source localisation performance for AI-LCMV compared to that of the conventional method (LCMV), further attempts were made to improve the localisation performance considering the limitations of AI-LCMV, such as possible temporal delay mismatch for the additional constraint and the lower accuracy for spatially close correlated sources. Later in the thesis, we introduced the ABMC pipeline, in which, by using the sparse Bayesian algorithm, we try to exclude the effect of the correlated sources from the input covariance and fix the temporal delay mismatch using a new constraint based on the cross-correlation between the beamformer's output and the desired source. The results of the ABMC beamformer indicated another step towards having a robust and accurate source localisation tool for identifying the source of DRs and IEDs. In addition, the ABMC method developed and employed in Method introduced in Chapter 5 was used to investigate the source of IEDs and DRs, revealing that the most IEDs are likely to originate from the same region as DRs. This is an important finding as it demonstrates the relation between the source of IEDs and epileptogenic regions in the brain. Finally, the hybrid tensor decomposition time-distributed array processing algorithm introduced in Chapter 6 aims to further improve the consistency and reliability of the ABMC beamformer for localising the IEDs and DRs. Tensor decomposition has been employed to increase the SNR of the input and capture more relevant information related to DRs and IEDs. Additionally, estimating the optimal weights for the beamformer in a time-distributed fashion over multiple data segments after sufficient iterations can help increase the consistency and adaptability of the algorithm for each subject.

The methods developed in this thesis offer deeper insights into the underlying mechanisms of epilepsy and provide more reliable tools for clinical applications, including SOZ identification. This is especially true for the DRE cases who undergo intracranial electrode implantation and are the possible candidates for resection surgery. This progress holds the promise of more efficient and cost-effective treatments in the future, instilling a sense of hope and optimism in the field of epilepsy research and treatment.

7.2 AREAS FOR IMPROVEMENT AND FUTURE DIRECTION FOR FUTURE

Having mentioned the aims and results of this thesis, there are areas that can be improved in the future and topics worth pursuing.

The first area is the possible opportunities to alter stimulation during SPES sessions. Although the data used in this work was recorded from multiple cases from various SPES sessions, the stimulation parameters were fixed. Recent studies have shown that changing the stimulation parameters can help to better identify the epileptogenic regions possibly responsible for seizure generation. In a recent study [46], researchers

examined 15 patients undergoing intracranial EEG monitoring and SPES with different stimulation intensities. Key findings of the study indicate that at stimulation intensities of 2 mA and above, the increase in N1 amplitude (a component of ERs) was greater for responses within the SOZ compared to the non-SOZ. The distribution of SOZ responses was maximised at stimulation intensities between 4-6 mA. The authors concluded that differences in ER amplitude over a range of current intensities can improve the ability to discriminate SOZ regions.

A more comprehensive investigation of the relationship between the E and I periods, SPES, and neuronal firing rates is required. Considering that a significant number of neurons firing in close proximity can imply E, and a period of no firing can imply I, it will be helpful to further explore the relationship between E or I with stimulation and related parameters. Investigating the correlation between pre-stimulus firing rates and the duration of E and I after stimulation, as well as any possible irregularities in segments where DRs are visible in the data compared to segments from normal regions, will be beneficial.

While initial results from the adaptive SSA pipeline employed to separate E and I activities indicated an increase in the I-to-E ratio immediately after ERs and before DRs, implying a period of increased I before the appearance of DRs in the majority of segments with visible DRs [54], examining the differences between various regions before stimulation and their correlation with neuronal firing rates and the period of E and I activities can help to better pinpoint the abnormalities expected in the epileptogenic regions compared to normal areas. Another area for improvement is the electrode localisation, head model, and leadfield estimation for more accurate results. The head model and leadfield estimation and electrode localisation in this work are performed using available open-source software, including Filedtrip [174], LeGUI [209] and Leadfield [205]. In this work, pre-surgery MRI and post-surgery CT scans are used to localise the positions of the implanted intracranial electrodes and to measure the head model and leadfield matrix, which serve as the linear operator linking brain activity sources to the recording signals for the beamforming algorithm. Pre-operative MRI and post-operative CT co-registration is performed through a pipeline implemented in Lead-DBS [205]. In this process, the CT images are first registered to the MRIs, then the volumes are normalised, and finally, any potential brain shift due to the surgery is compensated for [206–208]. Although using the available software, we tried to have the most accurate electrode localisation and leadfield estimation, there is still some error in MRI-CT coregistration due to various factors. The accuracy of CT-MRI coregistration in DBS surgery is influenced by multiple factors related to both MRI and CT imaging. In MRI, higher magnetic field strengths, optimised imaging sequences, and careful attention to slice thickness and voxel size enhance anatomical detail and precision. Geometric distortions and artefacts, particularly from metal implants or patient movement, must be corrected for accurate coregistration [227] [228]. Similarly, in CT imaging, optimising

slice thickness, spacing, and voxel size is crucial, along with managing artefacts like beam hardening. General factors such as the quality of coregistration algorithms, consistent patient positioning, and minimising the temporal gap between scans also play significant roles.

Developing more accurate image processing pipelines for coregistration and more accurate head models can help to have a more realistic leadfield vector and increase the overall reliability of the source localisation pipeline.

The aim of the proposed localisation methods introduced in this thesis is to develop accurate pipelines for identifying the source of responses to SEPS and other epileptiform activity like IEDs to pinpoint regions responsible for seizure generation. Despite significant improvement, the proposed beamforming methods assume a planar mat array as input for the algorithm, which is not fully accurate due to the brain's convexity.

The shape and geometry of the input array for the beamforming algorithm is an important factor. Larger spacing provides broader beamwidth with lower resolution [229, 230]. For uniform linear arrays (ULAs), the standard beamwidth is inversely proportional to the array length. The relationship between beamwidth and array length can be expressed as $\theta_B = \frac{2\pi}{\mathbf{L}}$, where $\mathbf{L}$ is the array length in wavelengths [153]. To avoid spatial aliasing, the element spacing should be less than half the wavelength of the highest frequency of interest. However, smaller spacing can lead to mutual coupling between elements, which degrades performance [231]. Beyond ULAs, other array geometries like uniform circular arrays (UCAs) and uniform rectangular arrays (URAs) offer different performance characteristics. UCAs provide 360-degree coverage but lower resolution than ULAs, while URAs can achieve high resolution in two dimensions at the cost of increased complexity [232]. Non-uniform and sparse array designs have also been proposed to optimise the performance metrics like sidelobe levels and directivity while reducing the number of elements. By establishing the current research on array geometry impacts, future work could focus on developing novel array configurations and signal processing techniques to enhance resolution and beamwidth performance, particularly for applications with size, cost, or computational constraints. Adaptive and cognitive beamforming approaches that dynamically optimise the array geometry could be another promising direction.

Finally, as mentioned in Chapter 5, the physical shape and positioning of the subdural mat as the array input are other areas worth investigating for source localisation pipelines based on beamforming algorithms. Research indicates that the spatial arrangement of array elements influences key beamforming parameters such as directivity, sidelobe levels, and beam steering capabilities [233, 234]. The sensor array geometry and the spacing between sensors determine the resolution and beamwidth of the beamformer: smaller inter-sensor spacing allows for higher spatial resolution and narrower beamwidth, while larger spacing provides broader beamwidth with lower resolution [229, 230]. For ULAs, the standard beamwidth is inversely proportional to

the spacing between sensors. The relationship between beamwidth and array length can be expressed as $\theta_B = \frac{2\pi}{\mathbf{L}}$, where $\mathbf{L}$ is the array length in wavelengths [153]. To avoid spatial aliasing, the element spacing should be less than half the wavelength of the highest frequency of interest. However, smaller spacing can lead to mutual coupling between elements, which degrades performance [231]. Beyond ULAs, other array geometries like UCAs and URAs offer different performance characteristics. UCAs provide 360-degree coverage but lower resolution than ULAs, while URAs can achieve high resolution in two dimensions at the cost of increased complexity [232, 235]. Non-uniform and sparse array designs have also been proposed to optimise the performance metrics like sidelobe levels and directivity while reducing the number of elements.

By establishing the current research on array geometry impacts, future work could focus on developing novel array configurations and signal processing techniques to enhance resolution and beamwidth performance, particularly for applications with size, cost, or computational constraints. Adaptive and cognitive beamforming approaches that can dynamically optimise the array geometry could be another promising direction.

BIBLIOGRAPHY

[1] Richard SJ Frackowiak. *Human brain function*. Elsevier, 2004.

[2] Michal Teplan et al. "Fundamentals of EEG measurement." In: *Measurement science review* 2.2 (2002), pp. 1–11.

[3] Gary H Glover. "Overview of functional magnetic resonance imaging." In: *Neurosurgery Clinics* 22.2 (2011), pp. 133–139.

[4] Saeid Sanei and Jonathon A Chambers. *EEG Signal Processing and Machine Learning*. John Wiley & Sons, 2021.

[5] Sebastianus Petrus van den Broek, F Reinders, M Donderwinkel, and MJ Peters. "Volume conduction effects in EEG and MEG." In: *Electroencephalography and clinical neurophysiology* 106.6 (1998), pp. 522–534.

[6] Gonzalo Alarcón and Antonio Valentín. *Introduction to epilepsy*. Cambridge University Press, 2012.

[7] World Health Organization. *Epilepsy*. Accessed: [Insert access date here]. 2023. URL: https://www.who.int/health-topics/epilepsy.

[8] Joseph I Sirven. "Epilepsy: a spectrum disorder." In: *Cold Spring Harbor perspectives in medicine* 5.9 (2015), a022848.

[9] S Wigglesworth, A Neligan, JM Dickson, A Pullen, E Yelland, T Anjuman, and M Reuber. "The incidence and prevalence of epilepsy in the United Kingdom 2013–2018: A retrospective cohort study of UK primary care data." In: *Seizure: European Journal of Epilepsy* 105 (2023), pp. 37–42.

[10] Aidan Neligan, Guleed Adan, Sarah J Nevitt, Angie Pullen, Josemir W Sander, Laura Bonnett, and Anthony G Marson. "Prognosis of adults and children following a first unprovoked seizure." In: *Cochrane Database of Systematic Reviews* 1 (2023).

[11] Linda Kalilani, Xuezheng Sun, Barbara Pelgrims, Matthias Noack-Rink, and Vicente Villanueva. "The epidemiology of drug-resistant epilepsy: a systematic review and meta-analysis." In: *Epilepsia* 59.12 (2018), pp. 2179–2193.

[12] Susan Spencer and Linda Huh. "Outcomes of epilepsy surgery in adults and children." In: *The Lancet Neurology* 7.6 (2008), pp. 525–537.

[13] Orrin Devinsky, Deana Gazzola, and W Curt LaFrance Jr. "Differentiating between nonepileptic and epileptic seizures." In: *Nature Reviews Neurology* 7.4 (2011), pp. 210–220.

[14] Carl E Stafstrom and Lionel Carmant. "Seizures and epilepsy: an overview for neuroscientists." In: *Cold Spring Harbor perspectives in medicine* 5.6 (2015), a022426.

[15] Haleema Anwar, Qudsia Umaira Khan, Natasha Nadeem, Iqra Pervaiz, Muhammad Ali, and Fatima Fayyaz Cheema. "Epileptic seizures." In: *Discoveries* 8.2 (2020).

[16] Sarah Fullam and Daniel J Costello. "Clinical characteristics of patients with refractory non-epileptic seizures." In: *Epilepsy & Behavior* 155 (2024), p. 109783.

[17] Richard J Brown and Markus Reuber. "Psychological and psychiatric aspects of psychogenic non-epileptic seizures (PNES): a systematic review." In: *Clinical Psychology Review* 45 (2016), pp. 157–182.

[18] Taeho Kim, Phuc Nguyen, Nhat Pham, Nam Bui, Hoang Truong, Sangtae Ha, and Tam Vu. "Epileptic seizure detection and experimental treatment: a review." In: *Frontiers in Neurology* 11 (2020), p. 701.

[19] Bahman Abdi-Sargezeh, Sepehr Shirani, Saeid Sanei, Clive Cheong Took, Oana Geman, Gonzalo Alarcon, and Antonio Valentin. "A review of signal processing and machine learning techniques for interictal epileptiform discharge detection." In: *Computers in Biology and Medicine* (2023), p. 107782.

[20] Antonio Valentin, M Anderson, Gonzalo Alarcon, JJ García Seoane, Richard Selway, CD Binnie, and CE Polkey. "Responses to single pulse electrical stimulation identify epileptogenesis in the human brain in vivo." In: *Brain* 125.8 (2002), pp. 1709–1718.

[21] Gonzalo Alarcón, Ioannis Stavropoulos, and Antonio Valentin. "Single-pulse electrical stimulation: Where do we stand?" In: *Clinical Neurophysiology: Official Journal of the International Federation of Clinical Neurophysiology* (2022), S1388–2457.

[22] Antonio Valentín, Gonzalo Alarcón, Mrinalini Honavar, Jorge J García Seoane, Richard P Selway, Charles E Polkey, and Colin D Binnie. "Single pulse electrical stimulation for identification of structural abnormalities and prediction of seizure outcome after epilepsy surgery: a prospective study." In: *The Lancet Neurology* 4.11 (2005), pp. 718–726.

[23] Mayo Clinic. *Seizure - Diagnosis and treatment*. Accessed on 1 July 2024. Mayo Clinic, 2023. URL: https://www.mayoclinic.org/diseases-conditions/seizure/diagnosis-treatment/drc-20365730.

[24] CURE Epilepsy. *Diagnosing Epilepsy: Tests and Tools*. Accessed on 1 July 2024. CURE Epilepsy, 2023. URL: https://cureepilepsy.org/for-patients/understanding/diagnosing-epilepsy/tests-and-tools/.

[25] Johns Hopkins Medicine. *Diagnosing Seizures and Epilepsy*. Accessed on 1 July 2024. Johns Hopkins Medicine, 2023. URL: https://www.hopkinsmedicine.org/health/conditions-and-diseases/epilepsy/diagnosing-seizures-and-epilepsy.

[26] Ritam Bandopadhyay, Tanveer Singh, Mohammed M Ghoneim, Sultan Alshehri, Efthalia Angelopoulou, Yam Nath Paudel, Christina Piperi, Javed Ahmad, Nabil A Alhakamy, Mohamed A Alfaleh, et al. "Recent developments in diagnosis of epilepsy: scope of MicroRNA and technological advancements." In: *Biology* 10.11 (2021), p. 1097.

[27] Christian J Hartmann, Sabine Fliegen, Stefan J Groiss, Lars Wojtecki, and Alfons Schnitzler. "An update on best practice of deep brain stimulation in Parkinson's disease." In: *Therapeutic Advances in Neurological Disorders* 12 (2019), p. 1756286419838096.

[28] Robert S Fisher and Ana Luisa Velasco. "Electrical brain stimulation for epilepsy." In: *Nature Reviews Neurology* 10.5 (2014), pp. 261–270.

[29] Ying-Chang Wu, Ying-Siou Liao, Wen-Hsiu Yeh, Sheng-Fu Liang, and Fu-Zen Shaw. "Directions of deep brain stimulation for epilepsy and Parkinson's disease." In: *Frontiers in Neuroscience* 15 (2021), p. 680938.

[30] Andres M Lozano, Nir Lipsman, Hagai Bergman, Peter Brown, Stephan Chabardes, Jin Woo Chang, Keith Matthews, Cameron C McIntyre, Thomas E Schlaepfer, Michael Schulder, et al. "Deep brain stimulation: current challenges and future directions." In: *Nature Reviews Neurology* 15.3 (2019), pp. 148–160.

[31] Michael Kogan, Matthew McGuire, and Jonathan Riley. "Deep brain stimulation for Parkinson disease." In: *Neurosurgery Clinics* 30.2 (2019), pp. 137–146.

[32] Michał Sobstyl, Angelika Stapińska-Syniec, and Marcin Rylski. "Deep brain stimulation for the treatment of refractory and super-refractory status epilepticus." In: *Seizure* 81 (2020), pp. 58–62.

[33] Ali Olamat, Pinar Ozel, and Aydin Akan. "Synchronization Analysis In Epileptic EEG Signals Via State Transfer Networks Based On Visibility Graph Technique." In: *International Journal of Neural Systems* 32.02 (2022), p. 2150041.

[34] Hilgo Bruining, Richard Hardstone, Juarez-Martinez, et al. "Measurement of excitation-inhibition ratio in autism spectrum disorder using critical brain dynamics." In: *Scientific Reports* 10.1 (2020), pp. 1–15.

[35] Osame Kinouchi and Mauro Copelli. "Optimal dynamical range of excitable networks at criticality." In: *Nature Physics* 2.5 (2006), pp. 348–351.

[36] Gina G Turrigiano and Sacha B Nelson. "Homeostatic plasticity in the developing nervous system." In: *Nature Reviews Neuroscience* 5.2 (2004), pp. 97–107.

[37] Kevin Staley. "Molecular mechanisms of epilepsy." In: *Nature Neuroscience* 18.3 (2015), pp. 367–372.

[38] Li-Rong Shao, Christa W Habela, and Carl E Stafstrom. "Pediatric epilepsy mechanisms: expanding the paradigm of excitation/inhibition imbalance." In: *Children* 6.2 (2019), p. 23.

[39] Riki Matsumoto, Dileep R Nair, Eric LaPresto, Imad Najm, William Bingaman, Hiroshi Shibasaki, and Hans O Lüders. "Functional connectivity in the human language system: a cortico-cortical evoked potential study." In: *Brain* 127.10 (2004), pp. 2316–2330.

[40] Antonio Valentin, Gonzalo Alarcon, Jorge J Garcia-Seoane, ME Lacruz, SD Nayak, M Honavar, Richard P Selway, CD Binnie, and CE Polkey. "Single-pulse electrical stimulation identifies epileptogenic frontal cortex in the human brain." In: *Neurology* 65.3 (2005), pp. 426–435.

[41] Riki Matsumoto, Dileep R Nair, Eric LaPresto, William Bingaman, Hiroshi Shibasaki, and Hans O Lüders. "Functional connectivity in human cortical motor system: a cortico-cortical evoked potential study." In: *Brain* 130.1 (2007), pp. 181–197.

[42] Josef Parvizi and Sabine Kastner. "Human intracranial EEG: promises and limitations." In: *Nature neuroscience* 21.4 (2018), p. 474.

[43] Sara Kruge Nossen. "Automatic Deviance Detection in the Human Auditory Cortex and Temporoparietal Junction." MA thesis. 2023.

[44] Takumi Mitsuhashi, Masaki Sonoda, Hirotaka Iwaki, Aimee F Luat, Sandeep Sood, and Eishi Asano. "Effects of depth electrode montage and single-pulse electrical stimulation sites on neuronal responses and effective connectivity." In: *Clinical Neurophysiology* 131.12 (2020), pp. 2781–2792.

[45] Gonzalo Alarcón, Juan Martinez, Shashivadan V Kerai, Maria E Lacruz, Rodrigo Quian Quiroga, Richard P Selway, Mark P Richardson, Jorge J García Seoane, and Antonio Valentín. "In vivo neuronal firing patterns during human epileptiform discharges replicated by electrical stimulation." In: *Clinical Neurophysiology* 123.9 (2012), pp. 1736–1744.

[46] Mark A Hays, Rachel J Smith, Yujing Wang, Christopher Coogan, Sridevi V Sarma, Nathan E Crone, and Joon Y Kang. "Cortico-cortical evoked potentials in response to varying stimulation intensity improves seizure localization." In: *Clinical Neurophysiology* 145 (2023), pp. 119–128.

[47] Takeharu Kunieda, Yukihiro Yamao, Takayuki Kikuchi, and Riki Matsumoto. "New approach for exploring cerebral functional connectivity: review of cortico-cortical evoked potential." In: *Neurologia medico-chirurgica* 55.5 (2015), pp. 374–382.

[48] Yuichi Kubota, Rei Enatsu, Jorge Gonzalez-Martinez, Juan Bulacio, John Mosher, Richard C Burgess, and Dileep R Nair. "In vivo human hippocampal cingulate connectivity: a corticocortical evoked potentials (CCEPs) study." In: *Clinical Neurophysiology* 124.8 (2013), pp. 1547–1556.

[49] Takayuki Kikuchi, Riki Matsumoto, Nobuhiro Mikuni, Yohei Yokoyama, Atsuhito Matsumoto, Akio Ikeda, Hidenao Fukuyama, Susumu Miyamoto, and Nobuo Hashimoto. "Asymmetric bilateral effect of the supplementary motor area proper in the human motor system." In: *Clinical neurophysiology* 123.2 (2012), pp. 324–334.

[50] Rei Enatsu, Riki Matsumoto, Zhe Piao, Timothy O'Connor, Karl Horning, Richard C Burgess, Juan Bulacio, William Bingaman, and Dileep R Nair. "Cortical negative motor network in comparison with sensorimotor network: a cortico-cortical evoked potential study." In: *Cortex* 49.8 (2013), pp. 2080–2096.

[51] Danny Flanagan, Antonio Valentín, Jorge J García Seoane, Gonzalo Alarcón, and Stewart G Boyd. "Single-pulse electrical stimulation helps to identify epileptogenic cortex in children." In: *Epilepsia* 50.7 (2009), pp. 1793–1803.

[52] Vasileios Kokkinos, Gonzalo Alarcón, Richard P Selway, and Antonio Valentín. "Role of single pulse electrical stimulation (SPES) to guide electrode implantation under general anaesthesia in presurgical assessment of epilepsy." In: *Seizure* 22.3 (2013), pp. 198–204.

[53] Li-Rong Shao, Christa W Habela, and Carl E Stafstrom. "Pediatric epilepsy mechanisms: expanding the paradigm of excitation/inhibition imbalance." In: *Children* 6.2 (2019), p. 23.

[54] Sepehr Shirani, Antonio Valentin, Gonzalo Alarcon, Farhana Kazi, and Saeid Sanei. "Separating inhibitory and excitatory responses of epileptic brain to single-pulse electrical stimulation." In: *International Journal of Neural Systems* 33.02 (2023), p. 2350008.

[55] Sepehr Shirani, Antonio Valentin, Bahman Abdi-Sargezeh, Gonzalo Alarcon, and Saeid Sanei. "Localization of Epileptic Brain Responses to Single-Pulse Electrical Stimulation by Developing an Adaptive Iterative Linearly Constrained Minimum Variance Beamformer." In: *International Journal of Neural Systems* (2023), pp. 2350050–2350050.

[56] Dinesh Nayak, Antonio Valentín, Richard P Selway, and Gonzalo Alarcón. "Can single pulse electrical stimulation provoke responses similar to spontaneous interictal epileptiform discharges?" In: *Clinical Neurophysiology* 125.7 (2014), pp. 1306–1311.

[57] Sepehr Shirani, Bahman Abdi-Sargezeh, Antonio Valentin, Gonzalo Alarcon, Jordan Bird, and Saeid Sanei. "Do Interictal Epileptiform Discharges and Brain Responses to Electrical Stimulation Come from the Same Location? An Advanced Source Localization Solution." In: (2024).

[58] Will D Penny, Stephan J Kiebel, James M Kilner, and Mick D Rugg. "Event-related brain dynamics." In: *Trends in neurosciences* 25.8 (2002), pp. 387–389.

[59] Geoffrey F Woodman. "A brief introduction to the use of event-related potentials in studies of perception and attention." In: *Attention, Perception, & Psychophysics* 72 (2010), pp. 2031–2046.

[60] Shravani Sur and Vinod Kumar Sinha. "Event-related potential: An overview." In: *Industrial psychiatry journal* 18.1 (2009), pp. 70–73.

[61] Hamid R Mohseni, Edward L Wilding, and Saeid Sanei. "Single trial estimation of event-related potentials using particle filtering." In: *2008 IEEE International Conference on Acoustics, Speech and Signal Processing*. IEEE. 2008, pp. 465–468.

[62] Delaram Jarchi, Saeid Sanei, Jose C Principe, and Bahador Makkiabadi. "A new spatiotemporal filtering method for single-trial estimation of correlated ERP subcomponents." In: *IEEE Transactions on Biomedical Engineering* 58.1 (2010), pp. 132–143.

[63] Sadaf Monajemi, Delaram Jarchi, Sim-Heng Ong, and Saeid Sanei. "Cooperative particle filtering for tracking ERP subcomponents from multichannel EEG." In: *Entropy* 19.5 (2017), p. 199.

[64] Vangelis P Oikonomou, A Tzallas, Spiros Konitsiotis, D Tsalikakis, and D Fotiadis. "The use of Kalman filter in biomedical signal processing." In: *Kalman Filter: Recent Advances and Applications* (2009).

[65] Shirin Enshaeifar, Loukianos Spyrou, Saeid Sanei, and Clive Cheong Took. "A regularised EEG informed Kalman filtering algorithm." In: *Biomedical Signal Processing and Control* 25 (2016), pp. 196–200.

[66] Zhe Chen et al. "Bayesian filtering: From Kalman filters to particle filters, and beyond." In: *Statistics* 182.1 (2003), pp. 1–69.

[67] Karl J Friston. "Functional and effective connectivity in neuroimaging: a synthesis." In: *Human brain mapping* 2.1-2 (1994), pp. 56–78.

[68] Stephen M Smith, Peter T Fox, Karla L Miller, David C Glahn, P Mickle Fox, Clare E Mackay, Nicola Filippini, Kate E Watkins, Roberto Toro, Angela R Laird, et al. "Correspondence of the brain's functional architecture during activation and rest." In: *Proceedings of the national academy of sciences* 106.31 (2009), pp. 13040–13045.

[69] Xiaolu Kong, Ru Kong, Csaba Orban, Peng Wang, Shaoshi Zhang, Kevin Anderson, Avram Holmes, John D Murray, Gustavo Deco, Martijn van den Heuvel, et al. "Sensory-motor cortices shape functional connectivity dynamics in the human brain." In: *Nature communications* 12.1 (2021), p. 6373.

[70] Tahereh S Zarghami and Karl J Friston. "Dynamic effective connectivity." In: *Neuroimage* 207 (2020), p. 116453.

[71] Dengsheng Zhang and Dengsheng Zhang. "Wavelet transform." In: *Fundamentals of image data mining: Analysis, Features, Classification and Retrieval* (2019), pp. 35–44.

[72] Satish Sinha, Partha S Routh, Phil D Anno, and John P Castagna. "Spectral decomposition of seismic data with continuous-wavelet transform." In: *Geophysics* 70.6 (2005), P19–P25.

[73] M Sifuzzaman, M Rafiq Islam, and MZ Ali. "Application of wavelet transform and its advantages compared to Fourier transform." In: (2009).

[74] Maryse A van't Klooster, Maeike Zijlmans, Frans SS Leijten, Cyrille H Ferrier, Michel JAM Van Putten, and Geertjan JM Huiskamp. "Time–frequency analysis of single pulse electrical stimulation to assist delineation of epileptogenic cortex." In: *Brain* 134.10 (2011), pp. 2855–2866.

[75] Brian E Mouthaan, Maryse A van't Klooster, D Keizer, Gerrit Jan Hebbink, Frans SS Leijten, Cyrille H Ferrier, Michel JAM Van Putten, Maeike Zijlmans, and Geertjan JM Huiskamp. "Single Pulse Electrical Stimulation to identify epileptogenic cortex: Clinical information obtained from early evoked responses." In: *Clinical neurophysiology* 127.2 (2016), pp. 1088–1098.

[76] MA Van't Klooster, NEC Van Klink, D Van Blooijs, CH Ferrier, KPJ Braun, FSS Leijten, GJM Huiskamp, and M Zijlmans. "Evoked versus spontaneous high frequency oscillations in the chronic electrocorticogram in focal epilepsy." In: *Clinical Neurophysiology* 128.5 (2017), pp. 858–866.

[77] Behtash Babadi and Emery N Brown. "A review of multitaper spectral analysis." In: *IEEE Transactions on Biomedical Engineering* 61.5 (2014), pp. 1555–1564.

[78] E Oran Brigham. *The fast Fourier transform and its applications*. Prentice-Hall, Inc., 1988.

[79] Loukianos Spyrou, Min Jing, Saeid Sanei, and Alex Sumich. "Separation and localisation of P300 sources and their subcomponents using constrained blind source separation." In: *EURASIP Journal on Advances in signal Processing* 2007 (2006), pp. 1–10.

[80] Jasmin Kevric and Abdulhamit Subasi. "Comparison of signal decomposition methods in classification of EEG signals for motor-imagery BCI system." In: *Biomedical Signal Processing and Control* 31 (2017), pp. 398–406.

[81] Saeid Sanei and Jonathon A Chambers. *EEG signal processing*. John Wiley & Sons, 2013.

[82] Javier Corsini, Leor Shoker, Saeid Sanei, and Gonzalo Alarcón. "Epileptic seizure predictability from scalp EEG incorporating constrained blind source separation." In: *IEEE Transactions on biomedical Engineering* 53.5 (2006), pp. 790–799.

[83] Riki Matsumoto, Dileep R Nair, Akio Ikeda, Tomoyuki Fumuro, Eric LaPresto, Nobuhiro Mikuni, William Bingaman, Susumu Miyamoto, Hidenao Fukuyama, Ryosuke Takahashi, et al. "Parieto-frontal network in humans studied by cortico-cortical evoked potential." In: *Human brain mapping* 33.12 (2012), pp. 2856–2872.

[84] Matthew A Howard, IO Volkov, R Mirsky, PC Garell, MD Noh, M Granner, H Damasio, Mitchell Steinschneider, RA Reale, JE Hind, et al. "Auditory cortex on the human posterior superior temporal gyrus." In: *Journal of Comparative Neurology* 416.1 (2000), pp. 79–92.

[85] Talal Almashaikhi, Sylvain Rheims, Julien Jung, Karine Ostrowsky-Coste, Alexandra Montavont, Julitta De Bellescize, Alexis Arzimanoglou, Pascale Keo Kosal, Marc Guénot, Olivier Bertrand, et al. "Functional connectivity of insular efferences." In: *Human Brain Mapping* 35.10 (2014), pp. 5279–5294.

[86] Talal Almashaikhi, Sylvain Rheims, Karine Ostrowsky-Coste, Alexandra Montavont, Julien Jung, Julitta De Bellescize, Alexis Arzimanoglou, Pascal Keo Kosal, Marc Guénot, Olivier Bertrand, et al. "Intrainsular functional connectivity in human." In: *Human brain mapping* 35.6 (2014), pp. 2779–2788.

[87] CL Wilson, M Isokawa, TL Babb, and PH Crandall. "Functional connections in the human temporal lobe: I. Analysis of limbic system pathways using neuronal responses evoked by electrical stimulation." In: *Experimental brain research* 82 (1990), pp. 279–292.

[88] CL Wilson, M Isokawa, TL Babb, PH Crandall, MF Levesque, and Jr Engel. "Functional connections in the human temporal lobe: II. Evidence for a loss of functional linkage between contralateral limbic structures." In: *Experimental Brain Research* 85 (1991), pp. 174–187.

[89] Riki Matsumoto and Takeharu Kunieda. "Cortico-cortical evoked potential mapping." In: *Invasive studies of the human epileptic brain: Principles and practice of invasive brain recordings and stimulation in epilepsy (Part IV: Human brain mapping, Chapter 32)* (2018), pp. 431–452.

[90] Hyunjin Jo, Dongyeop Kim, Jooyeon Song, and Dae-Won Seo. "New approach of using cortico-cortical evoked potential for functional brain evaluation." In: *Annals of Clinical Neurophysiology* 23.2 (2021), pp. 69–81.

[91] Riki Matsumoto, Takeharu Kunieda, and Dileep Nair. "Single pulse electrical stimulation to probe functional and pathological connectivity in epilepsy." In: *Seizure* 44 (2017), pp. 27–36.

[92] Christopher S Parker, Jonathan D Clayden, M Jorge Cardoso, Roman Rodionov, John S Duncan, Catherine Scott, Beate Diehl, and Sebastien Ourselin. "Structural and effective connectivity in focal epilepsy." In: *NeuroImage: Clinical* 17 (2018), pp. 943–952.

[93] Julien Krieg, Laurent Koessler, Jacques Jonas, Sophie Colnat-Coulbois, Jean-Pierre Vignal, Christian G Bénar, and Louis G Maillard. "Discrimination of a medial functional module within the temporal lobe using an effective connectivity model: A CCEP study." In: *NeuroImage* 161 (2017), pp. 219–231.

[94] Mikail Rubinov and Olaf Sporns. "Complex network measures of brain connectivity: uses and interpretations." In: *Neuroimage* 52.3 (2010), pp. 1059–1069.

[95] David Prime, Matthew Woolfe, David Rowlands, Steven O'Keefe, and Sasha Dionisio. "Comparing connectivity metrics in cortico-cortical evoked potentials using synthetic cortical response patterns." In: *Journal of Neuroscience Methods* 334 (2020), p. 108559.

[96] Tianfeng Chai, Roland R Draxler, et al. "Root mean square error (RMSE) or mean absolute error (MAE)." In: *Geoscientific model development discussions* 7.1 (2014), pp. 1525–1534.

[97] Meinard Müller. "Dynamic time warping." In: *Information retrieval for music and motion* (2007), pp. 69–84.

[98] Jason Lines and Anthony Bagnall. "Time series classification with ensembles of elastic distance measures." In: *Data Mining and Knowledge Discovery* 29 (2015), pp. 565–592.

[99] Christopher Meek, David Maxwell Chickering, and David Heckerman. "Autoregressive tree models for time-series analysis." In: *Proceedings of the 2002 SIAM International Conference on Data Mining*. SIAM. 2002, pp. 229–244.

[100] Boualem Boashash. *Time-frequency signal analysis and processing: a comprehensive reference*. Academic press, 2015.

[101] Zhihao Guo, Baotian Zhao, Wenhan Hu, Chao Zhang, Xiu Wang, Yao Wang, Chang Liu, Jiajie Mo, Lin Sang, Yanshan Ma, et al. "Effective connectivity among the hippocampus, amygdala, and temporal neocortex in epilepsy patients: A cortico-cortical evoked potential study." In: *Epilepsy & Behavior* 115 (2021), p. 107661.

[102] Katsuya Kobayashi, Kenneth N Taylor, Hossein Shahabi, Balu Krishnan, Anand Joshi, Michael J Mackow, Lauren Feldman, Omar Zamzam, Takfarinas Medani, Juan Bulacio, et al. "Effective connectivity relates seizure outcome to electrode placement in responsive neurostimulation." In: *Brain Communications* 6.1 (2024), fcae035.

[103] Golnoosh Kamali, Rachel June Smith, Mark Hays, Christopher Coogan, Nathan E Crone, Joon Y Kang, and Sridevi V Sarma. "Transfer function models for the localization of seizure onset zone from cortico-cortical evoked potentials." In: *Frontiers in Neurology* 11 (2020), p. 579961.

[104] Golnoosh Kamali, Rachel J Smith, Mark Hays, Christopher Coogan, Nathan E Crone, Sridevi V Sarma, and Joon Y Kang. "Localizing the seizure onset zone from single pulse electrical stimulation responses using transfer function models." In: *2020 42nd Annual International Conference of the IEEE Engineering in Medicine & Biology Society (EMBC)*. IEEE. 2020, pp. 2524–2527.

[105] R Rabenstein. "Transfer function models for multidimensional systems with bounded spatial domains." In: *Mathematical and Computer Modelling of Dynamical Systems* 5.3 (1999), pp. 259–278.

[106] Yonglin Dou, Jing Xia, Mengmeng Fu, Yunpeng Cai, Xianghong Meng, and Yang Zhan. "Identification of epileptic networks with graph convolutional network incorporating oscillatory activities and evoked synaptic responses." In: *NeuroImage* 284 (2023), p. 120439.

[107] Bowen Yang, Baotian Zhao, Chao Li, Jiajie Mo, Zhihao Guo, Zilin Li, Yuan Yao, Xiuliang Fan, Du Cai, Lin Sang, et al. "Localizing seizure onset zone by a cortico-cortical evoked potentials-based machine learning approach in focal epilepsy." In: *Clinical Neurophysiology* 158 (2024), pp. 103–113.

[108] Yann LeCun, Yoshua Bengio, and Geoffrey Hinton. "Deep learning." In: *nature* 521.7553 (2015), pp. 436–444.

[109] Ian Goodfellow. *Deep Learning*. MIT Press, 2016.

[110] Graham W Johnson, Leon Y Cai, Derek J Doss, Jasmine W Jiang, Aarushi S Negi, Saramati Narasimhan, Danika L Paulo, Hernán FJ González, Shawniqua Williams Roberson, Sarah K Bick, et al. "Localizing seizure onset zones in surgical epilepsy with neurostimulation deep learning." In: *Journal of neurosurgery* 138.4 (2022), pp. 1002–1007.

[111] Jamie Norris, Aswin Chari, Gerald Cooray, Martin Tisdall, Karl Friston, and Richard Rosch. "Localising the Seizure Onset Zone from Single-Pulse Electrical Stimulation Responses with a Transformer." In: *arXiv preprint arXiv:2403.20324* (2024).

[112] Loukianos Spyrou and Saeid Sanei. "Source localization of event-related potentials incorporating spatial notch filters." In: *IEEE Transactions on Biomedical Engineering* 55.9 (2008), pp. 2232–2239.

[113] Saeid Sanei, Saideh Ferdowsi, Kianoush Nazarpour, and Andrzej Cichocki. "Advances in electroencephalography signal processing [Life Sciences]." In: *IEEE Signal Processing Magazine* 30.1 (2012), pp. 170–176.

[114] Hamid R Mohseni and Saeid Sanei. "A new beamforming-based MEG dipole source localization method." In: *2010 IEEE International Conference on Acoustics, Speech and Signal Processing*. IEEE. 2010, pp. 558–561.

[115] Loukianos Spyrou and Saeid Sanei. "A new beamforming approach for the localisation of event related potentials." In: *2007 15th European Signal Processing Conference*. IEEE. 2007, pp. 2489–2493.

[116] Hossein Hassani. "Singular spectrum analysis: methodology and comparison." In: (2007).

[117] Steffen Merte. "Estimating heat wave-related mortality in Europe using singular spectrum analysis." In: *Climatic change* 142.3 (2017), pp. 321–330.

[118] Hossein Hassani and Dimitrios Thomakos. "A review on singular spectrum analysis for economic and financial time series." In: *Statistics and its Interface* 3.3 (2010), pp. 377–397.

[119] Saeid Sanei and Hossein Hassani. *Singular Spectrum Analysis of Biomedical Signals*. CRC press, 2015.

[120] Mansoureh Ghodsi, Hossein Hassani, and Saeid Sanei. "Extracting fetal heart signal from noisy maternal ECG by multivariate singular spectrum analysis." In: *Statistics and its Interface* 3.3 (2010), pp. 399–411.

[121] E García Plaza and PJ Núñez López. "Surface roughness monitoring by singular spectrum analysis of vibration signals." In: *Mechanical systems and signal processing* 84 (2017), pp. 516–530.

[122] Roya Cody, Jinane Harmouche, and Sriram Narasimhan. "Leak detection in water distribution pipes using singular spectrum analysis." In: *Urban Water Journal* 15.7 (2018), pp. 636–644.

[123] CL Wu and Kwok Wing Chau. "Rainfall–runoff modeling using artificial neural network coupled with singular spectrum analysis." In: *Journal of Hydrology* 399.3-4 (2011), pp. 394–409.

[124] Aapo Hyvärinen and Erkki Oja. "Independent component analysis: algorithms and applications." In: *Neural networks* 13.4-5 (2000), pp. 411–430.

[125] Norden E Huang, Zheng Shen, Steven R Long, Manli C Wu, Hsing H Shih, Quanan Zheng, Nai-Chyuan Yen, Chi Chao Tung, and Henry H Liu. "The empirical mode decomposition and the Hilbert spectrum for nonlinear and non-stationary time series analysis." In: *Proceedings of the Royal Society of London. Series A: mathematical, physical and engineering sciences* 454.1971 (1998), pp. 903–995.

[126] Gabriel Rilling, Patrick Flandrin, Paulo Goncalves, et al. "On empirical mode decomposition and its algorithms." In: *IEEE-EURASIP workshop on nonlinear signal and image processing*. Vol. 3. 3. Grado: IEEE. 2003, pp. 8–11.

[127] Mehdi Zare and Nowrouz Mohammad Nouri. "End-effects mitigation in empirical mode decomposition using a new correlation-based expansion model." In: *Mechanical Systems and Signal Processing* 194 (2023), p. 110205.

[128] Stéphane Mallat. *A wavelet tour of signal processing*. Elsevier, 1999.

[129] Richard C Burgess. "Intracranial electrodes." In: *Journal of Clinical Neurophysiology* 9.2 (1992), pp. 305–313.

[130] Yue Chen, Isuru Godage, Hao Su, Aiguo Song, and Hong Yu. "Stereotactic systems for MRI-guided neurosurgeries: a state-of-the-art review." In: *Annals of biomedical engineering* 47 (2019), pp. 335–353.

[131] Jerome Engel Jr. "Update on surgical treatment of the epilepsies: summary of the second international palm desert conference on the surgical treatment of the epilepsies (1992)." In: *Neurology* 43.8 (1993), pp. 1612–1612.

[132] James B Elsner and Anastasios A Tsonis. *Singular spectrum analysis: a new tool in time series analysis*. Springer Science and Business Media, 1996.

[133] Saeid Sanei, Tracey KM Lee, and Vahid Abolghasemi. "A new adaptive line enhancer based on singular spectrum analysis." In: *IEEE Transactions on Biomedical Engineering* 59.2 (2011), pp. 428–434.

[134] Foad Ghaderi, Hamid R Mohseni, and Saeid Sanei. "Localizing heart sounds in respiratory signals using singular spectrum analysis." In: *IEEE Transactions on Biomedical Engineering* 58.12 (2011), pp. 3360–3367.

[135] Samaneh Kouchaki, Saeid Sanei, Emma L Arbon, and Derk-Jan Dijk. "Tensor based singular spectrum analysis for automatic scoring of sleep EEG." In: *IEEE Transactions on Neural Systems and Rehabilitation Engineering* 23.1 (2014), pp. 1–9.

[136] Saeid Sanei, Mansoureh Ghodsi, and Hossein Hassani. "An adaptive singular spectrum analysis approach to murmur detection from heart sounds." In: *Medical Engineering and Physics* 33.3 (2011), pp. 362–367.

[137] Michael Ghil and Ning Jiang. "Recent forecast skill for the El Nino/Southern oscillation." In: *Geophysical Research Letters* 25.2 (1998), pp. 171–174.

[138] Kerry Patterson, Hossein Hassani, Saeed Heravi, and Anatoly Zhigljavsky. "Multivariate singular spectrum analysis for forecasting revisions to real-time data." In: *Journal of Applied Statistics* 38.10 (2011), pp. 2183–2211.

[139] A Olenko, Kainam Thomas Wong, H Mir, and H Al-Nashash. "Generalised correlation index for quantifying signal morphological similarity." In: *Electronics Letters* 52.22 (2016), pp. 1832–1834.

[140] Dinesh Nayak, Antonio Valentín, Richard P Selway, and Gonzalo Alarcón. "Can single pulse electrical stimulation provoke responses similar to spontaneous interictal epileptiform discharges?" In: *Clinical Neurophysiology* 125.7 (2014), pp. 1306–1311.

[141] Angelique C Paulk, Rina Zelmann, Britni Crocker, et al. "Local and distant cortical responses to single pulse intracranial stimulation in the human brain are differentially modulated by specific stimulation parameters." In: *Brain Stimulation* 15.2 (2022), pp. 491–508.

[142] Zeynep Akalin Acar and Scott Makeig. "Effects of forward model errors on EEG source localization." In: *Brain topography* 26 (2013), pp. 378–396.

[143] Munsif Ali Jatoi, Nidal Kamel, Aamir Saeed Malik, Ibrahima Faye, and Tahamina Begum. "A survey of methods used for source localization using EEG signals." In: *Biomedical Signal Processing and Control* 11 (2014), pp. 42–52.

[144] Munsif Ali Jatoi, Nidal Kamel, Ibrahima Faye, Aamir Saeed Malik, Jose Miguel Bornot, and Tahamina Begum. "BEM based solution of forward problem for brain source estimation." In: *2015 IEEE International Conference on Signal and Image Processing Applications (ICSIPA)*. IEEE. 2015, pp. 180–185.

[145] S Baillet, JJ Riera, G Marin, JF Mangin, J Aubert, and L Garnero. "Evaluation of inverse methods and head models for EEG source localization using a human skull phantom." In: *Physics in medicine & biology* 46.1 (2001), p. 77.

[146] Giovanni Pellegrino, Tanguy Hedrich, Rasheda Arman Chowdhury, Jeffery A Hall, Francois Dubeau, Jean-Marc Lina, Eliane Kobayashi, and Christophe Grova. "Clinical yield of magnetoencephalography distributed source imaging in epilepsy: A comparison with equivalent current dipole method." In: *Human brain mapping* 39.1 (2018), pp. 218–231.

[147] Tae-Seong Kim, Yongxia Zhou, Sungheon Kim, and Manbir Singh. "EEG distributed source imaging with a realistic finite-element head model." In: *IEEE Transactions on Nuclear Science* 49.3 (2002), pp. 745–752.

[148] Tulaya Limpiti, Barry D Van Veen, and Ronald T Wakai. "Cortical patch basis model for spatially extended neural activity." In: *IEEE Transactions on Biomedical Engineering* 53.9 (2006), pp. 1740–1754.

[149] Christoph M Michel and Bin He. "EEG source localization." In: *Handbook of clinical neurology* 160 (2019), pp. 85–101.

[150] B Neil Cuffin. "EEG dipole source localization." In: *IEEE engineering in medicine and biology magazine* 17.5 (1998), pp. 118–122.

[151] Fa-Hsuan Lin, Thomas Witzel, Seppo P Ahlfors, Steven M Stufflebeam, John W Belliveau, and Matti S Hämäläinen. "Assessing and improving the spatial accuracy in MEG source localization by depth-weighted minimum-norm estimates." In: *Neuroimage* 31.1 (2006), pp. 160–171.

[152] Munsif Ali Jatoi, Nidal Kamel, Aamir Saeed Malik, and Ibrahima Faye. "EEG based brain source localization comparison of sLORETA and eLORETA." In: *Australasian physical & engineering sciences in medicine* 37 (2014), pp. 713–721.

[153] Barry D Van Veen and Kevin M Buckley. "Beamforming: A versatile approach to spatial filtering." In: *IEEE assp magazine* 5.2 (1988), pp. 4–24.

[154] Dimitrios Pantazis and Amir Adler. "MEG source localization via deep learning." In: *Sensors* 21.13 (2021), p. 4278.

[155] Song Cui, Lijuan Duan, Bei Gong, Yuanhua Qiao, Fan Xu, Juncheng Chen, and Changming Wang. "EEG source localization using spatio-temporal neural network." In: *China Communications* 16.7 (2019), pp. 131–143.

[156] Jeff Craley, Christophe Jouny, Emily Johnson, David Hsu, Raheel Ahmed, and Archana Venkataraman. "Automated seizure activity tracking and onset zone localization from scalp EEG using deep neural networks." In: *PloS one* 17.2 (2022), e0264537.

[157] Daniele Grattarola, Lorenzo Livi, Cesare Alippi, Richard Wennberg, and Taufik A Valiante. "Seizure localisation with attention-based graph neural networks." In: *Expert systems with applications* 203 (2022), p. 117330.

[158] Daniel A Griffith and Daniel A Griffith. *Spatial filtering*. Springer, 2003.

[159] A Vander Lugt. "Signal detection by complex spatial filtering." In: *IEEE Transactions on information theory* 10.2 (1964), pp. 139–145.

[160] Henry Cox, Robertm Zeskind, and Markm Owen. "Robust adaptive beamforming." In: *IEEE Transactions on Acoustics, Speech, and Signal Processing* 35.10 (1987), pp. 1365–1376.

[161] Joe C Chen, Kung Yao, and Ralph E Hudson. "Source localization and beamforming." In: *IEEE Signal Processing Magazine* 19.2 (2002), pp. 30–39.

[162] Jacob Benesty, Jingdong Chen, and Yiteng Huang. "Conventional beamforming techniques." In: *Microphone array signal processing* (2008), pp. 39–65.

[163] Jacob Benesty, Jingdong Chen, Yiteng Huang, and Jacek Dmochowski. "On microphone-array beamforming from a MIMO acoustic signal processing perspective." In: *IEEE Transactions on Audio, Speech, and Language Processing* 15.3 (2007), pp. 1053–1065.

[164] Brian G Ferguson. "Minimum variance distortionless response beamforming of acoustic array data." In: *The Journal of the Acoustical Society of America* 104.2 (1998), pp. 947–954.

[165] Jing Liu, Alex B Gershman, Zhi-Quan Luo, and Kon Max Wong. "Adaptive beamforming with sidelobe control: A second-order cone programming approach." In: *IEEE Signal Processing Letters* 10.11 (2003), pp. 331–334.

[166] John C Mosher, Sylvain Baillet, and Richard M Leahy. "EEG source localization and imaging using multiple signal classification approaches." In: *Journal of Clinical Neurophysiology* 16.3 (1999), pp. 225–238.

[167] John C Mosher and Richard M Leahy. "Source localization using recursively applied and projected (RAP) MUSIC." In: *IEEE Transactions on signal processing* 47.2 (1999), pp. 332–340.

[168] John C Mosher and Richard M Leahy. "EEG and MEG source localization using recursively applied (RAP) MUSIC." In: *Conference Record of The Thirtieth Asilomar Conference on Signals, Systems and Computers*. IEEE. 1996, pp. 1201–1207.

[169] Richard Roy and Thomas Kailath. "ESPRIT-estimation of signal parameters via rotational invariance techniques." In: *IEEE Transactions on acoustics, speech, and signal processing* 37.7 (1989), pp. 984–995.

[170] Emanuël AP Habets, Jacob Benesty, Sharon Gannot, Patrick A Naylor, and Israel Cohen. "On the application of the LCMV beamformer to speech enhancement." In: *2009 IEEE Workshop on Applications of Signal Processing to Audio and Acoustics*. IEEE. 2009, pp. 141–144.

[171] Barry D Van Veen, Wim Van Drongelen, Moshe Yuchtman, and Akifumi Suzuki. "Localization of brain electrical activity via linearly constrained minimum variance spatial filtering." In: *IEEE Transactions on biomedical engineering* 44.9 (1997), pp. 867–880.

[172] Amit Jaiswal, Jukka Nenonen, Matti Stenroos, Alexandre Gramfort, Sarang S Dalal, Britta U Westner, Vladimir Litvak, John C Mosher, Jan-Mathijs Schoffelen, Caroline Witton, et al. "Comparison of beamformer implementations for MEG source localization." In: *NeuroImage* 216 (2020), p. 116797.

[173] Armin Fuchs. "Beamforming and its applications to brain connectivity." In: *Handbook of brain connectivity*. Springer, 2007, pp. 357–378.

[174] Robert Oostenveld, Pascal Fries, Eric Maris, and Jan-Mathijs Schoffelen. "FieldTrip: open source software for advanced analysis of MEG, EEG, and invasive electrophysiological data." In: *Computational intelligence and neuroscience* 2011.1 (2011), p. 156869.

[175] John Ashburner, Gareth Barnes, Chun-Chuan Chen, Jean Daunizeau, Guillaume Flandin, Karl Friston, Stefan Kiebel, James Kilner, Vladimir Litvak, Rosalyn Moran, et al. "SPM12 manual." In: *Wellcome Trust Centre for Neuroimaging, London, UK* 2464.4 (2014).

[176] François Tadel, Sylvain Baillet, John C Mosher, Dimitrios Pantazis, and Richard M Leahy. "Brainstorm: A user-friendly application for MEG/EEG analysis." In: *Computational intelligence and neuroscience* 2011.1 (2011), p. 879716.

[177] Alexandre Gramfort, Martin Luessi, Eric Larson, Denis A Engemann, Daniel Strohmeier, Christian Brodbeck, Roman Goj, Mainak Jas, Teon Brooks, Lauri Parkkonen, et al. "MEG and EEG data analysis with MNE-Python." In: *Frontiers in Neuroinformatics* 7 (2013), p. 267.

[178] Bandh R Breed and Jeff Strauss. "A short proof of the equivalence of LCMV and GSC beamforming." In: *IEEE Signal Processing Letters* 9.6 (2002), pp. 168–169.

[179] Stefan Werner, JOSÉ A Apolinario, and Marcello LR de Campos. "On the equivalence of RLS implementations of LCMV and GSC processors." In: *IEEE Signal Processing Letters* 10.12 (2003), pp. 356–359.

[180] R Tyrrell Rockafellar. "Lagrange multipliers and optimality." In: *SIAM review* 35.2 (1993), pp. 183–238.

[181] Kensuke Sekihara, Srikantan S Nagarajan, David Poeppel, Alec Marantz, and Yasushi Miyashita. "Reconstructing spatio-temporal activities of neural sources using an MEG vector beamformer technique." In: *IEEE transactions on biomedical engineering* 48.7 (2001), pp. 760–771.

[182] Anthony T Herdman, Alexander Moiseev, and Urs Ribary. "Localizing event-related potentials using multi-source minimum variance beamformers: a validation study." In: *Brain Topography* 31 (2018), pp. 546–565.

[183] Otis Lamont Frost. "An algorithm for linearly constrained adaptive array processing." In: *Proceedings of the IEEE* 60.8 (1972), pp. 926–935.

[184] Leonardo S Resende, Joao Marcos T Romano, and Maurice G Bellanger. "A fast least-squares algorithm for linearly constrained adaptive filtering." In: *IEEE Transactions on Signal Processing* 44.5 (1996), pp. 1168–1174.

[185] Xiansheng Guo, Lei Chu, and Baocang Li. "Robust adaptive LCMV beamformer based on an iterative suboptimal solution." In: *Radioengineering* 24.2 (2015), pp. 572–582.

[186] Leonardo S Resende, Joao Marcos T Romano, and Maurice G Bellanger. "A fast least-squares algorithm for linearly constrained adaptive filtering." In: *IEEE Transactions on Signal Processing* 44.5 (1996), pp. 1168–1174.

[187] Xiansheng Guo, Lei Chu, and Baocang Li. "Robust adaptive LCMV beamformer based on an iterative suboptimal solution." In: *Radioengineering* 24.2 (2015), pp. 572–582.

[188] Vejay N Vakharia, John S Duncan, Juri-Alexander Witt, et al. "Getting the best outcomes from epilepsy surgery." In: *Annals of Neurology* 83.4 (2018), pp. 676–690.

[189] Robert Oostenveld, Pascal Fries, Eric Maris, and Jan-Mathijs Schoffelen. "FieldTrip: open source software for advanced analysis of MEG, EEG, and invasive electrophysiological data." In: *Computational Intelligence and Neuroscience* 2011 (2011), pp. 1–9.

[190] Pradip Chauhan, Shalom Elsy Philip, Girish Chauhan, and Simmi Mehra. "The anatomical basis of seizures." In: *Epilepsy* (2022).

[191] Maciej Jedynak, Anthony Boyer, Chanteloup-Forêt, et al. "Variability of Single Pulse Electrical Stimulation Responses Recorded with Intracranial Electroencephalography in Epileptic Patients." In: *Brain Topography* 36.1 (2023), pp. 119–127.

[192] Luis Garcia Dominguez, Apameh Tarazi, Taufik Valiante, and Richard Wennberg. "Beamforming seizures from the temporal lobe using magnetoencephalography." In: *Canadian Journal of Neurological Sciences* 50.2 (2023), pp. 201–213.

[193] Dinesh Nayak, Antonio Valentín, Richard P Selway, and Gonzalo Alarcón. "Can single pulse electrical stimulation provoke responses similar to spontaneous interictal epileptiform discharges?" In: *Clinical Neurophysiology* 125.7 (2014), pp. 1306–1311.

[194] Gonzalo Alarcón, Diego Jiménez-Jiménez, Antonio Valentín, and David Martín-López. "Characterizing EEG cortical dynamics and connectivity with responses to single pulse electrical stimulation (SPES)." In: *International Journal of Neural Systems* 28.06 (2018), p. 1750057.

[195] Sepehr Shirani, Antonio Valentin, Gonzalo Alarcon, Farhana Kazi, and Saeid Sanei. "Response to the Discussion on S. Shirani, A. Valentin, G. Alarcon, F. Kazi and S. Sanei, Separating Inhibitory and Excitatory Responses of Epileptic Brain to Single-Pulse Electrical Stimulation, International Journal of Neural Systems, Vol. 3, No. 2 (2023) 2350008." In: *International Journal of Neural Systems* (2023), p. 2375002.

[196] S Parmigiani, E Mikulan, S Russo, et al. "Simultaneous stereo-EEG and high-density scalp EEG recordings to study the effects of intracerebral stimulation parameters." In: *Brain Stimulation* 15.3 (2022), pp. 664–675.

[197] Mustafa Aykut Kural, Lene Duez, Vibeke Sejer Hansen, Pål G Larsson, Stefan Rampp, Reinhard Schulz, Hatice Tankisi, Richard Wennberg, Bo M Bibby, Michael Scherg, et al. "Criteria for defining interictal epileptiform discharges in EEG: a clinical validation study." In: *Neurology* 94.20 (2020), e2139–e2147.

[198] A Bruce Janati, Naif Saad ALGhasab, Maram Youseef Aldaife, Roohi Khan, Imran Khan, Ahmad Abdullah, Aslam Khan, and Tarek Abdelwahed. "Atypical interictal epileptiform discharges in electroencephalography." In: *Journal of Epilepsy Research* 8.2 (2018), p. 55.

[199] Jan Pyrzowski, Jean-Eudes Le Douget, Amal Fouad, Mariusz Siemiński, Joanna Jędrzejczak, and Michel Le Van Quyen. "Zero-crossing patterns reveal subtle epileptiform discharges in the scalp EEG." In: *Scientific Reports* 11.1 (2021), p. 4128.

[200] JW Puspita, G Soemarno, AI Jaya, and E Soewono. "Interictal Epileptiform Discharges (IEDs) classification in EEG data of epilepsy patients." In: *Journal of Physics: Conference Series*. Vol. 943. 1. IOP Publishing. 2017, p. 012030.

[201] Sarang S Dalal, Kensuke Sekihara, and Srikantan S Nagarajan. "Modified beamformers for coherent source region suppression." In: *IEEE Transactions on Biomedical Engineering* 53.7 (2006), pp. 1357–1363.

[202] Chang Cai, Yuanshun Long, Sanjay Ghosh, Ali Hashemi, Yijing Gao, Mithun Diwakar, Stefan Haufe, Kensuke Sekihara, Wei Wu, and Srikantan S Nagarajan. "Bayesian adaptive beamformer for robust electromagnetic brain imaging of correlated sources in high spatial resolution." In: *IEEE Transactions on Medical Imaging* (2023).

[203] Zhilin Zhang and Bhaskar D Rao. "Sparse signal recovery with temporally correlated source vectors using sparse Bayesian learning." In: *IEEE Journal of Selected Topics in Signal Processing* 5.5 (2011), pp. 912–926.

[204] TL Babb, WJ Brown, and J Jr Engel. "Surgical treatment of the epilepsies." In: *New York, NY* (1987).

[205] Andreas Horn and Andrea A Kühn. "Lead-DBS: a toolbox for deep brain stimulation electrode localizations and visualizations." In: *Neuroimage* 107 (2015), pp. 127–135.

[206] Siobhan Ewert, Andreas Horn, Francisca Finkel, Ningfei Li, Andrea A Kühn, and Todd M Herrington. "Optimization and comparative evaluation of nonlinear deformation algorithms for atlas-based segmentation of DBS target nuclei." In: *Neuroimage* 184 (2019), pp. 586–598.

[207] Brian B Avants, Charles L Epstein, Murray Grossman, and James C Gee. "Symmetric diffeomorphic image registration with cross-correlation: evaluating automated labeling of elderly and neurodegenerative brain." In: *Medical Image Analysis* 12.1 (2008), pp. 26–41.

[208] Thomas Schönecker, A Kupsch, AA Kühn, G-H Schneider, and K-T Hoffmann. "Automated optimization of subcortical cerebral MR imaging- atlas coregistration for improved postoperative electrode localization in deep brain stimulation." In: *American Journal of Neuroradiology* 30.10 (2009), pp. 1914–1921.

[209] Tyler S Davis, Rose M Caston, Brian Philip, Chantel M Charlebois, Daria Nesterovich Anderson, Kurt E Weaver, Elliot H Smith, and John D Rolston. "LeGUI: a fast and accurate graphical user interface for automated detection and anatomical localization of intracranial electrodes." In: *Frontiers in Neuroscience* 15 (2021), p. 769872.

[210] Michael I Jordan, Zoubin Ghahramani, Tommi S Jaakkola, and Lawrence K Saul. "An introduction to variational methods for graphical models." In: *Machine Learning* 37 (1999), pp. 183–233.

[211] Chang Cai, Ali Hashemi, Mithun Diwakar, Stefan Haufe, Kensuke Sekihara, and Srikantan S Nagarajan. "Robust estimation of noise for electromagnetic brain imaging with the champagne algorithm." In: *NeuroImage* 225 (2021), p. 117411.

[212] David Wipf and Srikantan Nagarajan. "A unified Bayesian framework for MEG/EEG source imaging." In: *NeuroImage* 44.3 (2009), pp. 947–966.

[213] Kensuke Sekihara and Srikantan S Nagarajan. *Electromagnetic brain imaging: A Bayesian perspective*. Springer, 2015.

[214] Jie Lian, Garth Garner, Dirk Muessig, and Volker Lang. "A simple method to quantify the morphological similarity between signals." In: *Signal Processing* 90.2 (2010), pp. 684–688.

[215] S Parmigiani, E Mikulan, S Russo, S Sarasso, FM Zauli, A Rubino, A Cattani, M Fecchio, D Giampiccolo, J Lanzone, et al. "Simultaneous stereo-EEG and high-density scalp EEG recordings to study the effects of intracerebral stimulation parameters." In: *Brain Stimulation* 15.3 (2022), pp. 664–675.

[216] Tamara G Kolda and Brett W Bader. "Tensor decompositions and applications." In: *SIAM Review* 51.3 (2009), pp. 455–500.

[217] Evrim Acar, Daniel M Dunlavy, and Tamara G Kolda. "A scalable optimization approach for fitting canonical tensor decompositions." In: *Journal of Chemometrics* 25.2 (2011), pp. 67–86.

[218] Xuan Bi, Annie Qu, and Xiaotong Shen. "Multilayer tensor factorization with applications to recommender systems." In: (2018).

[219] Yanqing Zhang, Xuan Bi, Niansheng Tang, and Annie Qu. "Dynamic tensor recommender systems." In: *Journal of machine learning research* 22.65 (2021), pp. 1–35.

[220] Zhengyu Chen, Sibo Gai, and Donglin Wang. "Deep tensor factorization for multi-criteria recommender systems." In: *2019 IEEE International Conference on Big Data (Big Data)*. IEEE. 2019, pp. 1046–1051.

[221] Bahman Abdi-Sargezeh, Antonio Valentin, Gonzalo Alarcon, and Saeid Sanei. "Incorporating Uncertainty in Data Labeling into Automatic Detection of Interictal Epileptiform Discharges from Concurrent Scalp-EEG via Multi-way Analysis." In: *International Journal of Neural Systems* (2021), p. 2150019. ISSN: 0129-0657. URL: https://doi.org/10.1142/S0129065721500192.

[222] Bahman Abdi-Sargezeh, Antonio Valentin, Gonzalo Alarcon, David Martin-Lopez, and Saeid Sanei. "Higher-order tensor decomposition based scalp-to-intracranial EEG projection for detection of interictal epileptiform discharges." In: *Journal of Neural Engineering* 18.6 (2021), p. 066039.

[223] Bahman Abdi-Sargezeh, Antonio Valentin, Gonzalo Alarcon, and Saeid Sanei. "Detection of brain interictal epileptiform discharges from intracranial EEG by exploiting their morphology in the tensor structure." In: *2021 29th European Signal Processing Conference (EUSIPCO)*. IEEE. 2021, pp. 1167–1171.

[224] Tamara Gibson Kolda. *Multilinear operators for higher-order decompositions.* Tech. rep. Sandia National Laboratories (SNL), Albuquerque, NM, and Livermore, CA ..., 2006.

[225] Jason Uher, Tadeusz A Wysocki, and Beata J Wysocki. "Review of distributed beamforming." In: *Journal of Telecommunications and Information Technology* 1 (2011), pp. 78–88.

[226] Guoliang Peng, Lihui Jiang, Xiaohui Tao, Yan Zhang, and Rui Cao. "A Real-Time Adaptive Station Beamforming Strategy for Next Generation Phased Array Radio Telescopes." In: *Sensors (Basel, Switzerland)* 24.14 (2024).

[227] Felix S Gubler, Onur Alptekin, Linda Ackermans, Pieter L Kubben, Mark L Kuijf, Ersoy Kocabicak, and Yasin Temel. "Impact of preoperative computed tomography image slice thickness on the planning of deep brain stimulation surgery: A phantom study." In: *Deep Brain Stimulation* 2 (2023), pp. 6–14.

[228] John F Burke, Dominic Tanzillo, Philip A Starr, Daniel A Lim, and Paul S Larson. "CT and MRI image fusion error: an analysis of co-registration error using commercially available deep brain stimulation surgical planning software." In: *Stereotactic and Functional Neurosurgery* 99.3 (2021), pp. 196–202.

[229] Hamid Krim, Mats Viberg, et al. "Sensor array signal processing: two decades later." In: (1995).

[230] Harry L Van Trees. *Optimum array processing: Part IV of detection, estimation, and modulation theory*. John Wiley & Sons, 2002.

[231] Lal C Godara. "Application of antenna arrays to mobile communications. II. Beam-forming and direction-of-arrival considerations." In: *Proceedings of the IEEE* 85.8 (1997), pp. 1195–1245.

[232] Panayiotis Ioannides and Constantine A Balanis. "Uniform circular and rectangular arrays for adaptive beamforming applications." In: *IEEE antennas and wireless propagation letters* 4 (2005), pp. 351–354.

[233] Ahmed Alzin, Fraser K Coutts, Jamie Corr, Stephan Weiss, Ian K Proudler, and Jonathon A Chambers. "Adaptive broadband beamforming with arbitrary array geometry." In: (2015).

[234] Chenfeng Meng, Yongwei Zhang, Murat Temiz, and Ahmed El-Makadema. "A Multiobjective Array Beamforming Method for Arrays of Flexible Shape." In: *Electronics* 13.4 (2024), p. 752.

[235] Muhammad Asfar Saeed and Augustine O Nwajana. "A review of beamforming microstrip patch antenna array for future 5G/6G networks." In: *Frontiers in Mechanical Engineering* 9 (2024), p. 1288171.